Escola de Camins
Escola Tècnica Superior d'Enginyeria de Camins, Canals i Ports
UPC BARCELONATECH

TREBALL FINAL DE MÀSTER

THE PRESENT STATE OF THE LIBERIAN COAST: CONTRIBUTIONS TO COASTAL VULNERABILITY AND COASTAL PROTECTION MASTERPLAN

Treball realitzat per:
John C L Mayson II

Dirigit per:
Dr. Vicente Gracia
Associate Professor
Laboratori d'Enginyeria Marítima (LIM/UPC)
Centre Internacional d'Investigació dels Recursos Costaners (CIIRC)

Màster en:
COASTAL AND MARINE ENGINEERING AND MANAGEMENT (CoMEM)

Barcelona, 15 June 2018

Departament d'Enginyeria de Camins, Canals i Ports

ERASMUS +: ERASMUS MUNDUS MOBILITY PROGRAMME

Master of Science in

COASTAL AND MARINE ENGINEERING AND MANAGEMENT

CoMEM

THE PRESENT STATE OF THE LIBERIAN COAST: CONTRIBUTIONS TO COASTAL VULNERABILITY AND COASTAL PROTECTION MASTERPLAN

Universitat Politécnica de Catalunya (UPC)
15 June 2018

John C L Mayson II

The Erasmus+: Erasmus Mundus MSc in Coastal and Marine Engineering and Management is an integrated programme including mobility organized by five European partner institutions, coordinated by Norwegian University of Science and Technology (NTNU).

The joint study programme of 120 ECTS credits (two years full-time) has been obtained at two or three of the five CoMEM partner institutions:

- Norges Teknisk- Naturvitenskapelige Universitet (NTNU) Trondheim, Norway
- Technische Universiteit (TU) Delft, The Netherlands
- Universitat Politècnica de Catalunya (UPC). BarcelonaTech. Barcelona, Spain
- University of Southampton, Southampton, Great Britain
- City University London, London, Great Britain

During the first three semesters of the programme, students study at two or three different universities depending on their track of study. In the fourth and final semester an MSc project and thesis has to be completed. The two-year CoMEM programme leads to a multiple set of officially recognized MSc diploma certificates. These will be issued by the universities that have been attended by the student. The transcripts issued with the MSc Diploma Certificate of each university include grades/marks and credits for each subject.

Information regarding the CoMEM programme can be obtained from the programme coordinator:

Øivind A. Arntsen, Dr.ing.
Associate professor in Marine Civil Engineering
Department of Civil and Environmental Engineering
NTNU Norway
Mob.: +4792650455 Fax: + 4773597021
Email: oivind.arntsen@ntnu.no

CoMEM URL: https://www.ntnu.edu/studies/mscomem

CoMEM Thesis

This thesis was completed by:
John C L Mayson II

Under supervision of:
Dr. Vicente Gracia
Associate Professor
Laboratori d'Enginyeria Marítima (LIM/UPC)
Centre Internacional d'Investigació dels Recursos Costaners (CIIRC)

As a requirement to attend the degree of
Erasmus+: Erasmus Mundus Master in Coastal and Marine Engineering and Management (CoMEM)

Taught at the following educational institutions:

Norges Teknisk- Naturvitenskapelige Universitet (NTNU)
Trondheim, Norway

Universitat Politècnica de Catalunya, (UPC). BarcelonaTech.
Barcelona, Spain

University of Southampton,
Southampton, Great Britain

At which the student has studied from August 2016 to July 2018.

Abstract

A sea level rise of 1 meter exposes a land area of 95 square kilometers in Liberia to inundation (Wiles, 2005). Coastal towns in cities such as Monrovia and Liberia have been wiped away due to coastal erosion. The local government in collaboration with the United Nations Development Programme have been carrying out remedial works such as the construction of revetments and breakwaters. However, the factors influencing the decision on such adaptation strategies and unknown. This is due to a lack of relevant information regarding the coastal zone. From the hydrodynamics, to the sediment transport processes, and the subsequent morphology, very little is known about the natural and human induced processes occurring along the coast. This study attempts to use acceptable analytical methods practiced in Coastal Engineering and obtain rough estimates of wave and beach related parameters. Wave data from ERA-Interim (Hennermann, 2017) and Satellite-Derived Shoreline change rates data from Deltares (Netherlands) (Luijendijk et al., 2018) are used to calculate the bulk longshore sediment transport capacity of waves, and predict the shoreline retreat due to storm surge and Sea Level Rise (SLR) on medium, short, and long-term time and spatial scales respectively. The hope is that this document serves as a tool in understanding the coastal system from a very broad perspective. It is however noted that the results require validation before being used for any coastal management purpose.

Acknowledgement

I dedicate this dissertation to my beloved mother Miss. Georgian M. Patten, who brought me into this world and gave me all I needed to reach where I am today. My sincere thanks and appreciation go to my fiancée Wynitta who has supported me morally, physically, and spiritually throughout this entire academic journey. Finally, I want to say a big thank you to my thesis supervisor Dr. Vicente Gracia for his never-ending support and willingness to guide me. We did it Vicenç!!!

Table of Contents

CHAPTER 1: INTRODUCTION 1
1.1 Problem Statement 1
1.2 Motivation 2
1.3 Objectives 3
1.4 Area of Interest 4
1.5 Structure of the work 5
1.5.1 Literature review 5
1.5.2 The Liberian Coast 5
1.5.2 Evaluation of Data Sources 5
1.5.3 Methodology 5
1.5.4 Results and Discussion 6
1.5.5 Limitations 6
1.5.6 Conclusion and Recommendation 6
1.5.7 Appendices 6
CHAPTER 2: LITERATURE REVIEW 7
CHAPTER 3: THE LIBERIAN COAST 12
3.1 Geographical Features and Vegetation 12
3.2 Geology 13
3.3 Climate 14
3.4 Rivers 15
3.5 Bathymetry 16
3.6 Tides 19
3.7 Littoral Cells 19
3.8 Types of Coast 19
3.8.1 Tectonic Classification 19
3.8.2 Nature of Sediments 20
3.8.3 Inundation 20
3.8.4 Formation processes 21
3.8.5 Process-based 21
3.8.6 Morphology 21
3.9 Sediment characteristics of the beaches 21
CHAPTER 4: DATA SOURCES 23
4.1 ERA-Interim 23
4.1.1 Mean Sea Level Pressure and Wind Data 24

4.1.2 Ocean-wave data 24
4.2 Satellite Derived Shoreline Change Rate Data 26
CHAPTER 5: METHODOLOGY 27
5.1 Assessing the longshore sediment transport capacity of waves on medium term scale 27
5.1.1 ERA-Interim Wave Data Structure 28
5.1.2 A quality check for the effects of shoaling 29
5.1.3 Waves 29
5.1.4 Sorting 30
5.1.5 Frequency of Occurrence 32
5.1.6 Morphological Wave height and associated mean wave periods 33
5.1.7 Shoreline Orientations and waves angle of approach 34
5.1.8 Linear Wave Propagation 36
5.1.8.1 Propagation 37
5.1.9 Bulk Sediment Transport formulations 39
5.1.10 Satellite Derived Shoreline 44
5.2 Assessing the retreat of the shoreline under episodic (storm) conditions 44
5.2.1 Convolution Method – Kriebel et al (Kriebel et al., 1993) 44
5.2.2 Extreme Value Analysis 46
5.2.3 P.O.T vs Annual Maxima 50
5.2.4 Storm Surge 51
5.2.5 Total value for storm surge 54
5.2.6 Seasonal Variations 54
5.3 Assessing the shoreline retreat due to SLR on long-term time scales 55
5.3.1 The Bruun Rule 55
CHAPTER 6: RESULTS AND DISCUSSION 60
6.1 CERC vs Kamphius 60
6.2 Shoreline Orientation influence on sediment transport 62
6.3 Wave conditions and sediment transport 62
6.4 Kamphius' vs SDS data bulk transport predictions 62
6.5 Beach response to storm conditions for different return periods 64
6.6 Shoreline retreat rates for different RCP Scenarios 64
CHAPTER 7: LIMITATIONS OF THE STUDY 67
7.1 ERA-Interim wave data 67
7.2 Assumptions used in LWT Propagation 67
7.3 Uncertainty in SDS change rate data 67
7.4 Assumptions made for storm surge calculations 67

7.5 The Bruun Rule 67
7.6 Hallermeier's closure depth equation 68
7.7 Kriebel and Dean's convolution theory 68
CHAPTER 8: CONCLUSION AND RECOMMENDATIONS 69
CHAPTER 9: REFERENCES 70

TABLE OF FIGURES

Figure 1: An aerial view of the West Point community, one of the most vulnerable areas to coastal erosion *(Alamy Ltd, n.d.)* 1
Figure 2: Time and spatial scales of Stive et al *(Stive et al., 2002)*, modified by Woodroffe *(Woodroffe, 2007)* 4
Figure 3: Coast of Liberia 4
Figure 4: Sediment accumulation around the Mount Coffee Dam built in 1966 7
Figure 5: A 2005 image of the Port of Buchanan showing the accumulation of sediments west of the harbour 8
Figure 6: Global distribution of coastal barriers backed by tidal flats and/or lagoons (Amended after Pilkey 2003) in relation to tidal regime (Modified after Flemming 2005) 9
Figure 7: Map showing sediment size variation along the coast of Monrovia (OAU-ELWA) (Titus, 1990) 10
Figure 8: Graphical illustration of dominant grain size fractions along the Monrovia coastline (Titus, 1990) 10
Figure 9: Political map of Liberia (Maps of World, 2015) 12
Figure 10: Ecoregion map of Liberia (USAID; U.S. Geological Survey, n.d.) 13
Figure 11:Geological map of Liberia (British Geological Survey; Liberian Geological Survey, n.d.) 14
Figure 12: Annual rainfall (2014) observed at the St. Paul River hydrometric station (Liberian Hydrological Services, 2016) 15
Figure 13: Rivers of Liberia (Maps of World, 2013) 15
Figure 14: Bathymetry of continental margin off Liberia, modified from Robb, Schlee, and Behrendt (1973). Solid sounding track lines (numbered) are those of survey vessel R.V Unitedgeo I (1971); dashed track lines are those of survey vessel USNS Kane (1969) (Robb, James M.; Schlee, John; Behrendt, 1973). Red, blue, and green squares show the 3 sectors: northwest, central, and southeast. 17
Figure 15: Modified figure of Robb, Schlee, and Behrendt (1973). Left of the figure is the bathymetric profiles for the 3 sectors of the coast as mentioned in the bathymetry section. Horizontal scale approximate, vertical exaggeration about 10 times. Right of the figure shows the profiles of shelf edge, showing features belonging to a persistent zone of irregular topography (arrows). Horizontal scale approximate, vertical exaggeration about 10.5 times. Locations of profiles shown in figure 14.(Robb, James M.; Schlee, John; Behrendt, 1973) 18
Figure 16: A tectonic-based coastal classification after Inman and Nordstrom (1971) (Bosboom, Judith; Stive, 2015). The black square represents the location of Liberia 20
Figure 17: Global distribution of salt marshes and mangrove swamps. Black square circumscribes the Liberian Coast (Bosboom, Judith; Stive, 2015) 20
Figure 18: Hayes' coastal classification based on hydrodynamic energy (Davis & Hayes, 1984) 21
Figure 19: The canonical definition of sediment grain sizes as defined by geologist Chester K. Wentworth in a 1922 article in The Journal of Geology: "A Scale of Grade and Class Terms for Clastic Sediments" (The Bruce Murray Space Image Library, n.d.) 22
Figure 20: Location of data points in Google Earth. Each grid has a spacing of 0.25 degrees 28
Figure 21: Wave roses for 5 data points placed in order (1, 2, 3, 4, 5) from left to right 30
Figure 22: 32-point directional compass (Brosen_windrose.svg, n.d.) 32
Figure 23: Shoreline orientations from northwest to southeast along with the wave condition influencing the coastal processes for each orientation 34
Figure 24: An illustration of the angles discussed in the previous paragraph 35
Figure 25: Effects of breaker index of breaking wave heights 38

Figure 26: Wave characteristics at the breaker line using the different breaker index values 39
Figure 27: Fall velocities of sediment for fresh water with a temperature of 18 degrees Celsius (Sistermans, 2002) 42
Figure 28: Range of monthly Monrovia water temperature data (World Sea Temperature, 2018). ... 42
Figure 29: Effect of a change in water temperature from 40˚ F (≈ 4˚ C) to 80˚ F (≈ 27˚ C) on the fall velocity of quartz spheres of several sizes (Scott & Colby C. H., 1965) 43
Figure 30: Explanation of Colby and Scott (1965) graph shown in Figure 29 43
Figure 31: Assumed areas of influence of waves from the 5 offshore wave data points 47
Figure 32: CDF for wave heights above 1.55m threshold. Note that the values on the x-axis start from the threshold. 47
Figure 33: Weibull fit using values above 1.55m threshold for wave data point 1 48
Figure 34: Threshold selection criterion for method 2 49
Figure 35: Kamphius definition sketch for a storm surge for an open shore (Kamphuis, 2000) 51
Figure 36: Location of the point (green pin) on the shelf break used to calculate the wind contribution to the storm surge 52
Figure 37: Map showing the 2 shoreline orientations assumed for obtaining the worst possible wind direction 52
Figure 38: Wind rose for data point 1 53
Figure 39: Cross-section of the beach profile from the shoreline to the shelf break (right to left) 53
Figure 40: Spatial boundaries of the coastal zone showing the shoreface. The seaward boundary point of the shoreface is the depth of closure (Bosboom, Judith; Stive, 2015) 55
Figure 41: Ensemble mean regional relative sea level change (meters) for the RCP scenarios (a) 2.6, (b) 4.5, (c) 6.0, and (d) 8.5 between 1986-2005 and 2081-2100 (Church, J A; Clark, P U; A. Cazenave; Gregory, J M; Jevrejeva, S; Levermann, A; Merrifield, M A; Milne, G A; Nerem, R S; Nunn, P D; Payne, A J; Pfeffer, W T; Stammer, D; Unnikrishnan, 2013) 58
Figure 42: Net sediment transport prediction using CERC and Kamphius' equations. 60
Figure 43: Transport rates across shoreline orientations 61
Figure 44: Influence of shoreline orientation on sediment transport 62
Figure 45: Net sediment transport directions using the Kamphius and SDS methods 63
Figure 46: Net longshore sediment transport predictions using SDS data. Values below zero indicate a southeast transport direction. 63
Figure 47: Wave rose for wave data point 4. 64
Figure 48: Beach response in return period number of years 64
Figure 49: Shoreline retreat due to SLR for different RCP scenarios 65
Figure 50: Coastal conditions for shoreline orientation 66

Symbols, abbreviations, and their meanings

deg/^{o} = degrees

lat = latitude

lon = longitude

m = meters

cm = centimeters

s/sec = seconds

km = kilometers

UTC = Coordinated Universal Time

hPa = hectopascal (1 hPa = 100 Pa)

PVU = Potential Vorticity

NWP = Numerical Weather Prediction

Pi = Pi radians

NC = Mastercam Numerical Control File

g = gravitational acceleration

L_o = deep-water wavelength

T = wave period

Hs = Significant wave height of sea and swell

(-) = non dimensional

b = a subscript used to indicate wave breaking conditions

MSL = Mean Sea Level

SLR = Relative Sea Level Rise

RCP = Representative Concentration Pathways

CHAPTER 1: INTRODUCTION

In the face of rising sea levels, cities along the coast of Liberia, specifically in Grand Cape Mount, Montserrado, and Grand Bassa counties are being gradually lost to the Atlantic Ocean due to the coastal erosion phenomenon. The rise in sea levels due to climate change, combined with increasing storms and sea-surges have significant negative impacts on the lives and livelihoods of people in coastal areas (United Nations Development Programme, 2018). The erosion rate is further increased by illegal sand mining activities carried out along the coast, despite the efforts of the Liberian government to put a stop to through a ban in 2012 (Wilson, 2012). Because of the shoreline retreat in addition to the increasing proximity of homes to the coast, coastal inhabitants are being wiped away. For a country ranked 4th on a list of the poorest countries in the world according to their Gross Domestic Product (GDP) based on purchasing power parity (PPP) per capita in March 2017 (Barbara Tasch, 2017), immense pressure is put on the local government to provide new homes for the affected coastal inhabitants thereby placing additional financial constraints on an already poverty-stricken economy. The limited capacity to monitor, forecast, archive, analyse and communicate meteorological and hydrological data and climate change information highlight the limited knowledge of current climate variability in Liberia, thus resulting into a lack of planning for future climate change impacts (United Nations Development Programme, 2016). Due to this knowledge and information gap, managing the coastal zone in an efficient manner to combat coastal erosion is a huge challenge.

Figure 1: An aerial view of the West Point community, one of the most vulnerable areas to coastal erosion *(Alamy Ltd, n.d.)*

1.1 Problem Statement

To help address the challenges posed by coastal erosion along the coast of Liberia, the United Nations Development Programme (UNDP) launched a project along with the government of Liberia labelled in 2010: “Enhancing Resilience of Vulnerable Coastal Areas to Climate Change Risks in Liberia”. The project aimed to reduce vulnerability and build resilience of local communities and socio-economic sectors to withstand the threats of climate change in Liberia’s coastal areas and is being implemented in the three counties hard hit by the effects of climate change as mentioned in the preceding paragraph (United Nations Development Programme, 2018). Some of the measures taken so far include the construction of the 600-meter breakwater-revetment System along the critically eroded

Atlantic Street Beach front in Buchanan, the capitol city of Grand Bassa county. UNDP Liberia, together with the Government of Liberia and the Global Environment Facility (GEF) have also taken steps to reduce vulnerability and increase resilience by building coastal infrastructure, and by procuring and installing meteorological and hydrological equipment to develop an early warning system (United Nations Development Programme, 2016). A statement from the report reads:

> *To increase Liberia's capacity to adapt to the impacts of climate change, it will be necessary to generate appropriate climate information to monitor and predict slow-onset climate hazards such as seal level rise and increased temperatures, as well as rapid-onset hazards such as coastal surges and river floods, including flash-floods. This information needs to be disseminated to end-users through an Early Warning System (EWS).*

This is decent and quite approach to start with, as it will improve predictions of the marine climate and meteorological conditions and events. However, some critical questions arise as to what happens between now, and the future data collection time. What do we know now about the current erosional processes ongoing? Is it safe to assume that it is more dependent on SLR than other coastal processes? What can be predicted regarding the shoreline evolution and the factors responsible over different time scales? What information can we withdraw from the limited data available about the variability of the shoreline over different scales? Are we informed enough to make decisions on what kind of adaptation strategy to employ? This paper tends answer some of these questions by using the existing available data (23 years of recording used in the study, from 1984 to 2006) to make rough predictions about the shoreline variability over different scales due to waves, storm surge, and SLR.

1.2 Motivation

According to the Intergovernmental Panel on Climate Change (IPCC) in their fifth assessment report, it was predicted with high confidence that the increase of global mean surface temperature by the end of the 21st century (2081–2100) relative to 1986–2005 is likely to be 0.3°C to 1.7°C under RCP2.6, 1.1°C to 2.6°C under RCP4.5, 1.4°C to 3.1°C under RCP6.0 and 2.6°C to 4.8°C under RCP8.5 (Pachauri, 2014). Another study carried out in 2005 by Wiles predicted the following effects due to SLR:

> *It is projected that about 95 km2 of land in the coastal zone of Liberia will be inundated as a result of one meter sea level rise. About 50% (48 km2) of the total land loss due to inundation will be the sheltered coast. It is evident that with a one-meter sea level rise, parts of the capital city of Monrovia and its environs, West Point New Kru Town, River Cess, Buchanan and Robertsport will be lost due to the fact that the greater parts of these areas are below one meter. The mangrove systems along the coast will be lost. About 250 million United States Dollars worth of land and infrastructures such as Hotel Africa will also be lost. Inundation will be followed by shoreline retreat which would vary along the coast from 10 meters in the higher cliffed zone between Mamba Point and Sinkor to about 20 meters in the lowlands on the Bushrod Island. All the damages that occur along the coast are located on Bushrod Island, Buchanan, Cestos City, and Robertsport. These are the areas on the coast where erosion is most severe* (Wiles, 2005).

This implies that, with the earth expected to get warmer over the years, sea levels are also expected to rise and hence, there may be damaging effects for the coast. According to a recent study done for the coastline of Africa on a global scale using the Dynamic Interactive Vulnerability Assessment model (DIVA), the damage cost incurred due to sea level rise, without any adaptive measure by 2100 is roughly estimated at about 0.02% of the Gross Domestic Product (GDP) of Liberia (Hinkel et al., 2012). With adaptation, that value is cut into half and represents approximately 0.01% of the national GDP (Hinkel et al., 2012). This drop in percentage highlights the need for enhancing the resilience of the

coast through adaptive measures. Adaptation in this paper refers to hard and soft engineering methods being used to combat coastal erosion due to SLR. These methods include the construction of breakwaters, revetments, beach nourishments, etc (Wiles, 2005). Notwithstanding, as much as these measures aid in making the most vulnerable sections of the coastline resilient, it is crucial to understand what time and spatial scales are being considered regarding the evolution and variability of the shoreline (Stive et al., 2002). In other words, for how long will such measures be efficient in serving their respective purposes considering the projections for the increase in sea level rise due to climate change by the IPCC (Pachauri, 2014). It then draws up the question of whether the current adaptive measures taken are the most appropriate solutions. On a national scale, it is very difficult to evaluate such decisions in the absence of sufficient and reliable data (Hinkel et al., 2012).

However, before attempting to analyse the effects of SLR, it should be noted that there are existing processes and conditions occurring along the coast which in some way have influenced the morphology over time. Changes in the hydrodynamic forcing such as wind waves (generated locally by wind), swell (waves generated by a distant storm), and tides (generated by the difference between the gravitational pull on ocean water masses that are located at different distances from the sun and the moon (Bosboom, Judith; Stive, 2015)), as they propagate towards the shore from their respective generating locations, induce changes in the sediment transport rates. This phenomenon affects the morphological development of the coast which in turn changes the hydrodynamics again. A term for this continuous and variable cycle is coastal morphodynamics. How visible the evolution of the coast is, depends on the time and spatial scales considered.

It is therefore important to have a broad understanding of the changes undergone by the coast. Knowing the position and shape of the shoreline now, relative to where it was at a point in time gives an indication of how much it has moved landward and seaward over time. The general and dominant patterns of sediments' movements need to be identified. This leads to further questioning: What information is available to describe the effects of the hydrodynamic forcing? What are the features present along the coast? What are the inputs and outputs into the coastal system? Are there rivers emptying into the sea along the coast? If yes, how large are they and how much sediments do they add to the system? What are the dominant forces driving the change in sediment transport rates? How has the coast responded to these hydrodynamic forcing? Are the changes seasonal? All these questions require answers before carrying out adaptive measures to mitigate the effects of sea level rise on coastal erosion, as SLR does not happen in isolation of the other processes mentioned earlier. Without the sea and swell waves, storm surges, and the fluctuation in tidal heights, an increase in the mean water level due to SLR by itself may not cause significant coastal erosion. Significant is this context refers to the same order of magnitude as the shoreline retreat occurring today. Henceforth, improving our knowledge about the existing coastal processes happening in the coastal zone is of prime importance and should be delved into prior to selecting adaptive strategies to combat coastal erosion due to SLR.

1.3 Objectives

The aim of this paper is as follow:

- To assess the longshore sediment transport capacity of waves on medium-term scales.
- To predict the shoreline retreat and beach erosion due to storms on short-term scales (episodic and seasonal), and
- To estimate the shoreline retreat due to SLR over long-term scales.
- To estimate other parameters relevant for description of the conditions along the coast.

The definition of the time and spatial scales as outlined by Stive et al (2002) can be seen in Figure 2. Due to the limitations and uncertainties of the data used in the study, the values obtained in this study are first estimates intended to give an overall idea of how much sediment is moving along the coast, how the coast might respond to an episodic event (storm surge), and how much retreat is expected due to relative SLR. Therefore, they require validation using a robust data collection and analysis for the study area, before being used for coastal management purposes.

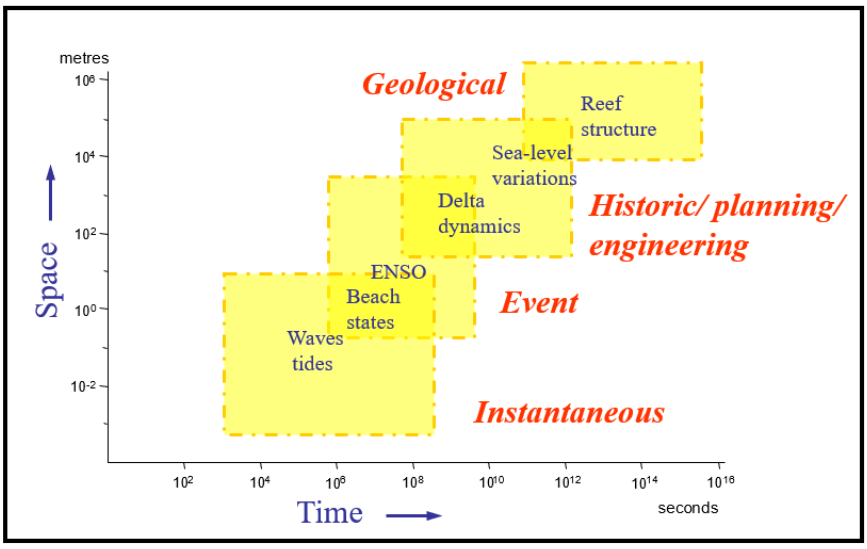

Figure 2: Time and spatial scales of Stive et al *(Stive et al., 2002)*, modified by Woodroffe *(Woodroffe, 2007)*

1.4 Area of Interest

The study covers the entire coast of Liberia which is approximately 559 kilometers long and spans from northwest to southeast. South of the coast is the Atlantic Ocean. A detailed description of the study area is given in chapter 3 of the paper.

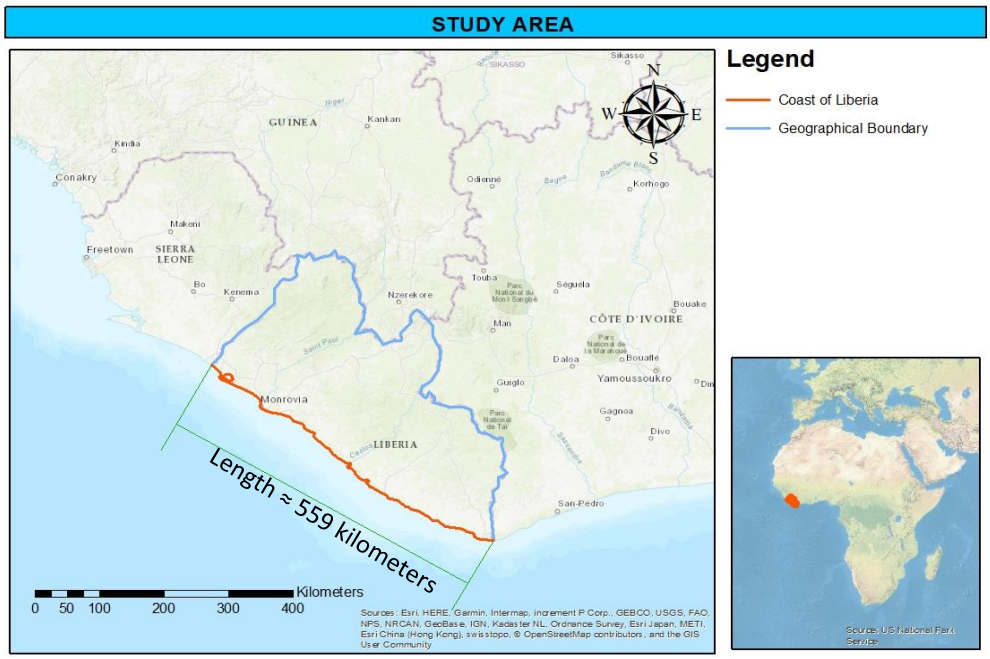

Figure 3: Coast of Liberia

1.5 Structure of the work

Chapter 1 introduces the problem the study is aiming to address, the motivation leading to the selection of the specific problem, the objectives of the study, and the structure of the paper. Below is an overview of the remaining chapters in this paper.

1.5.1 Literature review

Chapter 2 comprises of an overview of the existing literature available for the coast of Liberia. It summarizes the previous work done for the Liberian coast, identifies knowledge gaps, and highlights the need for further research.

1.5.2 The Liberian Coast

Chapter 3 describes the characteristics of the coast of Liberia (the study area). First, the coast is classified based on the type of sediments, plate tectonics, inundation, morphology, the existing coastal processes, and the kind of processes which shaped the coast. Next, the weather conditions and how they vary seasonally are presented. The geology of the coast is then described to give an overview of what sediments are found along the coast, their origin, and the weathering processes they might have undergone. The rivers which transport sediments to the coast are presented after, with an emphasis placed on the 6 major rivers. Also, the topographic length of the rivers, their physical shapes, the effects of intense rainfall on them, the extensions of their drainage basins or catchment areas, and the interceptions disrupting their flow are described. An overview of the bathymetry along the coast follows. The tidal range along the coast is then introduced, along with the variation in its amplitude which provides spring or neap tides. This is followed by an attempt to divide the coast into littoral cells based on the coastal orientation and the physical features existing on the coast. These cells are assumed to be unconfined as sediments still enter and leave them. Finally, the types of sediments and their characteristics are briefly introduced.

1.5.2 Evaluation of Data Sources

Chapter 4 introduces the data used in the study and their respective sources. This includes the method of collection, pre-processing, underlying assumptions, and limitations of the datasets.

1.5.3 Methodology

Chapter 5 presents the methods used to assess the longshore sediment transport over medium term scales, the shoreline response to episodic events and seasonal variations, and the long-term shoreline retreat due to SLR. 5 wave data points along the entire stretch of the coast are selected. For simplicity, the sections of the coast they influence are separated so that the difference in shoreline variability due to waves can be analysed.

1.5.3.1 Mean wave climate (medium-term scale)

The coast is broken down into 15 different shoreline orientations to account for the difference in bulk longshore sediment transport rates due to different wave approach angles to the shoreline. A breakdown of the sorting of wave data for the analysis is presented, followed by the method of propagation from deep water to the breaker line. Comparisons between the CERC and Kamphius formulas are made to decide on which formula is used to predict the bulk longshore sediment transport. The values are then compared with the transport volume calculated using Satellite-derived shoreline (SDS) change rate values.

1.5.3.2 Extreme wave climate and seasonal variations (short-term scale)

2 extreme value analysis methods are compared: the annual maxima method and the Peak over Threshold method. The method which provides the highest wave height at the breaker line is used for the analysis of the shoreline response to storm surge. To calculate the equilibrium beach response

and the eroded volume for 6 return periods (1, 5, 10, 25, 50, and 100 years), Kriebel and Dean's convolution method is used. The same procedure is applied separately for the dry and rainy seasonal wave data to see the temporal variation of the beach's response to storm surges.

1.5.3.3 Extreme wave climate (long-term scale)

In this section, the shoreline retreat due to SLR is calculated using Bruun's (1962) formula. The mean wave climate conditions are used to obtain wave-related parameters required for the calculations. Hallermeier's closure depth formulation is applied for use in Bruun's formula. Regional SLR projections from the IPCC's Fifth Assessment Report for the upper bound for RCP 4.5 and RCP 8.5 are used as relative SLR values in the calculations.

1.5.4 Results and Discussion

In chapter 6, the results from the analysis from the study are presented and organised in the same order as Chapter 3. The description of 1 of the 15 coastal stretches (complete result for all presented in appendices) is given in a tabular format, including the hydrodynamic, morphological, and sediment transport capacity of waves. The response of these sections to storm waves over short-term scales and to SLR over long-term scales are obtained based on the wave data point which influences them. This is further explained in Chapter 3. Once the results are presented, a discussion regarding the authenticity of the values obtained for few sections ensues. The different variables and their influences on the outcomes are assessed.

1.5.5 Limitations

Chapter 7 highlights uncertainty levels or confidence intervals of the values obtained in the analysis based on the limitations, assumptions, and simplifications of formulas or methods used in the analysis. The criticism of some of the formulas used and the justification for using them in the study are also discussed in this chapter.

1.5.6 Conclusion and Recommendation

Chapter 8 provides an insight of how the values obtained from the study can be calibrated or validated. Gaps of information required to be bridged and the need for further research to build on the study are also highlighted here.

1.5.7 Appendices

Chapter 9 displays the results for every section of the coast considered in the study.

1.5.8 References

Chapter 10 displays the sources of information used in the study.

CHAPTER 2: LITERATURE REVIEW

Over a 40 years span, not a lot of research related to coastal erosion has been done for the coast of Liberia. The earliest available work in existing literature dates to May 1990 in a report prepared by the United Nations Environment Programme, the World Meteorological Organisation (WMO), the United States Army Corps of Engineers, and the National Oceanic and Atmospheric Administration (NOAA) titled: "Changing Climate and the Coast" (Titus, 1990). This report contains information about works done along the coast related to coastal erosion issues. The first of these works was carried out in 1978 by the Japanese Agency for International Development who conducted a 3-week study to identify the causes of erosion along the Liberian coastline in 5 major coastal cities, namely: Robertsport, Greenville, Harper, Buchanan, and Monrovia (Titus, 1990). The 2 principal causes of erosion identified were the drifting of river outlets, and changes in the balance of littoral transport caused by blockage of natural sand drifting as a result of human activities in the coastal zone (Titus, 1990). Human activities in this context refers to the construction of hard engineering structures such as revetments or breakwaters, beach mining, and possible reduction of sand supply from the St. Paul river due to the construction of a Hydro-electric dam as shown in Figure 4 (Titus, 1990).

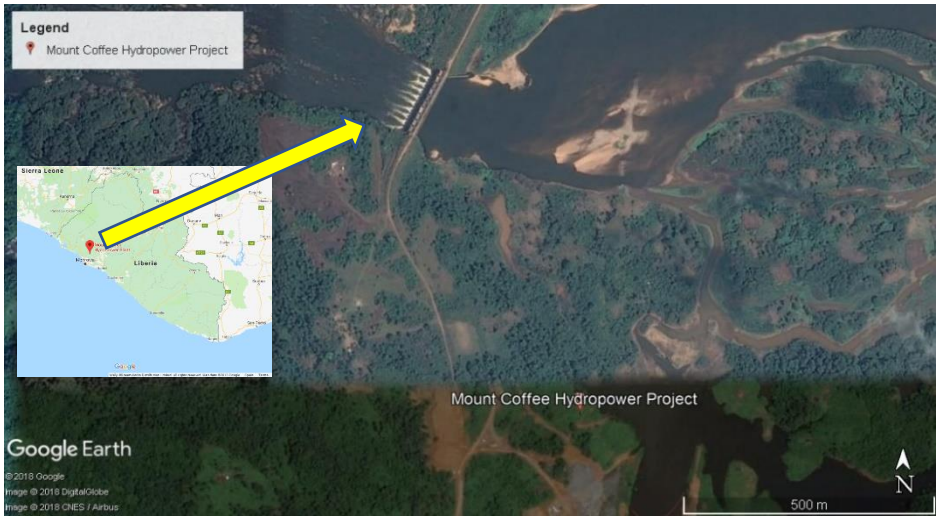

Figure 4: Sediment accumulation around the Mount Coffee Dam built in 1966

Along the coast of Liberia, there are few hard engineering interventions. 2 major harbours are present in the cities of Monrovia and Buchanan. For the latter, an increase in the rate of coastal erosion on the downdrift side of the coast was observed after the construction of the harbour's breakwaters (1 on each side of the harbour) (Titus, 1990). According to a report produced by the LAMCO J.V. Operating Company, sand was deposited east of the breakwaters to make up for the sediments blocked by the western breakwater at the harbour entrance (Titus, 1990). This however contradicts the assertion that the net littoral drift direction along the coast is northwest (west of harbour), except wherein the author's directional reference is from the land, facing seawards. Based on Satellite-derived shoreline (SDS) change rates for the Liberian coast obtained from a study of the state of the world's beaches (Luijendijk et al., 2018), the part of the coast immediately west of the breakwater is starved of sediments due to the accretional process east of the harbour (see Figure 5). In an effort by the government to reduce erosion downdrift of the coast at the time, 2 groins were constructed and it was reported to be effective (Titus, 1990). The positions and lengths of the groins were not given in the report. This is important as without said information, it is not clear what purpose the groins were

serving as the harbour was already blocking sediments coming from the southeast. It is therefore interesting to know the littoral drift direction of the sediments blocked by the groins. Revetments made of boulders were reported to have been constructed to reinforce the shoreline against erosion, and scheme was devised to monitor the extent of the beach erosion over time (Titus, 1990).

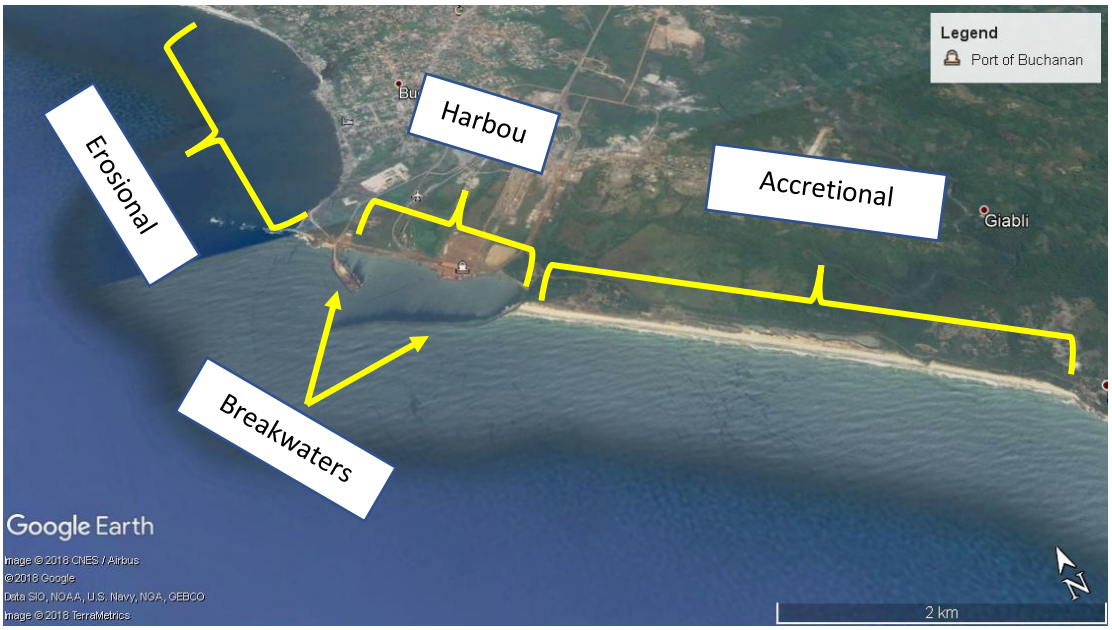

Figure 5: A 2005 image of the Port of Buchanan showing the accumulation of sediments west of the harbour

Between 1980 and 1982, Dr. Ntungwa Maasha conducted a study along the Monrovia coastline and concluded that 80% of the coastline consists of sandy beaches eroding at a rate of 0.5 to 4 meters per year (Titus, 1990). He also identified an accretional area, the West Point community, located south of the Freeport of Monrovia (Titus, 1990). This might be due to the presence of the Monrovia harbour. Interestingly, today, this depositional area is now eroding and has a small beach width as shown in Figure 1. He also reported that the littoral drift goes from southeast to northwest and that the long-shore current velocity varies between 16 and 31 cm/sec (Titus, 1990).

In 1983, a 3-man team of Hans Hanson, Lennart Jonsson, and Bo Broms from Sweden conducted a 1 week study along selected areas of the Liberian coast (Titus, 1990). They asserted that the harbours and other human interferences aggravated the erosion problem. An estimated volume of 50,000 and 60,000 cubic meters of sand were reported as accretional and erosional volumes of sediments on the southeast and northwest sides of the Free Port of Monrovia respectively (Titus, 1990). They also reported that the St. Paul River transports about 1.5 million cubic meters of sand to the coast. Considering that the Mount Coffee Dam was already built at the time of this report, coupled with report made by the Japanese Agency highlighting a 'possible reduction' of sediment supply from the St. Paul River due to the presence of the dam as a principal cause of coastal erosion (Titus, 1990), it is very important to estimate the changes in sediment volume before and after the dam was constructed. The most frequent waves reaching the coast were observed from the south to southwest, with heights ranging from 1.3 m to 0.6 m, changing seasonally (Titus, 1990). A morphological wave height of 1.1 m was said to be representative for littoral transport (Titus, 1990). However, the wave height values seem to be underestimated based on existing data and other research done for the coast of Liberia, or West Africa in general. This could be due to a bias towards the local wind-generated waves and a lack of consideration for the swell waves approaching the coast. A semidiurnal tide with a tidal range of about 1 – 1.5m was observed (Titus, 1990), which falls below the value given in *Figure*

6. The tide induces long-shore currents with ebb and flood velocities of 15-45 m/sec and 5-15 m/s (Titus, 1990).

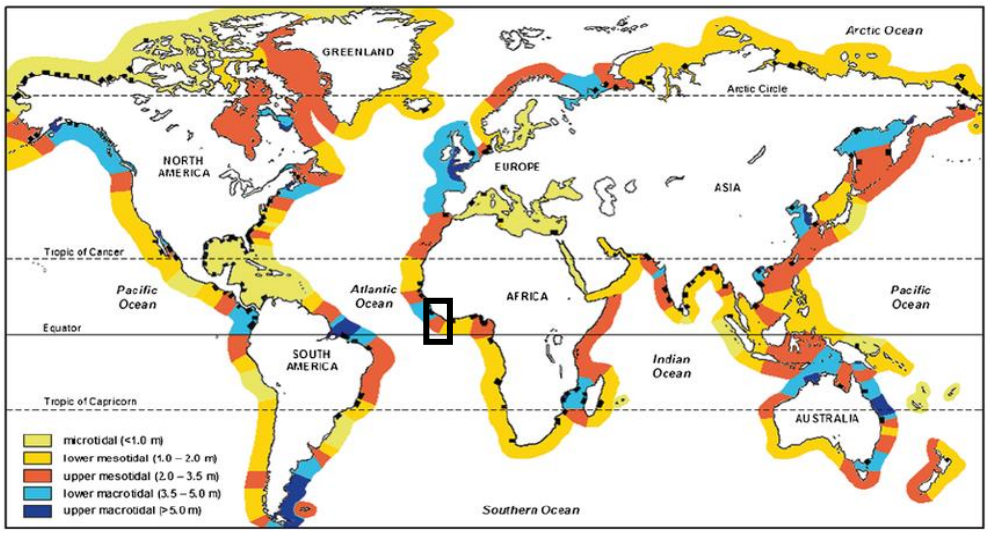

Figure 6: Global distribution of coastal barriers backed by tidal flats and/or lagoons (Amended after Pilkey 2003) in relation to tidal regime (Modified after Flemming 2005)

An extensive study was also done for the Monrovia coastline (coastal stretch from OAU Village to ELWA) by the Liberian Geological Survey; Department of Mineral Explorations and Environmental Research, Ministry of Lands, Mines and Energy; the University of Liberia, other government agencies and foreign institutions (Titus, 1990). The following conclusions were drawn:

- Waves approach the shoreline at oblique angles which increase in areas north of Cape Mesurado until the depth contours become parallel to the shoreline orientation.
- Average direction of wind-generated waves is South 38 degrees West, or 218 degrees referenced to the true north.
- The Coastline receives winds coming predominantly from the southwest at the beginning of the rainy season (May-June).
- A breaking wave height of 10.4 m with a mean period of 12.96 seconds.
- Waves break mainly by plunging, with spilling breaker types observed in a few places.
- Beaches are characterised by medium to coarse-grained sand, consisting of mostly quartz, with iron stains that give a brownish-white appearance.
- Littoral drift is towards the northwest.
- Morphological representative wave height is 1.3 m.
- Energy flux of 9.68 joules/sec and a longshore sediment transport rate of 7.26 x 104 m3/yr.
- Energy flux of 17.47 joules/sec and a longshore sediment transport rate of 1.31 x 105 m3/yr along the strip immediately north of Cape Mesurado.

Representative histograms of the beach sand with respect to locality and the dominant size fractions are shown in Figure 7. In Figure 8, a generalized variation line and the local deviations from it are shown (Titus, 1990). These deviations were observed in areas with rocky shorelines, where the grain size is apparently larger (Titus, 1990).

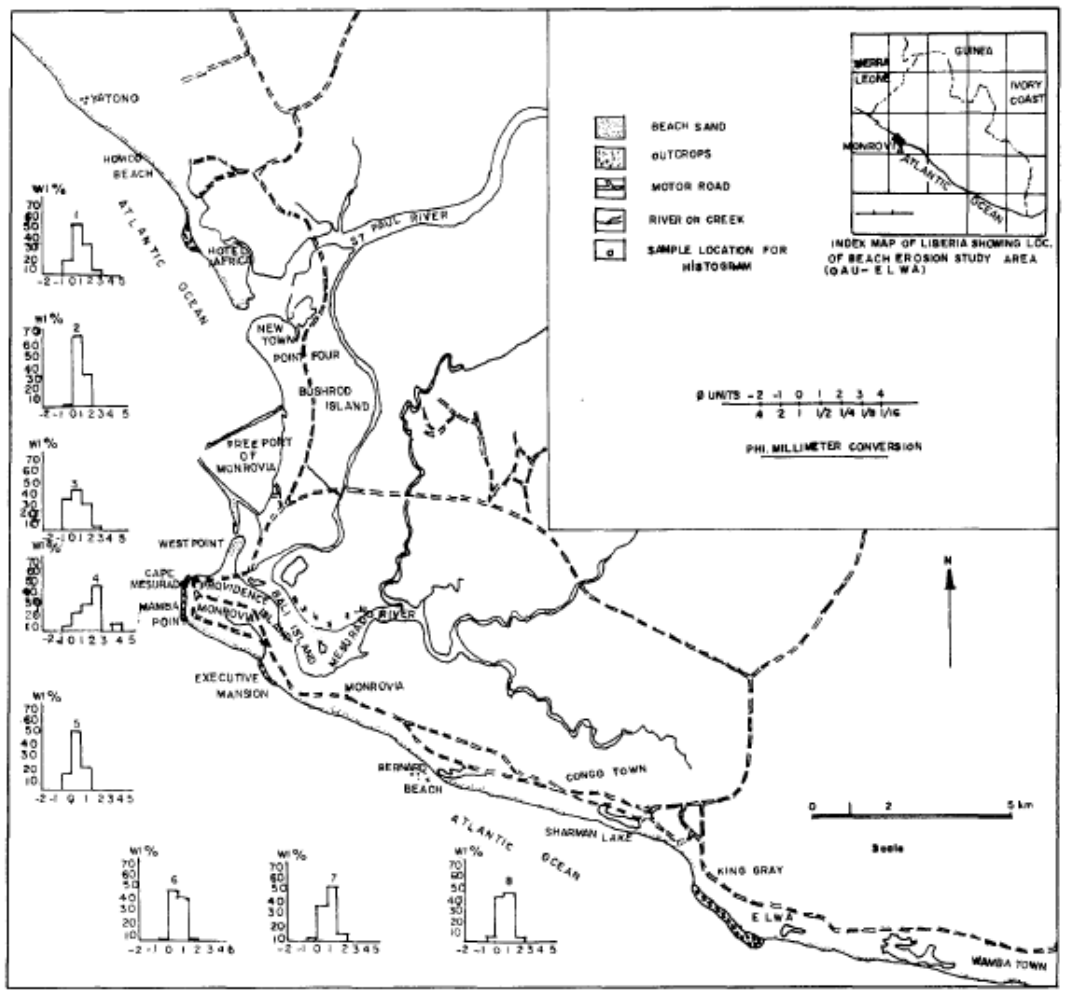

Figure 7: Map showing sediment size variation along the coast of Monrovia (OAU-ELWA) (Titus, 1990)

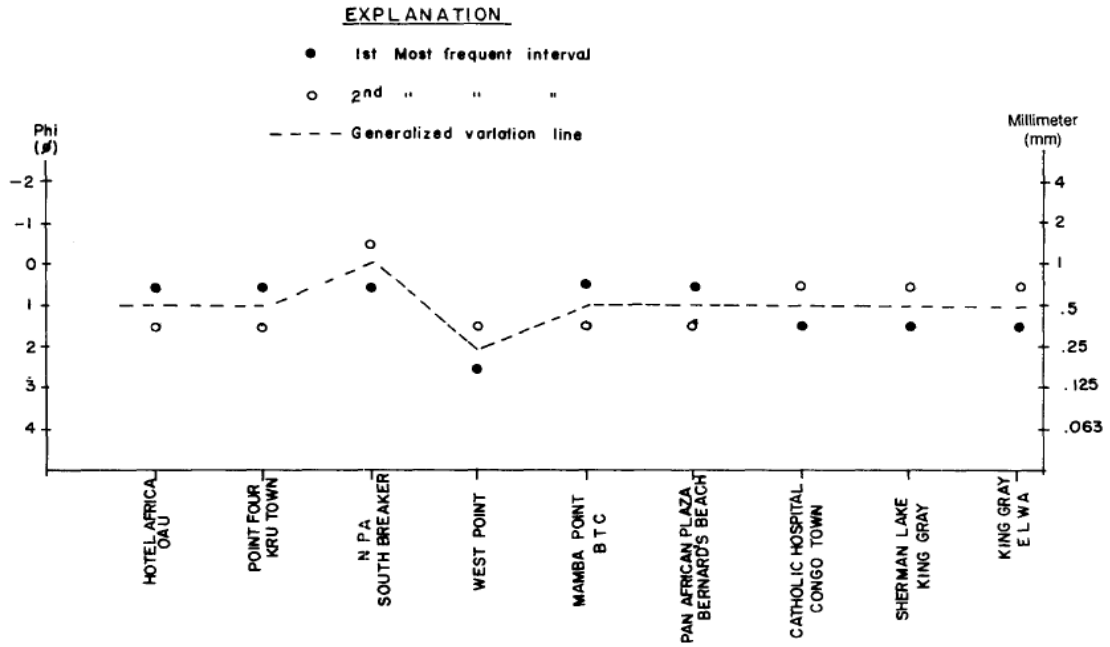

Figure 8: Graphical illustration of dominant grain size fractions along the Monrovia coastline (Titus, 1990)

A more generic study describing the conditions of the south-eastern section of the coastline was published in the Ocean and Coastal Management journal in 2006 (Sorensen, 2006). The paper, named "Coastal Conditions of West Africa" establishes the following about the West African Coast in general:

- The continental shelf is narrow.
- The coast is exposed to oceanic forces due to the absence of offshore islands.
- A semi-diurnal tide occurs with an average range of 1 meter and increases in the far east.
- Annual variation in mean sea level about 0.1-0.2m.
- The waves reaching the coast are of two distinctly different origins: the sea generated by the weak, local monsoon; and swell generated by storms in the southern part of the Atlantic Ocean.
- The locally generated waves rarely exceed 1.25 m in height; the maximum period is 3-4 s. They are generally weaker and are generated from the southwest.
- Storms occur around the 'roaring forties' throughout the year, but their violence peaks in the winter. The periods of these swells vary between 8 and 20 s, with an average of 12-13 s. Their average height in deep water is 1-1.5 m, although heights of 2-3 m and more can occur. They arrive from directions between south and south-west.

The lack of sufficient research and information available for the Liberian coast make it difficult to properly understand the evolution of coast over time. This section tried to summarise the existing information available for the Liberian coast. The studies complement each other in most aspects and can be used as references for current and future research.

CHAPTER 3: THE LIBERIAN COAST

Liberia is located along the west coast of Africa between latitudes 4˚20' and 8˚30' north of the equator and longitudes 7˚18' and 11˚20' west of the prime meridian and covers a total area of 111,370 sq. km. of which 15,050 sq. km is water and the remaining 96,320 sq. km is land (Wiles, 2005). It shares geographical borders of about 598 km with the Ivory Coast on the east, 370 km with Sierra Leone on the west, 540 km with Guinea up north. 560 km with the North Atlantic Ocean in the south (Wiles, 2005). Liberia has a population of about 3.5 million people based on a 2008 census done by the local government (Johnson-sirleaf, 2008). The country gained independence in 1847 from the American Colonisation society and its capital city is Monrovia. Liberia is divided into 15 political subdivisions called counties and is made up of 16 ethnic groups.

Figure 9: Political map of Liberia (Maps of World, 2015)

3.1 Geographical Features and Vegetation

Liberia is the 5th smallest country on the African Continent and the extreme south-eastern part of the country is closer to the equator than any other coastal part of West Africa (Wiles, 2005). The relief system consists of 4 relief belts parallel to the coast with increasing elevation towards the north, they are: the Coastal Belt – 15 meters above mean sea level (MSL), the Rolling Hills Belt – 100 meters above MSL, the Dissected Plateau – 300 meters MSL, and the Northern Highland – 1800 meters above MSL (Wiles, 2005). Located within the Tropical Rain Forest Vegetation Belt of West Africa, the forest zone covers all of Liberia except a narrow strip of the coast where mangrove vegetation alternates with coastal savanna (Wiles, 2005).

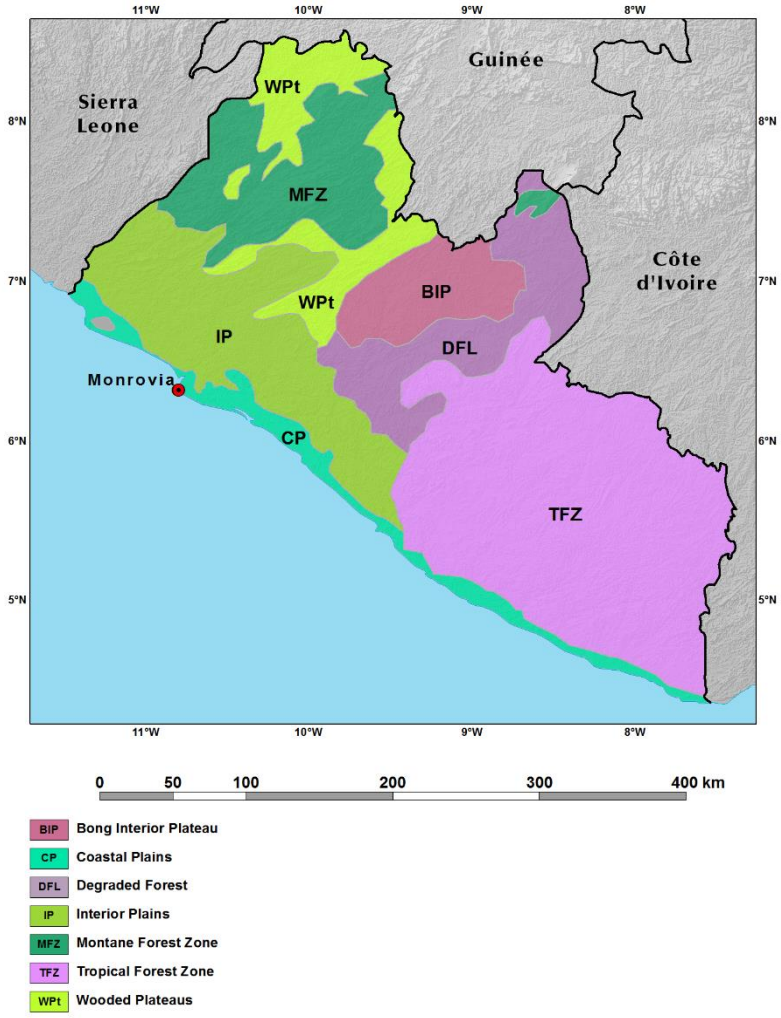

Figure 10: Ecoregion map of Liberia (USAID; U.S. Geological Survey, n.d.)

The coastal plains shown in *Figure 10* span about 560 kilometres long and extend up to 25 miles inland (Hadden, 2006). They are low and sandy, with miles of beaches interspersed with bar-enclosed lagoons, mangrove swamps, and a few rocky promontories (Hadden, 2006). The highest promontory is Cape Mount (305 meters above MSL in elevation) in the northwest, followed Cape Mesurado in Monrovia, and Cape Palmas in the southeast and its deepest extensions lie along the watercourses (Hadden, 2006). The shore is broken by river estuaries, tidal creeks, swamps, and a few rocky capes and promontories that appear as landmarks from the sea (Hadden, 2006). Except for the promontories and capes and an occasional small hill, the altitude of the coastal region usually rises no higher than 9 to 18 meters above MSL (Hadden, 2006).

3.2 Geology

Along the coast lie beds of sandstone, with occasional crystalline-rock outcrops (Hadden, 2006). The coastline is characterized by lagoons, mangrove swamps, and river-deposited sandbars. Rocks of Pan African age extend north-westerly along most parts of the coastline, from the Cestos shear zone (Hadden, 2006). They underlie an elongate, fault-bounded zone and comprise of metasedimentary and mafic meta-igneous rocks, containing granitic bodies and subordinate noritic intrusions (British Geological Survey; Liberian Geological Survey, n.d.).

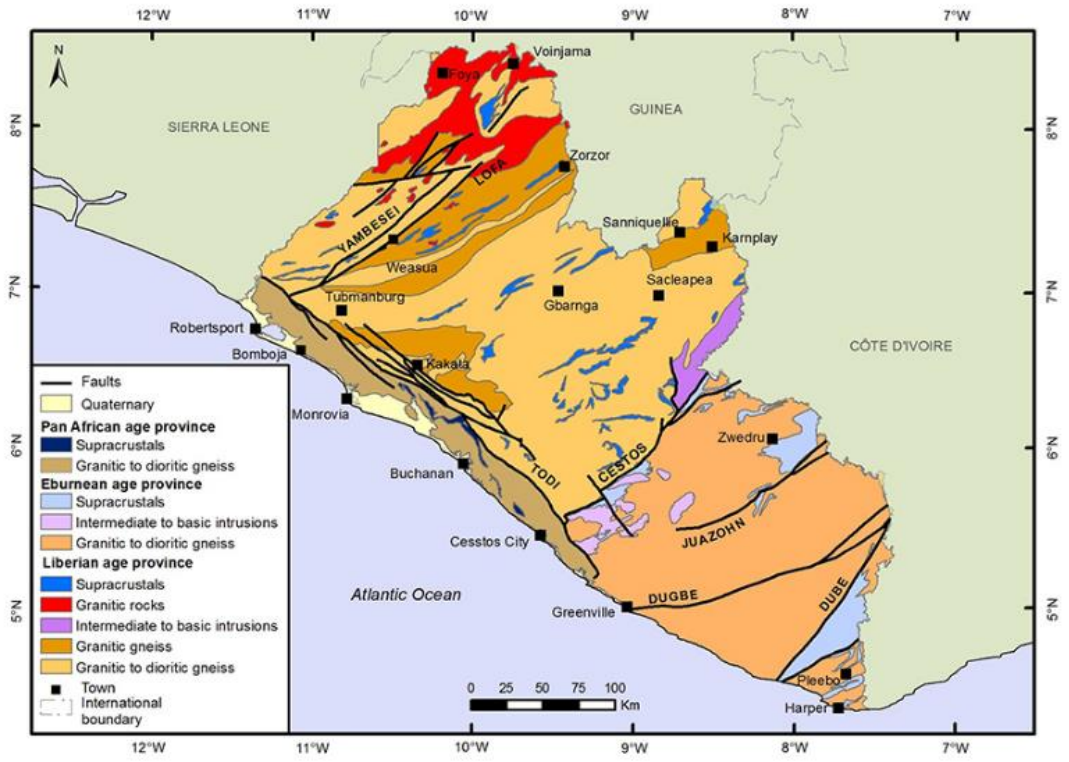

Figure 11:Geological map of Liberia (British Geological Survey; Liberian Geological Survey, n.d.)

3.3 Climate

The climate of Liberia is determined by the distribution of high and low pressure belts over the African Continent and the Atlantic Ocean (Wiles, 2005). There are 2 major seasons in Liberia: the rainy and dry seasons. The rainy season begins in April/May and ends in October, while the dry season is from November to March/April. These seasons are determined by the prevailing precipitation rather than a varying temperature as the temperature is more or less stable throughout the year (Wiles, 2005). The mean annual temperatures in Celsius range from the 20˚C (70˚F) to 27˚C (80˚F), with the mean monthly maxima decline from the low 30s (low 90s in ˚F) to the high 20s (high 80s in ˚F) during the rainy season, and the mean monthly minima range from 15-18˚C (low 60s in ˚F) in the highlands of the northwest to the low 20-24˚C (low 70s in ˚F) at Monrovia and along the coast (Hadden, 2006). An annual amount of rainfall measured around the St. Paul River area in 2014 is shown in *Figure 12*.

Due to Liberia's proximity to the equator, and the moderating influence of the nearby Atlantic Ocean, there is a fairly warm temperature throughout the year with a very high humidity (Wiles, 2005). The continental and maritime air masses of air (winds) alternate their movements back and forth, and from north to south, resulting in seasonal difference in rainfall intensity with the coastal region experiencing the heaviest rainfall (Hadden, 2006). This causes a very high humidity ranging from 90 percent to 100 percent during the rainy season; and 85 percent to 95 percent during the dry season (Wiles, 2005). The average annual rainfall near the coast amounts to 4770 mm, with annual and daily variations being evenly balanced due to Atlantic Ocean's moderating effect on temperature (Wiles, 2005). Sea water temperature along the coast of Liberia ranges from 27.4˚ C (81.4˚ F) to 30.5˚ C (86.6˚ F) (World Sea Temperature, 2018).

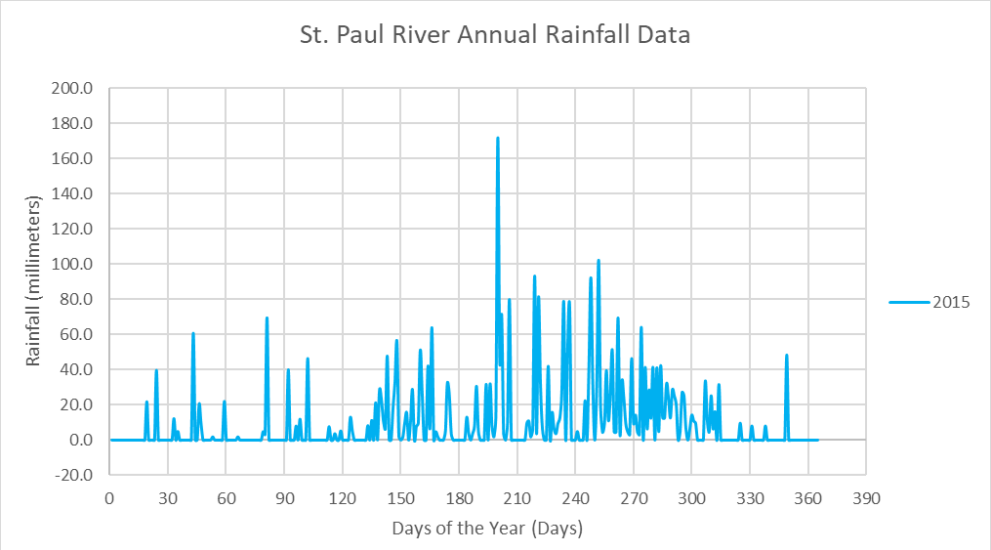

Figure 12: Annual rainfall (2014) observed at the St. Paul River hydrometric station (Liberian Hydrological Services, 2016)

3.4 Rivers

Most of the rivers in Liberia are perennial and are fed through rainfall (Liberian Hydrological Services, n.d.). This implies that the discharges into them vary between dry and rainy seasons. These rivers glow from northwest to southeast except the Cavalla River and its tributary, the Dougbe River which flow northeast to south (Wiles, 2005), and discharge into the Atlantic Ocean. . Many rivers flow along the coast for miles before they enter the Atlantic Ocean (Hadden, 2006).

Figure 13: Rivers of Liberia (Maps of World, 2013)

From *Figure 13*, it can be seen that majority of Liberian Rivers originate in Guinea (Wiles, 2005) and to a lesser extent Sierra Leone (Liberian Hydrological Services, n.d.). There are 6 international or major rivers in Liberia and many small ones. They are as follows:

- Cavalla River
- Cestos River
- Lofa River
- Mano River
- Morro River
- St. Paul River
- St. John River

The Mano and Morro rivers in the northwest and the Cavalla River in the southeast are boundary lines for part of the country. The influence of rivers along the coast varies seasonally. During dry seasons when the discharge into them reduces due to less rainfall, the tidal currents disrupt the flow of rivers and prevents them from removing sand bars and accumulations along the river banks (Hadden, 2006). On the contrary, rivers overflow their banks regularly during the rainy seasons and sometimes cause severe flooding along the coastal plains (Hadden, 2006). Due to the presence of sandbars which shift over time, and submerged rocks along the coast, the flow diverges at the river mouths thus disabling their ability to form natural harbours (Hadden, 2006). *Table 1* displays the lengths, the total basin areas, and the basin areas of the rivers within Liberia including their percentages. Note that only the largest rivers are shown in the table.

Name of the River	River length (km)	Total basin area (km^2)	Basin area in Liberia (km^2)	Basin area in Liberia (%)
Moa River	475	19,617	1,730	9
Mano River	391	7,520	5,539	74
Lofa River	410	10,612	9,189	87
St. Paul River	495	20,281	10,991	54
Farmington River	153	5,249	5,249	100
St. John River	464	16,930	14,363	85
Cestos River	476	12,709	10,389	82
Sehnkwehn River	230	5,659	5,659	100
Cavalla River	861	30,277	12,240	40

Table 1: Physical properties of the largest Liberian Rivers (Liberian Hydrological Services, n.d.)

3.5 Bathymetry

The U.S. Geological Survey team did an extensive study of the continental shelf along the coast of Liberia in 1971 and published their findings in their research journal (Robb, James M.; Schlee, John; Behrendt, 1973). This section summarises their work and gives a breakdown of the bathymetry along the coast. Citations are not repeated as all the information herein is obtained from their study.

The continental shelf along the coast of Liberia is relatively flat, narrow, and featureless, although irregularities are found in the very nearshore area. Small, irregular highs of 2 or 3 m relief occur on the middle and outer shelf in a few places but are more frequent southeast of longitude 8˚20' West, with these highs assumed to be a result of rock outcrops (Robb, James M.; Schlee, John; Behrendt, 1973). A constant zone of irregular topography occurs at depths of 80-120 m on the shelf edge, probably displaying relict strandlines and coralline or algal growths formed during lower periods of the MSL, and the depth at the shelf break ranges from 100 to 150 m.

The Continental shelf can be divided into 3 sectors (see *Figure 14* – modified to show the different sectors) characterised by different types of submarine topography: a northwest sector, Cape Mount to Buchanan; a central sector, Buchanan to east of Greenville; and a southeast sector, east of Greenville to Harper. The northwest and southeast sectors of the margin are narrow, and the slope is topographically complex. The central is wider and smoother. *Figure 15* shows the bathymetric profile and the profiles of the shelf edge for the 3 sectors.

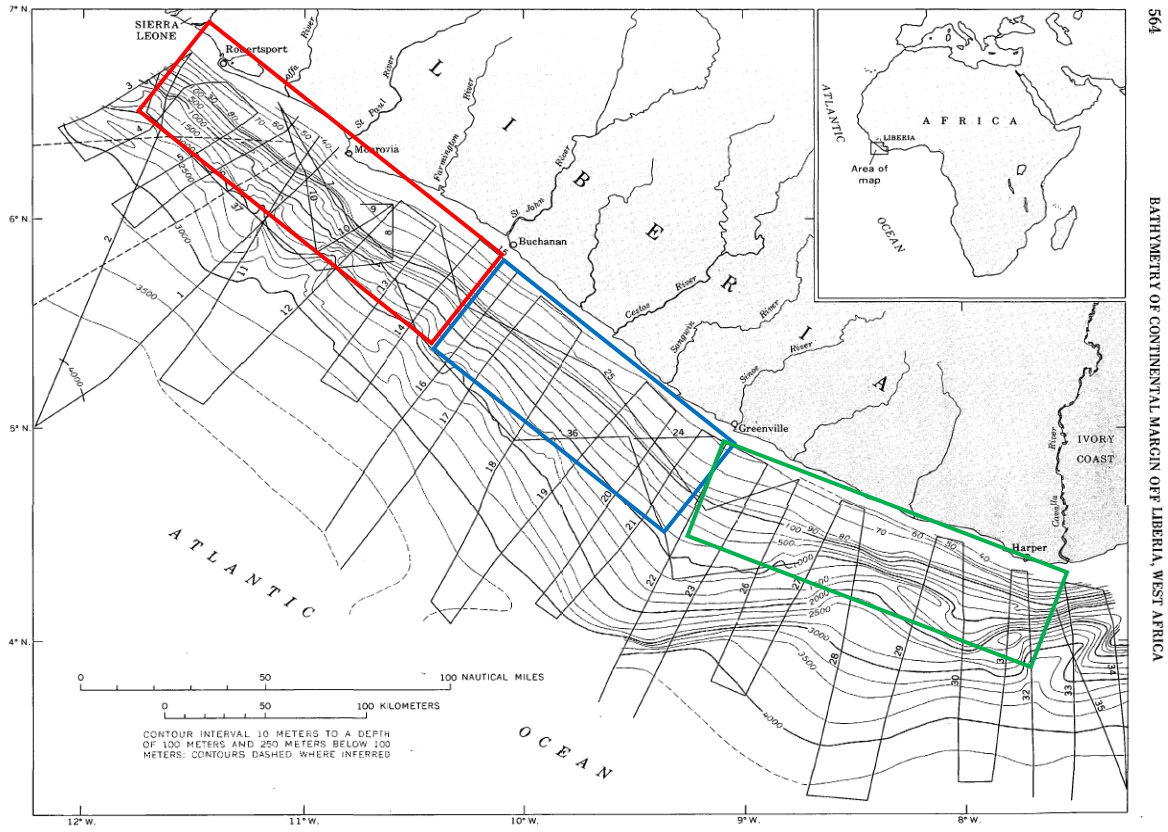

Figure 14: Bathymetry of continental margin off Liberia, modified from Robb, Schlee, and Behrendt (1973). Solid sounding track lines (numbered) are those of survey vessel R.V Unitedgeo I (1971); dashed track lines are those of survey vessel USNS Kane (1969) (Robb, James M.; Schlee, John; Behrendt, 1973). Red, blue, and green squares show the 3 sectors: northwest, central, and southeast.

The north-western is about 25 km wide, with a continental slope of 60 km wide, and an average slope of 3˚, a relatively constant shelf break depth of 134m, and is characterised by many features that resemble slump and landslide scars and rubble. At least 2 large submarine valleys cut the slope, off the St. Paul and Farmington Rivers. The upper slope between Cape Mount and Monrovia is extremely rough; it contains many small valleys averaging about 170 m in depth and spaced intervals of about 3 km.

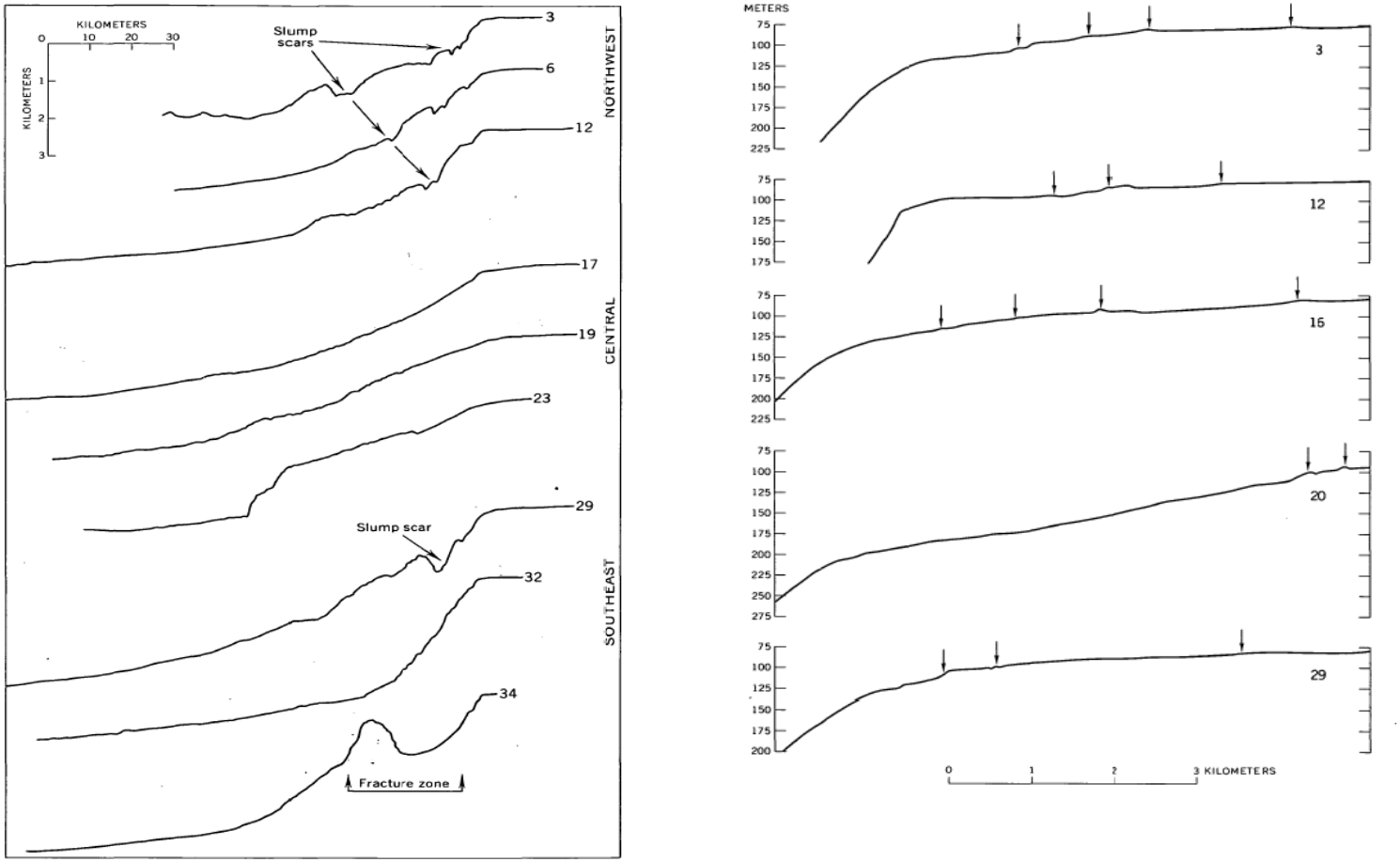

Figure 15: Modified figure of Robb, Schlee, and Behrendt (1973). Left of the figure is the bathymetric profiles for the 3 sectors of the coast as mentioned in the bathymetry section. Horizontal scale approximate, vertical exaggeration about 10 times. Right of the figure shows the profiles of shelf edge, showing features belonging to a persistent zone of irregular topography (arrows). Horizontal scale approximate, vertical exaggeration about 10.5 times. Locations of profiles shown in figure 14.(Robb, James M.; Schlee, John; Behrendt, 1973)

The central part of the slope is smoother, has smaller slump scars and no valleys, and a smoothly rounded transition from shelf to slope. The continental shelf width of this sector is about 45 km wide, with a slope length of about 95 km, and a slope of about 1.8˚.

The south-eastern part of the slope, near Cape Palmas, is crossed oblique to the shoreline by a structural valley that has been modified by large slumps or landslides. This valley may be the termination, at the continental margin, of an oceanic fracture zone. The continental shelf is about 20 km wide, a slope length of about 75 km wide, and an average slope (also has slopes of 10˚-15˚ of about 3˚. The shelf break in this sector occurs at depths of 100 – 150 m.

3.6 Tides

A semidiurnal tide has been observed along the Liberian coast with a tidal range of 1 – 1.5 m (Titus, 1990). The mean tidal range does not exceed 1.5 m and falls within the mesotidal category (Healy, Terry; Wang, Ying; Healy, 2002). Currently, there are no real-time data for tidal heights and ocean density currents along the coast.

3.7 Littoral Cells

The littoral drift along the coast of Liberia moves northwest and southeast with the net direction being northwest. Despite the presence of few human interventions along the coast (harbours, breakwaters etc.) and discontinuities (tidal inlets, river mouths, etc.), there are no observed self-contained coastal cells with respect to the common definition used in literature (Motyka & Brampton, 1993). Sediments move along the span of the entire coast. Further research needs to be made to establish the presence of coastal subcells. Capes and promontories may serve as drift divides, but there is no study available in existing literature to prove that sediment bypassing does not occur around these shoreline elongations. Furthermore, there have been recorded instances of dredging activities at the entrance of the Monrovia harbour (Titus, 1990), indicating that some sediments may have moved to the downdrift side of the harbour.

3.8 Types of Coast

There are many kinds of coastal classification schemes globally. However, there is no universally acceptable classification system (Finkl, 2004). It also depends on the timescale under consideration. In this study, the coast of Liberia is classified based on large-scale classifications such as the tectonic plate theory, the nature of sediments found on the coast, inundation, the coastal formation processes, and on regional and local scale variations in coastal landforms such as the existing coastal processes, and most importantly, the morphology.

3.8.1 Tectonic Classification

Using Inman and Nordstrom (1971) classification, the coast of Liberia falls within the trailing-edge category. This implies that the coast is located away from plate boundaries and are generally tectonically stable because the continent and adjoining ocean floor are of the same plate (Bosboom, Judith; Stive, 2015). The coast is further categorised into the Afro-trailing edge coasts (see *Figure 16*) category due to smaller sediment supply to the coastal zone compared to Amero-trailing edge coast (Bosboom, Judith; Stive, 2015). Because the coast is positioned in the middle of a crustal plate, there is no plate collision and henceforth, there is a lack of significant mountains from which rivers with large drainage basins delivering sediments to the coast originate from (Bosboom, Judith; Stive, 2015). Due to this effect, and the moderate-low wave energy conditions along the coast, smaller quantities of sediments are delivered to the coastal zone (Bosboom, Judith; Stive, 2015).

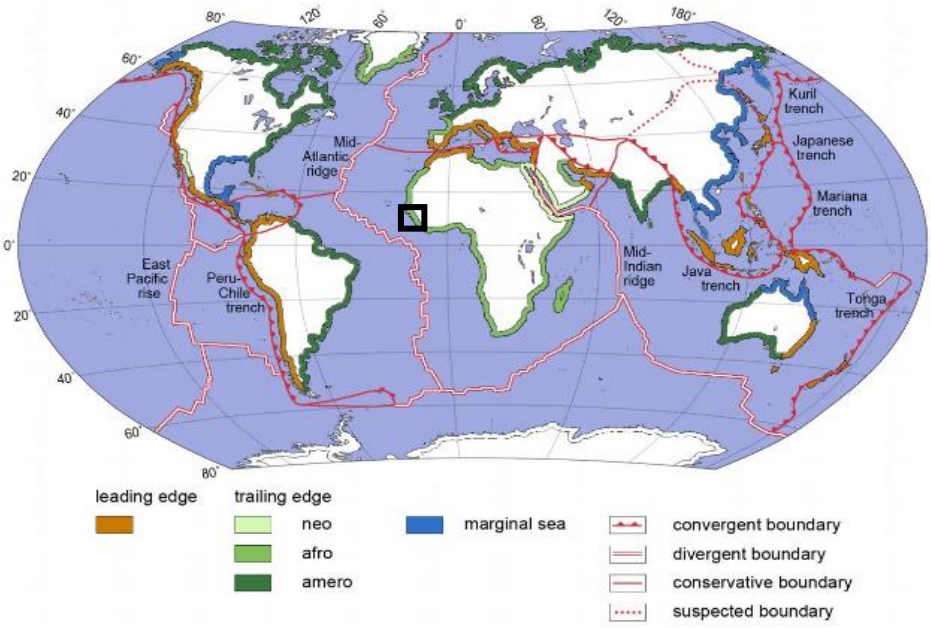

Figure 16: A tectonic-based coastal classification after Inman and Nordstrom (1971) (Bosboom, Judith; Stive, 2015). The black square represents the location of Liberia

3.8.2 Nature of Sediments

The coast of Liberia is a depositional coastal environment characterised mainly by very fine – medium – coarse grained sediments, based on Wentworth's classification (Titus, 1990). It is dominated by sandy beaches, although there are few stretches comprising of mangrove swamps as is shown in *Figure 17*. Continental sediments formed from weathered continental rock are the major type of sand found along the coast. The sand consists of mostly quartz and to a lesser extent, carbonate.

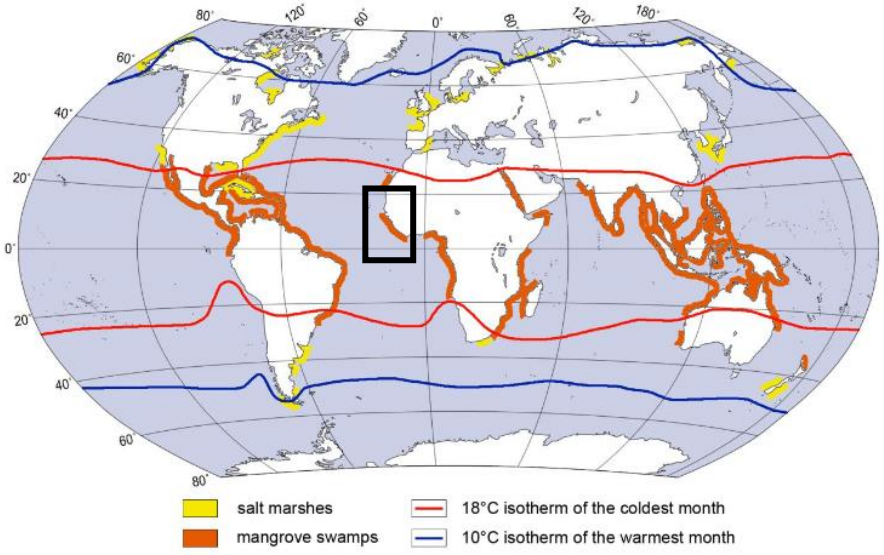

Figure 17: Global distribution of salt marshes and mangrove swamps. Black square circumscribes the Liberian Coast (Bosboom, Judith; Stive, 2015)

3.8.3 Inundation

Based on Valentin's (1952) coastal classification scheme, the coast of Liberia can be classified as a transgressive or advancing coast (Finkl, 2004). This is based on the features found on the coast, not the amount of recession the coast is undergoing currently due to SLR. The presence of raised beaches, coastal plains, lagoons, and estuaries on the coast validates its placement in this category.

3.8.4 Formation processes

Using Shepard's (1948) classification of coasts based on the processed from which the coast is shaped, the Liberian coast can be classified as a secondary coast. That is, the coast is shaped by marine processes such as erosion and deposition (Finkl, 2004).

3.8.5 Process-based

On a regional or local scale, coasts can be classified based on the dominant hydrodynamic forcing they are subjected to. Hayes (1975) based his classification largely on coasts with low to moderate energy, and with an intent to apply it to trailing edge, depositional coasts (Davis & Hayes, 1984). The coast of Liberia ticks these 2 boxes and henceforth can be classified using Hayes' classification. This classification uses the ratio of the tidal range to the mean annual nearshore wave height to determine which category the coast falls within. Figure 18 shows the relationship between the mean wave height and the tidal range. For the Liberian coast, this ratio falls between 0.5 to 1 and therefore the coast is classified as a wave-dominated coast.

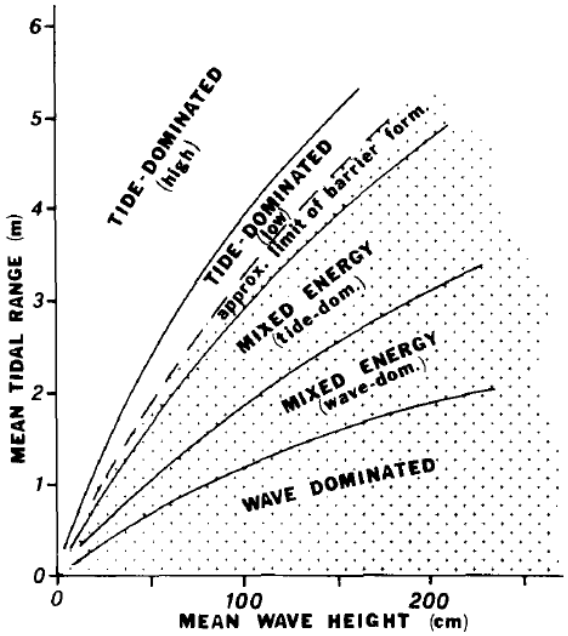

Figure 18: Hayes' coastal classification based on hydrodynamic energy (Davis & Hayes, 1984)

3.8.6 Morphology

Based on the morphology of most parts of the coast, it can be categorised as a barrier island coast due to the existence of lagoons, estuaries, and barrier beaches along the coast. However, some sections fall into the mangrove coast category. Also, the presence of promontories and capes indicate that parts of the coast can be termed as cliffed coasts.

3.9 Sediment characteristics of the beaches

Along the coast lie beds of sandstone, with occasional crystalline-rock outcrops (Hadden, 2006). Monrovia, the capital city of Liberia stands on such an outcropping ridge of diabase (a dark-coloured, fine-grained rock) which is a potential source of sediment supply to the coast via weathering processes (Hadden, 2006). Sandstone is a clastic sedimentary rock composed mainly of sand-sized between 0.0625 to 2 mm based on Wentworth's classification (see *Figure 19*) (Chester K. Wentworth, 2018), with mineral particles or rock fragments (Wikimedia Foundation Inc., 2018).

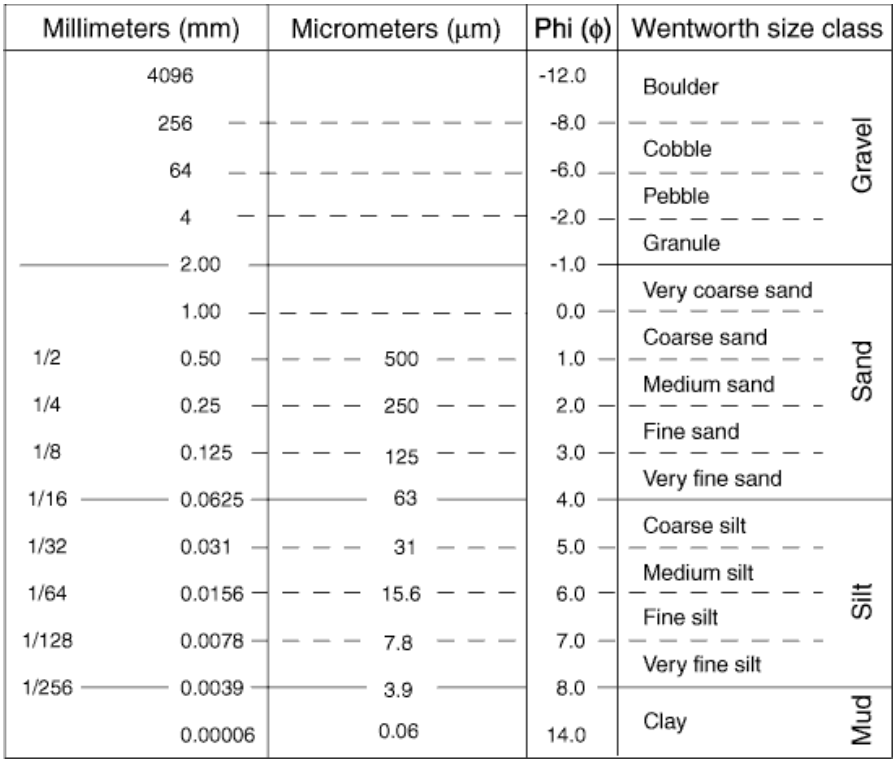

Figure 19: The canonical definition of sediment grain sizes as defined by geologist Chester K. Wentworth in a 1922 article in The Journal of Geology: "A Scale of Grade and Class Terms for Clastic Sediments" (The Bruce Murray Space Image Library, n.d.)

CHAPTER 4: DATA SOURCES

In this section, the data used for analysis in this paper is discussed. The sources from which the data were collected is briefly introduced. This is followed by an overview of how the data was collected and pre-processed, including but not limited to measures taken to reduce errors in the data. There are 4 kinds of data used in this paper: mean sea level pressure, wind data, ocean-wave data, and shoreline change rate data. The first 3 were obtained from the European Centre for Medium Range Weather Forecasts (ECMWF) ERA-Interim project, and the last were provided by Deltares, an independent institute for applied research in the field of water and subsurface with five areas of expertise (Deltares.nl, n.d.). The remaining parts of this section tend to explain about the data in this order: the source is outlined first, and the data obtained from them forms a subsection under the source heading.

4.1 ERA-Interim

ERA-Interim is a dataset, showing the results of a global climate reanalysis from 1979 to date. It is usually updated in near-real-time as new data becomes available(Hennermann, 2017). It originally ran from 1989, but a 10-year extension was produced in 2011(Berrisford et al., 2009). ERA stands for 'European Reanalysis' and refers to a series of research projects at ECMWF which produced various datasets, for example: ERA-Interim, ERA-40, etcetera (Hennermann, 2017).

The ERA-Interim data assimilation and forecast suite produces:

- four analyses per day, at 00, 06, 12 and 18 UTC;
- two 10-day forecasts per day, initialized from analyses at 00 and 12 UTC.

The analysis produced at 00 UTC on a given day involves observations taken between 15 UTC on the previous day and 03 UTC on the present day; the analysis at 12 UTC involves observations between 03 UTC and 15 UTC (Berrisford et al., 2009). Analysed data is described as instantaneous, though it does represent an average over a 30 minutes model time step (Hennermann, 2017). Depending on the parameter, forecast data in ERA-Interim is either instantaneous or accumulated from the beginning of the forecast (Hennermann, 2017). However, the data used in this paper is analysed data. That is, a value recorded at a particular time is independent of another value recorded earlier, at a given time interval.

A description of the product relevant to the study is shown below. The full information can be found on ECMWF's website (Hennermann, 2017).

- The temporal coverage is from 1 January 1979 to present
- The spatial coverage is global
- The spectral resolution is T255 (T255 spherical-harmonic representation of the basic dynamic fields)
- The native horizontal resolution is approximately 80 km (reduced Gaussian grid N128); about 83km/0.75 degree when interpolated to a regular lat/long grid

The ERA-Interim product generates parameters and places them in different groups (Berrisford et al., 2009). The groups are labelled as follow:

- Upper air parameters on model and pressure levels
- Upper air parameters on isentropic and $PV = \pm 2\ PVU$ surfaces

- Surface and single level parameters
- Additional vertical integrals for energy, mass, water and ozone budgets
- Ocean-wave data
- Additional fields accumulated from the physical parametrizations

The parameters used in this study fall under the 'surface and single level parameters' (mean sea level pressure and the 10 meters northward and eastward wind components), and the 'ocean-wave data' (Significant height of sea and swell, mean wave period, and mean wave direction).

The preceding paragraphs have given an overview of the ERA-Interim project and the description of its dataset. The next step is to outline and describe the specific parameters obtained from ERA-Interim dataset for this study. The first parameter is the mean sea level pressure, described together with the wind as both are produced on the same potential vorticity (PVU) surface. This is followed by the description of how parameters related to ocean waves are obtained.

4.1.1 Mean Sea Level Pressure and Wind Data

The mean sea level pressure measured in pascals is saved on the ERA-Interim model's Gaussian grid (Berrisford et al., 2009). The wind data however is broken down into eastward and northward components, with the reference being the true north. It is measured at a 10 meters elevation from a reference ground surface and given in meter per seconds units. Like the mean sea level pressure, it is also saved on a Gaussian grid. There is not much information available on the details of how the 2 parameters in this section are collected and processed. However, a detailed discussion of what is done with the data can be found in the methodology section of the paper.

4.1.2 Ocean-wave data

The 3 ocean-wave data parameters used in this study are as follow:

- Significant wave height of sea and swell
- Mean wave period
- Mean wave direction

An altimeter was used to obtain the wave heights. However, this information is not enough to describe the sea state and highlights the problem of having more degrees of freedom than observations (ECMWF, 2012). If the sea state is going to be analysed using 2-dimensional wave spectra, then there is a need decompose the wave height to obtain the sea and swell component of the spectra.

4.1.2.1 WAM and the action balance equation in spherical coordinates

To retrieve the sea and swell components of the spectra, the first step taken was to produce first-guess model heights using the wave model (WAM) (ECMWF, 2012). WAM is a third-generation wave model which solves the action balance equation in spherical coordinates with Sbeing the source term.

$$\frac{\vartheta}{\vartheta t}N + (cos\,\phi)^{-1}\frac{\vartheta}{\vartheta \phi}\left(\dot{\phi}\,cos\,\phi\,N\right) + \frac{\vartheta}{\vartheta \lambda}\left(\dot{\lambda}N\right) + \frac{\vartheta}{\vartheta \omega}(\dot{\omega}N) + \frac{\vartheta}{\vartheta \theta}\left(\dot{\theta}N\right) = S \qquad (1)$$

And

$$S = S_{in} + S_{nl} + S_{ds} + S_{bot} \qquad (2)$$

Where: S_{in} is the input from the wind;

S_{nl} is the input from wave-wave interactions;

S_{ds} input from dissipation due to whitecapping;

S_{bot} is the input from dissipation due to bottom friction;

N is the spectral action density in the Cartesian coordinate system, transformed to a spherical coordinate system through:

$$\widehat{N}\, d\omega\, d\theta\, d\phi\, d\lambda = N\, d\omega\, d\theta\, dx\, dy \qquad (3)$$

Or

$$\widehat{N} = NR^2 \cos\phi \qquad (4)$$

Where: ω is the angular velocity;

θ is the direction with reference to the true north;

ϕ is the latitude in spherical coordinates;

λ is the longitude in spherical coordinates;

And R is the radius of the earth

To further understand the full derivation of the transport equation, how processes like shoaling and refraction are considered in the transport equation, and how the components of the source term are parametrized, the IFS documentation for the ECMWF wave model (ECMWF, 2012) is recommended.

4.1.2.2 Optimum Interpolation

After the first-guess model wave heights are produced by WAM, they are interpolated to the locations of the altimeter observations using the optimum interpolation approach used by Lorenc in his paper on 'A Global Three-Dimensional Multivariate Statistical Interpolation Scheme (Lorenc, 1981), and with appropriate assumptions regarding the error covariances between the interpolated data and the observed altimeter wave heights (ECMWF, 2012).

Optimal interpolation is a technique for combining first-guess and observed quantities in a way consistent with the estimated accuracy of each (Lorenc, 1981). The statistical techniques of optimum interpolation lead naturally to a method of detecting data which are unlikely to be correct, as a means ensuring the quality of the data and subsequent analysis (Lorenc, 1981).

Finally, the field with the interpolated values is then used to retrieve the full two-dimensional wave spectrum from a first-guess spectrum, introducing additional assumptions to transform the information of a single wave height measurement into separate corrections for the wind sea and swell components of the spectrum (ECMWF, 2012). This method corrects the two-dimensional spectrum by introducing appropriate rescaling factors to the energy and frequency scales of the wind sea and swell components of the spectrum and updates the local forcing wind speed. Rescaling factors are computed for two classes of spectra (ECMWF, 2012):

- Wind sea spectra – rescaling factors are derived from fetch and duration growth relations.
- Swell spectra – assumed that wave steepness is conserved.

A simple classification into each of the 2 components depends on their percentage of energy with regards to the total energy. The wave spectra are regarded either as wind sea spectra, if the wind sea energy is larger than 3/4 times the total energy, or, if this condition is not satisfied, as swell (ECMWF, 2012).

4.2 Satellite Derived Shoreline Change Rate Data

The shoreline change rates data was provided by Deltares. These rates were obtained from satellite imagery. Image collections used were from NASA Landsat 4, 5, 7, 8 and ESA Sentinel 2. To study the SDS positional accuracy and application in coastline monitoring practice, the following steps were carried out as explained by Hagenaars et al in their paper (Hagenaars, de Vries, Luijendijk, de Boer, & Reniers, 2018):

- Automatic and unsupervised detection of the SDS position and calculation of its position relative to in-situ data;
- Definition of a benchmark case, in which all drivers that can cause inaccuracies are absent;
- Quantification of the drivers of inaccuracy in relation to the positional accuracy,
- Effect of an image composite processing technique on the mitigation of these drivers, and
- Comparison between the long-term coastline trend based on the SDS and in-situ shoreline (the Sand Engine in the Netherlands) data.

The shoreline position is tested for accuracy for 143 images against high resolution in-situ data obtained from topographic surveys and water level measurements along a coastal stretch near the Sand Motor (Hagenaars et al., 2018). It was concluded that structural trends can be detected for coastlines that have changed with at least the pixel resolution (10-30 meters) within the considered timespan and are less or equally dynamic as the one in the paper (Hagenaars et al., 2018), and that this technique can potentially be applied at other locations with large (structural) coastline trends with a good accuracy of composite images in combination with the worldwide availability of public satellite imagery covering the last decades (Hagenaars et al., 2018). A detailed description of the image processing techniques and shoreline position validation can be found using this reference: (Hagenaars et al., 2018).

CHAPTER 5: METHODOLOGY

This section presents the methods used to describe the state of the coast under mean, extreme, and long-term conditions. The bulk longshore sediment transport capacity is estimated on medium term scales. Next, the response of the beaches along the coast due to storm surge (short-term) conditions is quantified using the convolution method of Kriebel and Dean. Finally, the shoreline retreat due to future SLR predictions is assessed using the Bruun rule.

5.1 Assessing the longshore sediment transport capacity of waves on medium term scale

Longshore sediment transport is the net movement of sediment particles through a fixed vertical plane perpendicular to the shoreline (Bosboom, Judith; Stive, 2015). The direction of this transport is parallel to the shoreline and the depth contour lines (Bosboom, Judith; Stive, 2015). The longshore sediment transport is assumed to be wave-driven, and it depends on the hydrodynamics in the breaker zone and the sediment properties amongst other things (Bosboom, Judith; Stive, 2015). Notwithstanding, this transport only occurs if moveable sediment is available in a certain area, either in the seabed or in the water column through supply from an adjacent area (Bosboom, Judith; Stive, 2015). If the seabed is fixed (sediments unable to be removed from the bed due to vegetation, or lack of sediments on the bed), erosion is prevented (Bosboom, Judith; Stive, 2015). Depending on the hydrodynamics, the actual transport in this case may be less than the local transport capacity. The focus in this study is placed on the transport capacity of waves or wave-driven currents (Bosboom, Judith; Stive, 2015). The effects of tidal currents or other alongshore currents are not considered. It is also important to note that the sediment referred to here is sand. Henceforth, the terms ‘sediment transport’ and ‘sand transport’ are used interchangeably throughout the paper. Gravels, shingles, clays, silts, and other kinds of sediments are not a part of this study.

The overall aim of this section is to calculate the wave-driven bulk longshore sediment transport along the Liberian coast under mean wave climate conditions on medium-term time and spatial scales. Medium term here refers to a time scale of years to decades, and a spatial scale of 1 to 5 kilometers (Stive et al., 2002). The period under study is 23 years (1984 – 2006). The term ‘bulk sediment transport’ is used interchangeably with ‘bulk transport’ for the remainder of this paper. The term ‘net sediment transport’ represents the bulk transport moving in the dominant transport direction. The coastline of Liberia spans from northwest to southeast with reference to the true north. Therefore, the net sediment transport volume is found by calculating the difference between the bulk transport in opposite alongshore directions corresponding to the shoreline orientation. Transport rates are expressed in rate terms (volume per meter width of the surf zone).

The structure of this section is as follows: the wave data and its structure will be introduced at first, including a quality control check to ensure that the waves have not undergone transformation due to shoaling, refraction, and bottom friction. Next, the processing of the wave data to obtain a morphological wave height, an associated wave period (used interchangeably with period throughout this paper), and a frequency of occurrence for each of the directional range represented in the dataset are explained. These waves are then propagated using the Airy or Linear Waves Theory formulations to the point of breaking. A brief introduction of wave-driven longshore or littoral transport follows. The Kamphius and CERC formulas are then used to calculate the bulk transport over the entire width of littoral zone. The transport initiated by each breaking wave is multiplied by its individual frequency

of occurrence, and the net transport volume is calculated. A sensitivity analysis is carried out to determine which of the 2 formulas is more representative of the conditions along the coast.

5.1.1 ERA-Interim Wave Data Structure

The wave data was downloaded from the ECMWF's website via a python script. Based on the grid size requirements of ERA-Interim (Hennermann, 2017), points were chosen at the defined grid intersections seaward of the Liberian coast in Google Earth. The grid spacing is 0.75 degrees in the latitude and longitude direction. The coordinate system used in Google Earth is the World Geodetic System (WGS 84) spherical coordinate system.

Point Label	Latitude (deg)	Longitude (deg)	Number of Timesteps
A	6.75 S	-12 E	33604
B	6 S	-11.25 E	33604
C	5.25 S	-10 E	33604
D	4.5 S	-9.75 E	33604
E	3.75 S	-8.25 E	33604

Table 2: Coordinates of wave data points. Timesteps indicate the number of recorded values (data recorded at 6-hours interval for 23 years)

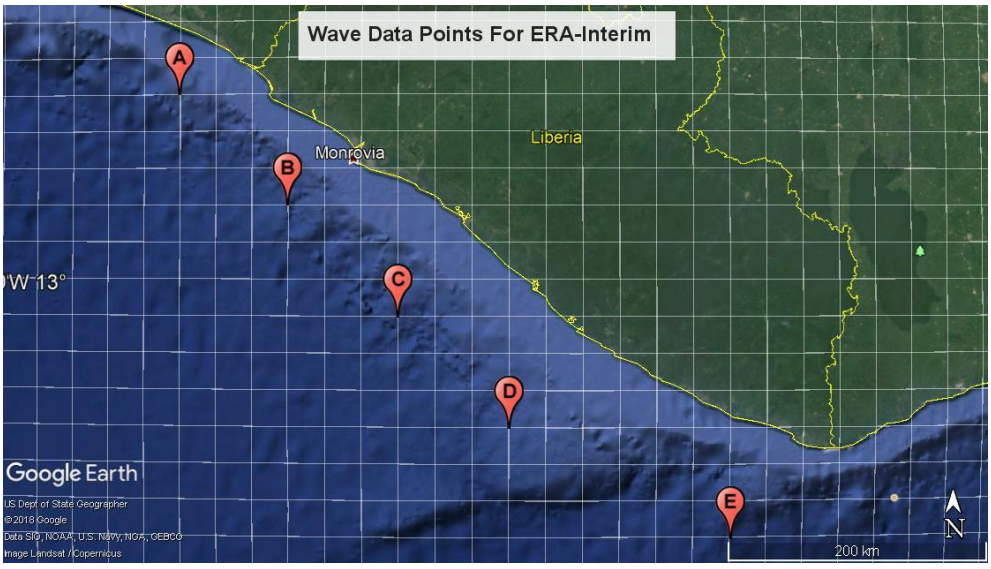

Figure 20: Location of data points in Google Earth. Each grid has a spacing of 0.25 degrees

A python script was generated to download the data and modified to extract the information for the study site and convert the data into a Mastercam Numerical Control File (nc file extension). The 3 parameters downloaded are the significant wave height of sea and swell, the mean wave period, and the mean wave direction. Each parameter is given as a 3-dimensional matrix comprising of a latitude, longitude, and the total number of timesteps for each point over the study period. The values are then extracted for the five points chosen for the study. For each parameter, values were recorded 4 times a day at 6-hour intervals. These values are independent of each other but represent the mean over each 6 hours of observation.

5.1.2 A quality check for the effects of shoaling

After downloading the data and extracting the information for the selected points, a simple check was carried out to ensure that the waves are not affected by the sea bed or the effects of shoaling. According to the Linear waves theory, for not too steep waves in deep water (Bosboom, Judith; Stive, 2015), the deep-water wavelength (L_o) is directly proportional to the square of the wave period multiplied by a factor of 1.56 (a ratio of 2 pi radian and a gravitational acceleration of approximately 9.81 meters per second square). The maximum wave period was found for each data point, and the deep-water wavelength for each of them was found using the formula below.

$$L_o = \frac{g}{2\pi} T^2 = 1.56T^2 \qquad (5)$$

The deep-water condition implies that the water depth is greater than half of the deep water wavelength (Bosboom, Judith; Stive, 2015). Therefore, the wavelength calculated was multiplied by a factor of 0.5 to obtain the maximum wavelength which satisfies the deep-water condition. To verify that the depths at the selected points satisfy this condition, a print screen of the bathymetry was taken from the Navionics website's chart viewer page using the snipping tool and saved as an image. The image was then georeferenced in ArcMap after verifying that the data frame properties of ArcMap and the map in Navionics were referenced to the same geographic coordinate system (WGS 84). A digitisation process was carried out in ArcMap for each bathymetry line on the Navionics map, and their respective depth values were added. The depth value of the closest digitised bathymetry line to each of the wave data point was considered as the water depth at that location. The depth values were then checked to see if they obeyed the deep-water condition using equation 6. The results of this check indicated that the waves for all data points have not been transformed due to shoaling, refraction, or bottom friction. In other words, the waves were not in contact with the sea bed at the locations of the data points and can thus be used for the analysis.

$$\frac{h}{L_o} > 0.5 \; or \; h > 0.5L_o \qquad (6)$$

5.1.3 Waves

The wave heights generally increase from northwest (point 1) to southeast (point 5). This could be due to a stronger influence of swell waves propagating from the south (Titus, 1990). An increase in frequency of waves from the south can also be seen along this trajectory. The most frequent arrive from directions ranging from the south to the southwest, and this is confirmed in existing literature (Titus, 1990). The waves reaching the coast are of two distinctly different origins: the sea generated by the weak, local monsoon; and swell generated by storms in the southern part of the Atlantic Ocean (Titus, 1990).

The wave record used in this study was measured over a 6-hour interval for 23 years (1984-2006). The wave height and period values recorded give the mean over the time interval. The total number of wave per each data point is 33604. How this data is used in the analysis is explained in succeeding sections.

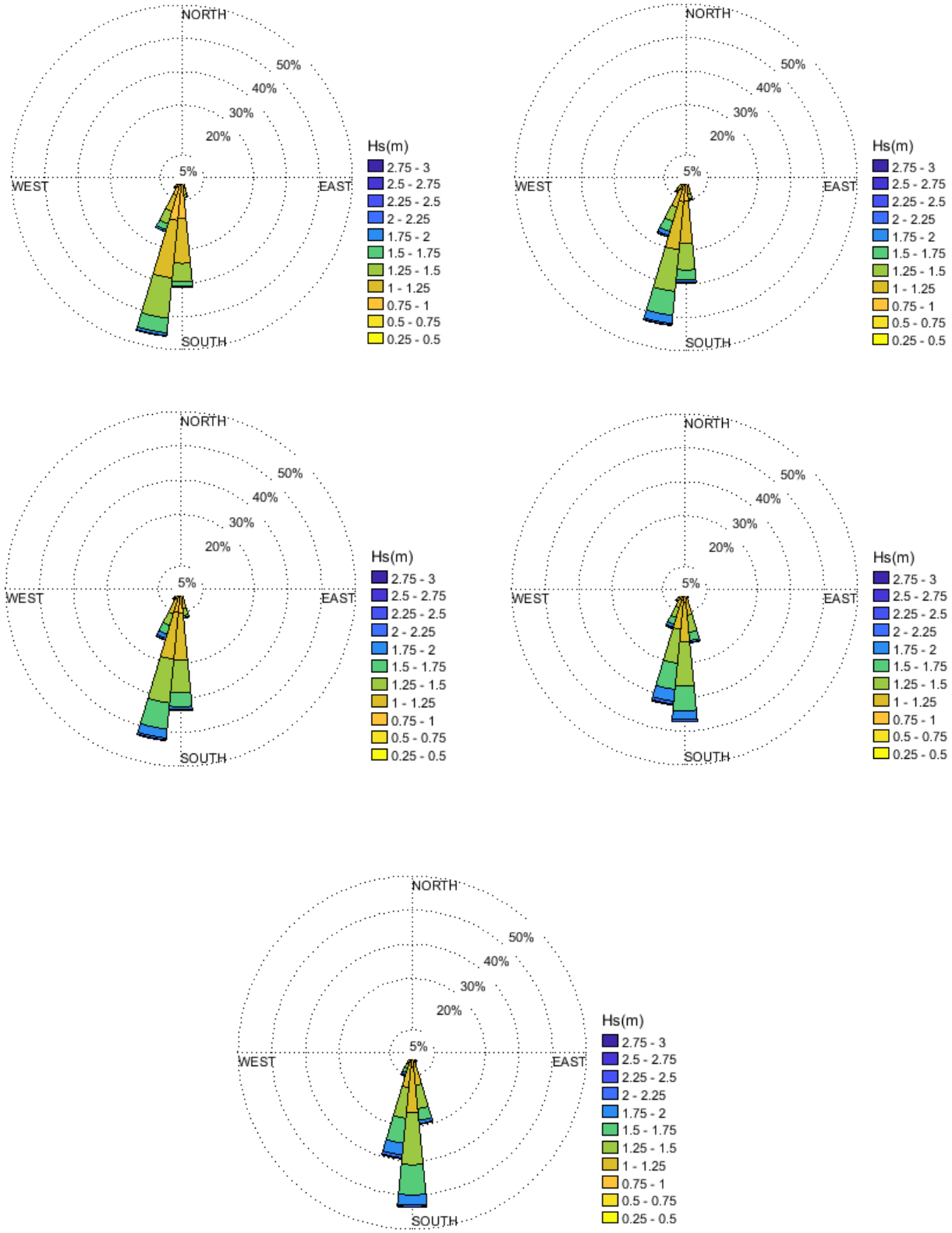

Figure 21: Wave roses for 5 data points placed in order (1, 2, 3, 4, 5) from left to right

5.1.4 Sorting

The wave heights and wave periods are separated by their directions using a 32-point directional compass with reference to the true north. The naming of the directional bins can be understood here: http://tamivox.org/dave/compass/index.html (Barber, 2008).

Directional Bin Number	Direction Name	Lower limit (degrees)	Upper limit (degrees)
1	N	354.375	5.625
2	NbE	5.625	16.875
3	NNE	16.875	28.125
4	NEbN	28.125	39.375
5	NE	39.375	50.625
6	NEbE	50.625	61.875
7	ENE	61.875	73.125
8	EbN	73.125	84.375
9	E	84.375	95.625
10	EbS	95.625	106.875
11	ESE	106.875	118.125
12	SEbE	118.125	129.375
13	SE	129.375	140.625
14	SEbS	140.625	151.875
15	SSE	151.875	163.125
16	SbE	163.125	174.375
17	S	174.375	185.625
18	SbW	185.625	196.875
19	SSW	196.875	208.125
20	SWbS	208.125	219.375
21	SW	219.375	230.625
22	SWbW	230.625	241.875
23	WSW	241.875	253.125
24	WbS	253.125	264.375
25	W	264.375	275.625
26	WbN	275.625	286.875
27	WNW	286.875	298.125
28	NWbW	298.125	309.375
29	NW	309.375	320.625
30	NWbN	320.625	331.875
31	NNW	331.875	343.125
32	NbW	343.125	354.375

Table 3: 32-point compass used. N = North, E = East, S = South, W = West.

Based on the data collected for the 5 points, the waves are spread across 11 directions, from South-South-East (SSE) to West (W). Within each directional bin, the waves are further sorted into selected wave height bins of 0.1 meter interval and period bins of 0.5 seconds interval respectively. *Table 4* displays what this sorting looks like for one direction. The wave data point B is chosen, and the selected direction is SSE. Note that the number of wave and period bins are less than the total (30 bins each), and that the intervals between the period bins are not consistent all through. The last 2 bins are used here for 2 reasons: first, because they are the only bins in which waves originating from the SSE are found considering the data point selected, and secondly, it gives a visual representation of how the sorting of waves is done.

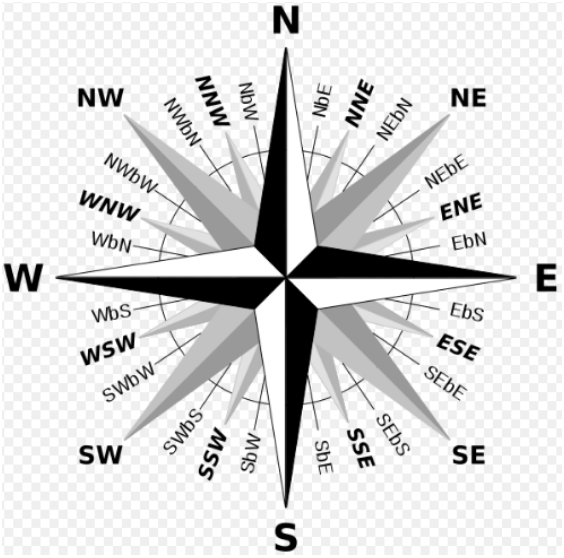

Figure 22: 32-point directional compass (Brosen_windrose.svg, n.d.)

Wave period bins

Wave height bins	Bin limits	0 – 0.5	0.5 - 1	1.5 - 2	2 – 2.5	8.5 – 9	9 – 9.5	Total number of waves
	0 - 0.1							
	0.1 - 0.2							
	0.2 - 0.3							
	0.3 - 0.4							
	0.4 - 0.5							
	0.5 - 0.6							
	0.6 - 0.7							
	0.7 - 0.8							
	0.8 - 0.9					1		
	0.9 - 1					1	2	
	1 - 1.1						2	
	1.1 - 1.2							
								33604

Table 4: Joint distribution of wave height and period bins

The minimum and maximum values of the wave heights and periods are found to guide the choice of the outer bin limits. Based on the wave data used for this study, the maximum value chosen for the wave height is 3 meters, and 15 seconds for the wave period. The total number of bins for each parameter is 30 considering the intervals chosen. The boxes shown in the table above were filled with the wave count for each combination of wave height and period bin.

5.1.5 Frequency of Occurrence

In the analysis of wave data, a key step is to try and represent the actual conditions in the best way possible. Therefore, the importance of estimating how often a condition occurs cannot be overlooked. A good practice is to calculate the frequency of occurrence of a specific wave climate condition. In the previous section, the number of waves for each wave height and period combination was obtained. The frequency of occurrence of waves in each joint bin in the table above is then calculated by dividing the value in the bin by the total number of waves extracted for a specific data point. The total number of waves for each wave data point in this study is 33604, and is found using the equation below:

$$N_{total} = N_{per\ day} * N_{days\ per\ year} * N_{ysp} \quad (7)$$

Where: $N_{per\ day}$ is the number of recorded measurements per day

$N_{days\ per\ year}$ is the number of days in a Gregorian calendar year including leap years

N_{ysp} is the number of years covered in the study

5.1.6 Morphological Wave height and associated mean wave periods

In accordance with the main aim of this chapter, which is to estimate the bulk sediment transport, we need to propagate the waves from deep water to the point where they break. A common way of defining the location where the waves break is at the seaward limit of the surf zone (Bosboom, Judith; Stive, 2015). To calculate the wave height at breaking, the representative values of the offshore wave heights from each direction are required for propagation using an acceptable method. For simplicity, those representative offshore wave heights are called 'morphological wave heights'. Note that this label is specifically used when it is involved in the estimation of the bulk sediment transport. The main ideology behind this label is highlighted in the definition of 'Coastal Morphodynamics', which is described as the mutual adjustment of morphology and hydrodynamic processes involving sediment transport (Bosboom, Judith; Stive, 2015). In simpler terms, morphodynamics is a feedback which exists between hydrodynamic processes and morphology, with the coupling between them provided by sediment transport (Bosboom, Judith; Stive, 2015).

The first step in obtaining the morphological wave height is to sum all the individual frequencies under each wave period bin, for all the wave height bins. For example, if there are 2 wave height bins (0.5m – 1m, and 1m – 1.5m), a single period bin will be considered. That is, the frequencies of each of the 2 wave height bins under that single period bin will be summed to obtain the total frequency for that period bin. This exercise will then be carried out for each period bin. Once the sum of the frequencies for each period bin is found, the next step is to calculate the morphological wave height for each period bin. Using the same example, each of the upper limits of the wave height bins (1m and 1.5m) are squared and multiplied by their respective frequencies of occurrence. The products are summed, and then divided by the total frequency of occurrence for a particular period bin. Taking the square root of this value gives the morphological wave height associated with that period bin. Once again, this operation is repeated for every other period bin. Morphological wave height values greater than zero are then selected and associated with the median of the period bin range they represent. A mathematical representation is shown below:

$For\ a\ selected\ period\ bin, let\ i = the\ first\ wave\ height\ bin$

$and\ i_2 = the\ second\ wave\ height\ bin$

$$H_{morph} = \sqrt{\frac{(HsUL_{i,1}{}^2 * f_{i,1}) + (HsUL_{i,2}{}^2 * f_{i,2}) + \ldots (HsUL_{i,n}{}^2 * f_{i,n})}{\sum_{i=1}^{n} f_i}} \quad (8)$$

$Where:$ $HsUL\ represents\ the\ upper\ limit\ of\ the\ wave\ height\ bin$

		Wave period bins	
	Bin limits	**8.5 – 9**	**9 – 9.5**
Wave height bins	0.8 - 0.9	2.98E-05	
	0.9 - 1	2.98E-05	5.95E-05
	1 - 1.1		5.95E-05
Total frequency		**5.95E-05**	**1.19E-04**
Morphological wave height		**0.95**	**1.05**

Table 5: Illustration of the joint wave height – wave period distribution

5.1.7 Shoreline Orientations and waves angle of approach

The equations used in this study to estimate the bulk longshore sediment transport establishes a strong dependence on the wave height and wave angle at the breaker point. The CERC formula shows that as long as the other parameters are constant, the transport magnitude increases with increasing wave angle at the breaker point until a maximum is reached at $\varphi_b = \pm 45^{\circ}$ (Bosboom, Judith; Stive, 2015). Similarly, the wave angle parameter used in the Kamphius' equation overpredicts the sediment transport rate (Kamphuis, 1991). Henceforth, it is important that reasonable estimates of the shoreline orientation are considered.

In this study, it is assumed that the bathymetry contour lines are parallel to the coast. Therefore, the angle a wave ray forms with a perpendicular from the shoreline gives the approach angle of the waves in deep water. To obtain this angle, lines were constructed with the aim of tracing the average shoreline orientation in ArcMap as shown in Figure 23. A total of 15 shoreline orientations are used. The slope of each orientation line is found using the latitudinal and longitudinal coordinates of the shoreline orientation's endpoints. Using the true north as a reference orientation, the angle (α) each shoreline orientation forms with the horizontal axis (West to East) is calculated by taking the inverse tangent of the slope. An angle of 90 degrees is added to α to find (ϕ), which is the angle formed between a line normal to the shoreline, and the horizontal reference. (θ) is the wave direction referenced to the true north. Now, consider a wave from the south with reference to the true north. This wave ray forms an angle (β) with the horizontal and forms another angle with the line normal to the shoreline. The latter angle is the approach angle (φ) in degrees and can be calculated by subtracting (α) from (β). The approach angle is also described as the angle the crest of a wave forms with the shoreline. Figure 24 gives a visual representation of the angles mentioned in this paragraph.

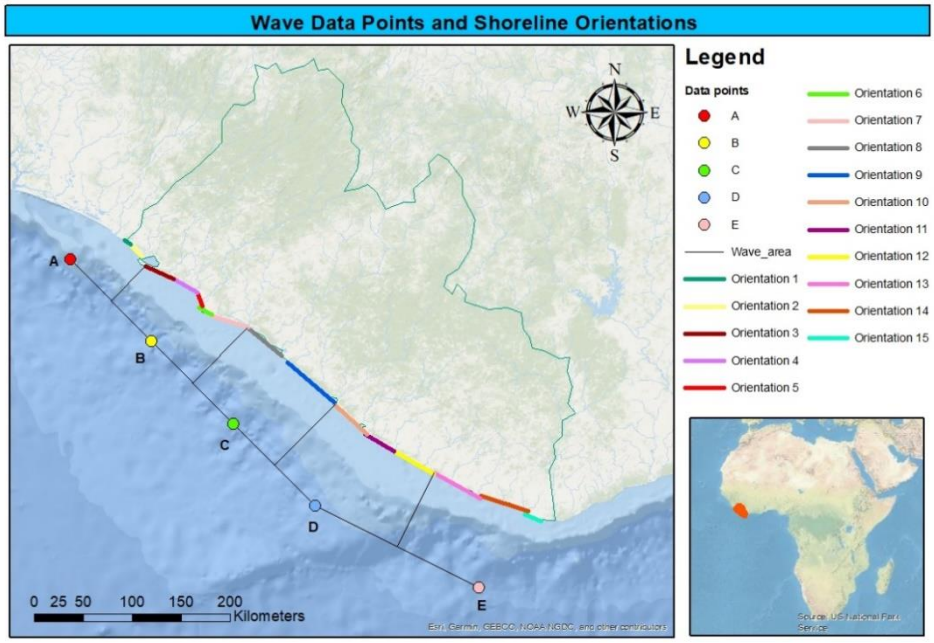

Figure 23: Shoreline orientations from northwest to southeast along with the wave condition influencing the coastal processes for each orientation

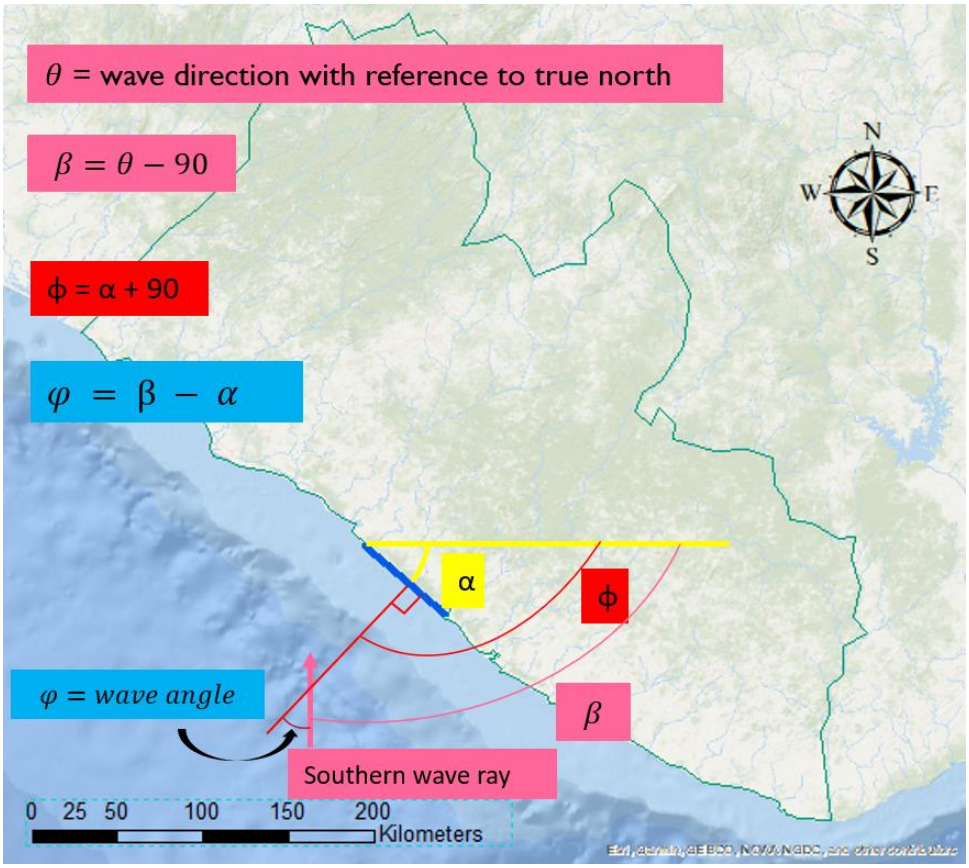

Figure 24: An illustration of the angles discussed in the previous paragraph

Orientation Label	Length of segment (meters)	Endpoint 1		Endpoint 2		α	ϕ
		Lon	Lat	Lon	Lat		
1	7442	-11.5050	6.9278	-11.4501	6.8899	35	125
2	16712	-11.4527	6.8886	-11.3479	6.7819	46	136
3	30908	-11.3100	6.6850	-11.0550	6.5759	23	113
4	26096	-11.0400	6.5650	-10.8380	6.4467	31	121
5	14643	-10.8380	6.4467	-10.7857	6.3268	67	157
6	14146	-10.8180	6.3117	-10.7070	6.2502	29	119
7	37897	-10.6930	6.2331	-10.3670	6.1356	17	107
8	45399	-10.3730	6.1264	-10.0570	5.8700	39	129
9	62602	-10.0050	5.8083	-9.5773	5.4449	40	130
10	43398	-9.5625	5.4199	-9.2784	5.1540	43	133
11	34241	-9.2923	5.1525	-9.0267	4.9980	30	120
12	46610	-9.0319	4.9995	-8.6690	4.7915	30	120
13	52830	-8.6538	4.8007	-8.2390	4.5708	29	119
14	51213	-8.2321	4.5898	-7.7934	4.4519	18	108
15	17500	-7.8276	4.4216	-7.6834	4.3591	24	114

Table 6: Geographic coordinates of endpoints of the shoreline orientations and their angles as explained in the previous paragraph. Coordinates are referenced to the WGS 84 Spheroid

As seen in Figure 23, the area of influence of each wave data point is approximated by constructing a line between the centers of successive data points from northwest to southeast. A perpendicular is then drawn from the midpoint of the connecting line between data points and projected shorewards to a point along the coast. This approximation is done to make it easier when selecting which wave condition to use for a shoreline orientation.

Wave data points	Subjected Shoreline Orientations	Number of Wave Directions
A	1 – 2	9
B	3 – 7	11
C	8 – 9	11
D	10 – 12	10
E	13 – 15	7

Table 7: Shoreline orientations and the wave data point they are subjected to.

The approach angle changes for different shoreline orientations wave directions. Table 8 displays angle of incidence values for shoreline orientation 3. The sign convention corresponds to the alignment of the approach angle. That is, a negative angle implies that the angle is formed on the left of the wave ray as shown in Figure 24 and vice versa.

Wave directions	α	φ (deg)	φ (rad)
SSE	23.30	-45.80	-0.80
SbE		-34.50	-0.60
S		-23.30	-0.41
SbW		-12.00	-0.21
SSW		-0.80	-0.01
SWbS		10.50	0.18
SW		21.70	0.38
SWbW		33.00	0.58
WSW		44.20	0.77
WbS		55.50	0.97
W		66.70	1.16

Table 8: Approach angles for shoreline orientation 3

5.1.8 Linear Wave Propagation

Due to the lack of detailed information for the coast of Liberia, the parameters required for a robust wave transformation simulation of waves as they propagate from deep water to the point where they break are not available. Therefore, models such as the Simulating Waves Nearshore (SWAN) model or other models are not used in this study. However, a simple propagation is carried out using the Small-Amplitude wave theory (Sorensen, 2006). The abbreviation 'LWT' will be used for the remainder of the study.

It is important to note that the focus here is not to give a deep insight of LWT. For detailed understanding of the assumptions used, derivation of the formulas, and limitations of the theory, books by Dalrymple (Dean & Dalrymple, 1991) and Sorensen (Sorensen, 2006) are recommended. Notwithstanding, the main formulas used for the propagation are presented. An important condition is required to verify the use of LWT: the wave height should be smaller when compared to the wavelength and the water depth (Sorensen, 2006). Based on the range of wave height values obtained from the data, the morphological wave heights determined, and the depth value of the bathymetric contour at the wave data extraction point, this condition is obeyed. Also, it has been shown in the

quality check for the wave data that the waves are in deep water. Henceforth, the theory can be used to propagate the waves. The next paragraphs outline the steps of the propagation.

5.1.8.1 Propagation

There are 3 key parameters required as inputs for the LWT formulation: an offshore representative wave height, its associated wave period, and the angle of approach (in radians) of the wave to the shoreline. The 2 wave transformations from deep water to the breaker line considered in this study are shoaling and refraction.

The water depth at the breaker line is unknown during the initial stage of the propagation. For simplicity, a constant breaker depth is assumed for all the waves at first. The propagated wave height is then calculated but is incorrect due to the previous assumption of a constant depth for the propagation. To solve this, McCowan's solitary wave formula relating the breaker depth to the breaking wave height through a certain breaker index (0.78) is used (Bosboom, Judith; Stive, 2015). This formula is used to calculate a breaking wave height.

$$\gamma_b = \frac{H_{M,b}}{h_b} \approx 0.78 \qquad (9)$$

However, Camenen and Larson in their paper on the 'Predictive Formulas for Breaker Depth Index and Breaker Type' investigated McCowan's breaker index value along with 5 other predictive values including Miche (1944), Ostendorf and Madsen (1979) etc., and provided a formula to predict the breaker index (Camenen & Larson, 2007). Their reasoning was that most breaker index predictions give an overestimation for smaller slopes (m > 0.1), despite working reasonably well for bigger slopes (0.02 < m < 0.1) (Camenen & Larson, 2007). They used Miche's (1944) formula as a basis and added a correction factor which is a function of the beach slope and offshore wave steepness (Camenen & Larson, 2007). This formula was validated using a larger and more extensive dataset and is shown below:

$$\gamma_b = \frac{0.284}{\sqrt{\lambda_o}} tanh\left[f_*(m, \lambda_o)\pi\sqrt{\lambda_o}\right] \qquad (10)$$

Where: $f_*(m, \lambda_o) = a\ function\ of\ an\ empirical\ fit\ to\ the\ experimental\ data$

And $\lambda_o = the\ offshore\ deep\ water\ wave\ steepness$

The breaker index value predicted by Gourlay (1994) (Saket, Peirson, Banner, & Allis, 1994), Allsop et al (2015) (Allsop, 2015), McCowan (1894) (Camenen & Larson, 2007), and the predictive approach of Camenen and Larson (2007) (Camenen & Larson, 2007) were used in a sensitivity analysis to see how they vary with respect to the breaking wave height. An offshore morphological (see *Table 9*) wave with the same deep-water parameters was propagated towards shoreline orientation 3 (≈31 kilometers long). The graph below shows the difference in transport rates for the 4 predictions.

Method	Y_b (-)	Hs_o (m)	Tm (s)	Θ (rad)	Hs_b (m)	h_b (m)
Allsop et al (1998)	0.42	0.95	8.75	-0.80	0.99	2.39
Gourlay (1994)	0.55	0.95	8.75	-0.80	1.04	1.90
McCowan (1894)	0.78	0.95	8.75	-0.80	1.09	1.41
Camenen and Larson (2007)	0.89	0.95	8.75	-0.80	1.12	1.27

Table 9: Wave characteristics in deep water and at the breaker line using different breaker index formulas

As seen in *Figure 25*, the Camenen and Larson (2007) formula gives the highest wave height at breaking. This is expected as the breaker index is inversely proportional to the water depth at breaking. Therefore, a higher index gives smaller water depths which increase the effect of shoaling. Also, for smaller water depths, the waves get in contact with the bottom early, assuming parallel contours to the shoreline. Thus, the effects of refraction are smaller, and the waves heights are reduced less. Camenen and Larson's formula (2007) also shows that steeper waves in deep water within the limits proposed by Miche (1944) (Bosboom, Judith; Stive, 2015) will have higher wave heights at breaking, holding all other factors constant.

Camenen and Larson's formula (2007) considers a wider slope range, irregular waves, the effect of the beach slope and offshore wave steepness and overall seems more representative of the actual beach conditions. However, its dependence on the slope makes it difficult to use in the iteration procedure carried out to find the breaker depth as discussed in the next paragraph. The constant predictive breaker index value of McCowan (1894) is preferred in the study as it is easier to use and is suitable for coasts exposed to waves with long fetches like the study site.

Obtaining the wave height at breaking using the breaker index allows the actual water depth to be found through an iterative process. To do this, breaking wave height found using the LWT is subtracted from the one found using the predictive breaker index value. An iteration is then performed by setting the difference between the wave heights to a value of 0.01, and then searching for a breaker depth value which satisfies that condition. The goal seek function in excel is used for the iteration. Once the breaker depth is found, all the other parameters dependent upon it automatically update and the actual breaking wave height to be used in the sediment transport formulations is now found.

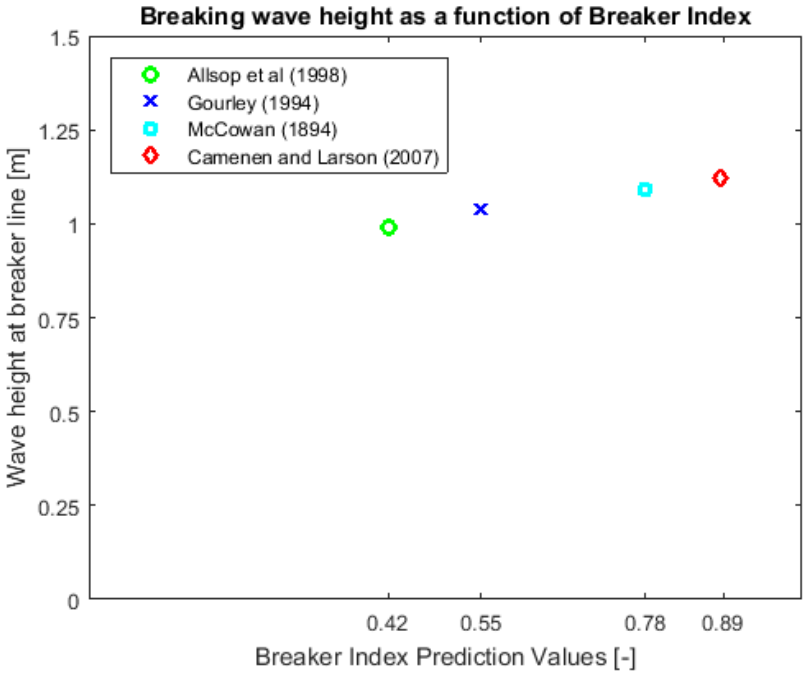

Figure 25: Effects of breaker index of breaking wave heights

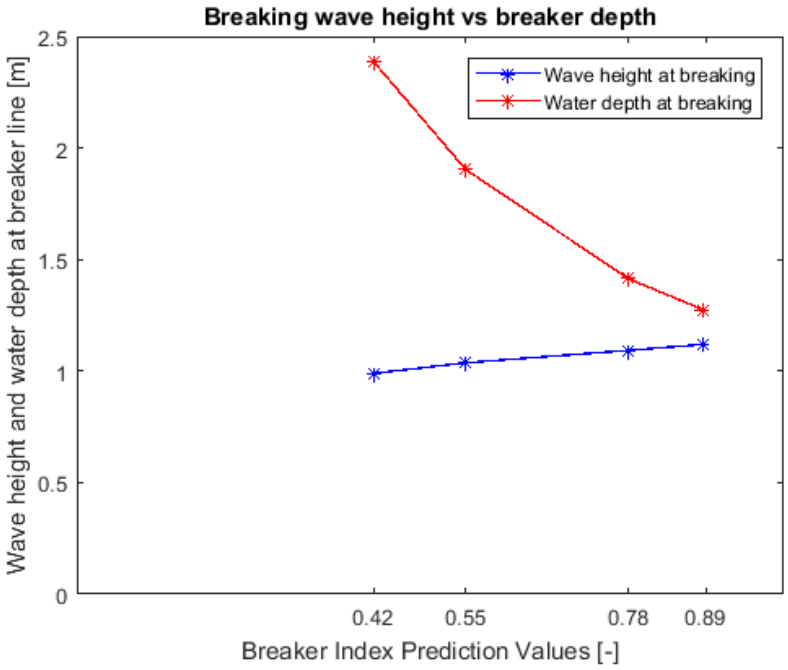

Figure 26: Wave characteristics at the breaker line using the different breaker index values

5.1.9 Bulk Sediment Transport formulations

The bulk transport formulas used in this study gives only takes the wave-induced current into account. It also gives the total transport over the entire width of the littoral or surf zone rather than the distribution over the surf zone, although they may resolve the cross-shore distribution (Bosboom, Judith; Stive, 2015). A major advantage of using these bulk transport formulas is that they are robust, and easy to calibrate and apply. However, the analysis done in this study does not include calibration. Assumptions will be made for certain parameters based on available literature for the study area. In this section, the dimensionally correct form of the CERC formula presented by Komar and Inman (1970) rewritten in terms of wave height parameters (Bosboom, Judith; Stive, 2015), and the Kamphius (1991) equation (Kamphuis, 1991), are used to calculate the bulk sediment transport for specific breaking wave characteristics. The results obtained using them will be compared against each other. A decision is then made on which formula is more representative of the actual site conditions. This is done by comparing both results with the transport volume obtained using the SDS change rate data.

5.1.9.1 CERC formula

CERC formula gives the total longshore sediment transport over the breaker zone due to the action of waves approaching the coast at an angle (Bosboom, Judith; Stive, 2015). It assumes that the longshore current is exclusively driven by waves. Note that a presentation of the origin of the CERC formula is not presented here. For a more detailed understanding of the derivation and original parameters, the Shore Protection Manual (SPM 1984) is recommended (DEPARTMENT OF THE ARMY, Waterways Experiment Station, Corps of Engineers, 1984). This section focuses on the dimensionally correct version of the CERC equation presented by Komar and Inman (1970) (Bosboom, Judith; Stive, 2015). The most general form of the equation is given as follows:

$$Q = \frac{I}{\rho g(s-1)(1-p)} = \frac{K}{\rho g(s-1)(1-p)} (Enc)_b \cos \varphi_b \sin \varphi_b \qquad (11)$$

Where: $Q = the\ deposited\ volume\ of\ sediment\ transport\ [m^3/s]$

$I = \ the\ immersed\ (underwater)\ weight\ of\ sediment\ transported\ [N/s]$

$\rho = density\ of\ water\ [kg/m^3]$

$s = the\ relative\ density\ of\ the\ sediment\ \ \rho_s/\rho\ [-]$

$p = porosity\ [-]$

$g = gravitational\ acceleration\ [m/s^2]$

$K = coefficient\ [-]$

$E = wave\ energy\ [J/m^2]$

$c = the\ wave\ phase\ velocity\ [m/s]$

$n = the\ ratio\ between\ group\ and\ phase\ velocity\ [-]$

$\varphi = the\ wave\ angle\ of\ incidence\ [rad]$

$b = subscript\ referring\ to\ breaking\ conditions$

Inman and Bagnold (1963) applied the energetics concept of Bagnold (1963) to the littoral zone, relating the immersed (underwater) weight of sediment transported, I, to the sine and cosine of the angle of incidence, $\cos\varphi_b \sin\varphi_b$, through a constant, K (Bosboom, Judith; Stive, 2015). The CERC formula can also be written in terms of wave height parameters by substituting $E = 1/8\,\rho g {H_b}^2$ (Bosboom, Judith; Stive, 2015). Considering that wave breaking at the outer edge of the surf zone is a function of reduced water depth, shallow water conditions are assumed such that $n_b = 1$, and that $c_b \approx \sqrt{g h_b}$. The breaking wave height and breaker depth relationship through the breaker index allows h_b to be replaced with H_b/γ. Recalling the double angle formula from trigonometry, $2\cos\varphi_b \sin\varphi_b = \sin 2\varphi_b$ (Bosboom, Judith; Stive, 2015). The CERC formula thereby reduces to the formula below:

$$\mathrm{Q} = \frac{\mathrm{K}}{16(\mathrm{s}-1)(1-\mathrm{p})}\sqrt{\frac{\mathrm{g}}{\gamma}}\,sin\,2\varphi_{\mathrm{b}}\,{\mathrm{H}_{\mathrm{b}}}^{2.5} \qquad (12)$$

The value of the constant K depends on whether the root mean square breaking wave height H_{rmsb} or the significant wave height H_{sb} is used at the breaker line (Bosboom, Judith; Stive, 2015). Komar and Inman (1970) derived a value of K for the H_{rmsb} as 0.77 based on a field study (Bosboom, Judith; Stive, 2015). In this study, the significant wave height at breaking is used. A relationship between the 2 wave heights assuming a Rayleigh distribution of the wave heights ($H_{sb} = \sqrt{2}H_{rmsb}$) for K is given by the equation below (Bosboom, Judith; Stive, 2015):

$$\mathrm{K}_{\text{for Hsb}} = (1/\sqrt{2})^{5/2}\mathrm{K}_{\text{for Hrmsb}} \approx 0.4\mathrm{K}_{\text{for Hrmsb}} \qquad (13)$$

Assuming the constant value of 0.77 for $K_{for\ Hrmsb}$ as proposed by Komar and Inman (1970), the $K_{for\ Hsb}$ used in this study is 0.31. The CERC equation can now be applied to calculate the total longshore sediment transport over the breaker zone.

5.1.9.2 Kamphius (1991) Equation

One key limitation of the CERC formula is that the sand transport is independent of the sand properties such as grain size (Bosboom, Judith; Stive, 2015). This is an important parameter, as the grain size plays a role in determining how the sediments form the beach slope along with the hydrodynamic conditions. The angle of repose, the force required to move the sediments, how far they can travel

under hydrodynamical forcing conditions are all in some way functions of the sediment properties. For example, using the Dean (1977) profile, knowledge of a certain shape parameter is required (Bosboom, Judith; Stive, 2015). Dean (1987) related this parameter to the fall velocity of the sediment, which in turn depends on the fluid's velocity and the sediment's diameter (Bosboom, Judith; Stive, 2015). To solve this, Kamphius (1991) developed an expression linking sediment transport rate to wave steepness, beach slope, and relative grain size, based on the results of 3-dimensional hydraulic model experiments performed with regular and irregular waves (Kamphuis, 1991). The expression also related the sediment transport to the wave breaking angle, but it is not made explicit here as the CERC formula also considered the same parameter. Kamphius' expression was then validated with published field data and compared well (Kamphuis, 1991). Assuming a medium dense sediment porosity of 32%, the Kamphius (1991) formula reads:

$$Q = 6.4x10^{4} * H_{sb}{}^{2} * T_{p}{}^{1.5} * m_{b}{}^{0.75} * D_{50}{}^{-0.25} * \sin^{0.6}(2\varphi_{b}) \qquad (14)$$

Where: $Q = the\ deposited\ volume\ of\ sediment\ transport\ [m^3/yr]$

$H_{sb} = the\ significant\ wave\ height\ at\ breaking\ [m]$

$T_p = the\ peak\ wave\ period\ (mean\ period\ is\ used\ here)\ [m]$

$m_b = the\ slope\ of\ the\ beach\ profile\ [-]$

$D_{50} = the\ median\ grain\ size\ diameter\ [m]$

$\varphi_b = the\ wave\ approach\ angle\ at\ breaking\ [rad]$

The 2 unknown parameters in Kamphius' equation as it relates to the study are the beach profile slope and the median grain size diameter. In the next 2 paragraphs, the methods used to obtain these 2 unknowns will be explained.

5.1.9.2.1 The median grain size diameter

Along the coast of Liberia lie beds of sandstone, with occasional crystalline-rock outcrops (Hadden, 2006). Sandstone is a clastic sedimentary rock composed mainly of sand-sized (0.0625 to 2 mm) mineral particles or rock fragments (Wikimedia Foundation Inc., 2018). Beach erosion studies done for the coast of Monrovia, the capital city of Liberia, classified the sediments along the coastal stretch as very fine – medium – coarse grained (Titus, 1990). The most prominent categories mentioned are the fine and medium grain sand, which ranges from 0.125 mm to 0.25 mm and from 0.25 mm to 0.50 mm respectively according to the Wentworth (1922) grain size classification (Chester K. Wentworth, 2018). For this study, the median (0.25 mm) of the entire range of fine to medium grain sand (0.125 mm to 0.50 mm) is used.

5.1.9.2.2 Beach Profile Slope

To find the beach profile slope, the Dean profile is used assuming a constant beach profile slope from the shoreline (refers to the line separating land from water while the beach is in equilibrium with hydrodynamic forcing) to the breaker line (Bosboom, Judith; Stive, 2015). It reads:

$$h_b = Ax^{2/3} \qquad (15)$$

Where: $h_b = the\ water\ depth\ at\ the\ breaker\ line\ [m]$

$A = the\ sediment\ shape\ parameter\ [-]$

$x = an\ offshore\ distance\ from\ the\ mean\ waterline\ [m]$

Moore (1982) related the shape parameter to the median grain size, showing that a coarser grain size implies a larger value of A and thus a steeper cross-shore profile (Bosboom, Judith; Stive, 2015). Dean (1987) then showed that this relation could be transformed to a relation using the fall velocity via the equation below:

$$\mathrm{A} = 0.5\mathrm{w_s}^{0.44} \qquad (16)$$

Where: $w_s = the\ sediment\ fall\ velocity\ [m/s]$

In this study, the sediment fall velocity is determined using Sistermans (2002) graph relating the grain size to the fall velocity at a water temperature of 18 degrees Celsius.

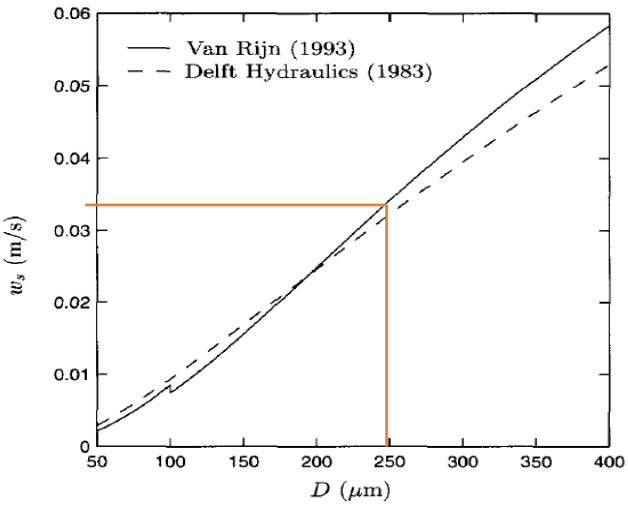

Figure 27: Fall velocities of sediment for fresh water with a temperature of 18 degrees Celsius (Sistermans, 2002)

Using the Van Rijn (1993) line in Sistermans (2002) graph, a sediment fall velocity of 0.0342 meters per second can be extrapolated for a grain size diameter of 250 micrometers ($0.25\ mm\ or\ 2.5E^{-4}$). To check whether the difference in temperature affects the fall velocity extrapolated from Sistermans (2002) graph, Colby and Scott (1965) graph relating the change in temperature to a change in the sediment fall velocity is used (Scott & Colby C. H., 1965). The sea water temperature along the coast of Liberia ranges from 27.4˚ C (81.4˚ F) to 30.5˚ C (86.6˚ F) (World Sea Temperature, 2018). Figure 28 shows the monthly sea water temperature for Monrovia, which is quite similar to other cities along the Liberian coast like Buchanan, Robertsport, and Harper.

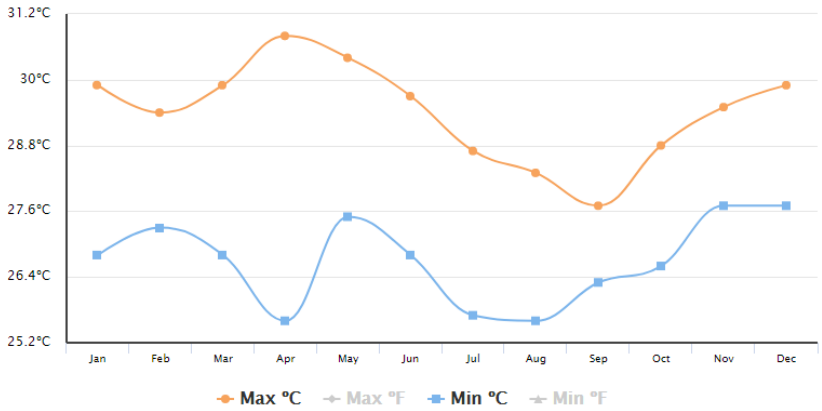

Figure 28: Range of monthly Monrovia water temperature data (World Sea Temperature, 2018).

Colby and Scott (1965) showed that for a grain size in the range of 250 to 500 micrometers, a 23˚ C increase in temperature increases the sediment fall velocity by 0.012 meters per second (≈ 1 cm/s) (Scott & Colby C. H., 1965). Figure 29 and Figure 30 illustrate how the change in water temperature affects the sediment fall velocity (Scott & Colby C. H., 1965). It is therefore safe to assume that Sistermans (2002) graph can be used to determine the sediment fall velocity for a grain size of 250 micrometers despite a temperature difference of approximately 10˚ C with the average sea water temperature along the coast of Liberia. Henceforth, a sediment fall velocity of 0.342 meters per second is used in the study.

Since the sediment fall velocity has been determined, the shape parameter can now be found using equation 16. For a fall velocity of 0.342 meters per second, the shape parameter to be used in the analysis is 0.31. Using the Dean (1977) profile, the offshore distance from the shoreline to the breaker line (x) can be calculated assuming the water depth at breaking (h_b) is known. By making (x) the subject, equation xxx now reads:

$$\mathrm{x} = \left(\frac{\mathrm{h_b}}{\mathrm{A}}\right)^{3/2} \qquad (17)$$

Once again, assuming a constant slope from the shoreline to the breaker line, the slope (m_b) can be found by dividing (h_b) by (x). Note that the slope differs for different wave heights and water depths.

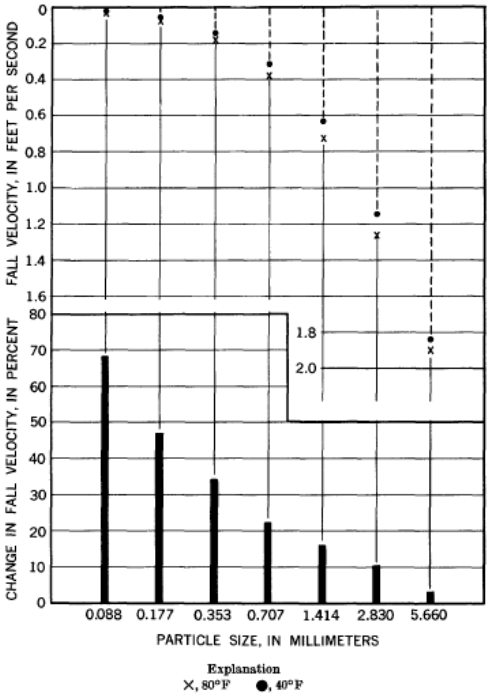

Figure 29: Effect of a change in water temperature from 40˚ F (≈ 4˚ C) to 80˚ F (≈ 27˚ C) on the fall velocity of quartz spheres of several sizes (Scott & Colby C. H., 1965)

Geometric mean size (*mm*)	(*ft*)	*Size range of spheres* (*mm*)
0.088	0.00029	0.062–0.125
.177	.00058	.125– .250
.353	.00116	.250– .500
.707	.00232	.500–1.000
1.414	.00464	1.000–2.000
2.830	.00928	2.000–4.000
5.660	.01856	4.000–8.000

Figure 30: Explanation of Colby and Scott (1965) graph shown in Figure 29

With the median grain size diameter, sediment fall velocity, offshore distance and the slope of the profile from the shoreline to the breaker line known, the Kamphius (1991) formula can be applied to obtain the bulk longshore sediment transport. The 2% wave run-up is calculate using Stockdon et al's formula (Stockdon, Holman, Howd, & Sallenger, 2006). The next section of this study introduces the Satellite Derived Shoreline (SDS) data and how it is processed prior to being used as a rough validation tool in the results and discussion chapter.

5.1.10 Satellite Derived Shoreline

Before using the SDS change rates in the analysis, a quality check was carried out to ensure that the SDS algorithm found a coastline on the transect. A geo-line was drawn between the origin and endpoint of each transect. Since the transect rates file contains retreat information and mean intercept, the values of the intercept were applied to the geo-line object to see if the shoreline position at that point is intersected by the transect. New coordinates were obtained in cases where the transects did not intersect the shoreline at the points of known mean intercept values. This was done to avoid using change rate values that sat beyond the position of the shoreline.

To calculate the bulk sediment transport volume using the SDS change rate data, the well-known Hallermeier's depth of closure concept was applied (Nicholls, Birkemeier, & Hallermeier, 1997). The Dean profile method was used to calculate the offshore distance from the shoreline (transect location) to the location of the depth of closure (Bosboom, Judith; Stive, 2015). Assuming a constant slope, the area of a triangle formula was used to calculate the area of sediment transport along a line spanning from the shoreline to the depth of closure location. For the transport volume calculations, a condition wherein no sediments are transported in the system from the most north-western transect was assumed. The area of sediments was then multiplied by alongshore length between the closest transect in the south-eastern direction to obtain the volume of bulk sediment transport. An analysis of the results will be given in the Results and Discussion chapter, including a comparison with the transport volume predicted using the CERC and Kamphius formulas.

5.2 Assessing the retreat of the shoreline under episodic (storm) conditions

Short-terms as per Stive et al (2002) classification refers to time scales from hours to years, and spatial scales ranging from 10 m to 1 km (Stive et al., 2002). The natural causes and factors of shoreline evolution or variability are waves, tides, and surge conditions (Stive et al., 2002). Season climate variations also play a part in shaping the coast over such scales. In this section, the focus is on the time-dependent beach-profile response to a severe storm surge and the volume eroded are calculated using Kriebel and Dean's (1993) convolution method (Kriebel, Dean, & Members, 1993). The impacts of seasonal variations will also be presented.

5.2.1 Convolution Method – Kriebel et al (Kriebel et al., 1993)

The convolution method provides a simplified procedure for computing cross-shore beach-profile response to time-varying water-level and wave conditions (Kriebel et al., 1993). It is based on the assumption that the beach is a linear-dynamic system (Kriebel et al., 1993). That is, the system output (the beach erosion response) is determined as a function of the system input (the erosion forcing due to variable water level and breaking waves) and the characteristic exponential beach response to any step-type forcing function (Kriebel et al., 1993). An exponential erosion rate is assumed for the beach's response to storms and the response is found to lag the erosion forcing in time (Kriebel et al., 1993). According to Kriebel et al (1993), this response rate is also damped relative to the maximum erosion potential such that only a fraction of the equilibrium response actually occurs (Kriebel et al., 1993).

An equilibrium profile with a sloping beach face is assumed in this study. The equilibrium response is given by:

$$R_\infty = \frac{S\,(x_b - \frac{h_b}{m})}{B + h_b - \frac{S}{2}} \qquad (18)$$

Where: $S = peak\ storm\ surge\ [m]$

$x_b = distance\ from\ the\ still\ water\ shoreline\ to\ the\ breaker\ depth\ location$

$h_b = water\ depth\ at\ the\ breaker\ line$

$m = slope\ of\ the\ beach\ profile\ (assumed\ to\ be\ linear)$

$B = berm\ height$

The term (x_b) is calculated using the Dean (1977) profile as discussed in section xxx. However, Kreibel et al (1993) found a useful relationship between the shape parameter (A) and the sediment fall velocity by fitting an expression through the empirical data presented by Dean (1987) (Kriebel et al., 1993). It reads:

$$A = 2.25\left(\frac{w^2}{g}\right)^{1/3} \qquad (19)$$

This is valid for sediment grain sizes in the range of 0.1 – 0.4 mm, and for water temperatures of about 20˚ C. It is assumed that this equation is valid for our study, as Colby and Scott (1965) showed that the effect of a change in temperature of 8˚ C (difference between the 20˚ C and the average sea water temperature along the Liberian coastline) on the fall velocity for the grain size used in the study is negligible (Scott & Colby C. H., 1965). The equation for x_b is used here depends on whether the depth at breaking (h_b) is bigger or smaller than the depth at which the linear slope is tangent to the concave profile (h_T) (Kriebel et al., 1993). The latter depth is found by:

$$h_T = \frac{4A^3}{9m^2} \qquad (20)$$

x_b can now be calculated using:

$$x_b = x_o + \left(\frac{h_b}{A}\right)^{3/2} \qquad (21)$$

Where: $x_o = the\ distance\ from\ the\ still - water\ shoreline\ to\ the\ virtual\ origin\ of\ the\ concave\ equilibrium\ profile\ form$

The term x_o is found by:

$$x_o = \frac{h_T}{3m} \qquad (22)$$

The reduce the dependency of x_b, h_b, x_o, and h_T on the slope m in the calculations, Sunamura's (1984) formula for the beach-face slope which is dependent on the breaking wave and sediment parameters (Okazaki & Sunamura, 1994)

$$m = {0.12(gT_p{}^2)^{1/4}D^{1/4}}\Big/{H_b{}^{1/2}} \qquad (23)$$

Where: $D = the\ sediment\ grain\ size\ diameter$

$T_p = the\ peak\ wave\ period$

The berm height is calculated using Sunamura (1982) formula which is said to have obtained reasonable results when applied to field data (Okazaki & Sunamura, 1994). The equation reads:

$$\mathrm{B} = 0.125(\mathrm{gT}^2)^{3/8}\,\mathrm{H_b}^{5/8} \qquad (24)$$

The volume eroded from above the original mean sea level at equilibrium is given by:

$$\mathrm{V_{M\infty}} = \mathrm{R_\infty B} + \frac{\mathrm{S}^2}{2\mathrm{m}} - \frac{2}{5}\frac{\mathrm{S}^{5/2}}{\mathrm{A}^{3/2}} \qquad (25)$$

The maximum potential volume eroded from above the peak storm surge level is given by:

$$\mathrm{V_{S\infty}} = \mathrm{R_\infty}(\mathrm{B} - \mathrm{S}) \qquad (26)$$

To calculate the time scale of the profile response, the equation below is used:

$$T_s = C_1 \frac{{H_b}^{3/2}}{g^{1/2}A^3}(1 + \frac{h_b}{B} + \frac{mx_b}{h_b})^{-1}$$

Where: $C_1 = a\ numerically\ derived\ coefficient\ by\ Kriebel\ et\ al = 320$

The rate parameter is then calculated by taking the reciprocal of the time scale of the profile response:

$$\alpha_{\mathrm{conv}} = \frac{1}{\mathrm{T_s}} \qquad (27)$$

5.2.2 Extreme Value Analysis

For the analysis of the extreme wave climate, the annual maxima and peak over threshold (P.O.T) methods are used to extract the offshore wave heights and peak periods prior to propagation using LWT. In this section however, the shoreline orientations in the mean wave climate section are not considered. Rather, the effect of storms on the entire coastal stretch assumed to be affected by the waves from each of the 5 wave data points is considered. A sensitivity analysis is carried out for the annual maxima and P.O.T methods based on their predictions of the breaking wave height.

5.2.2.1 Threshold selection for P.O.T method

For the sensitivity analysis, the wave data from Point 1 is used. To select the threshold for the P.O.T method, 2 methods are used. The first is to plot a normal distribution of all the offshore wave heights, obtain the mean and the standard deviation, and apply the famous 68-95-99.7% rule to get the threshold value by taking the mean plus 2 times the standard deviation. This implies that 95% of the values are below the selected threshold. The second method of obtaining the threshold is done by using a range of thresholds and selecting the one with the smallest standard error value.

To compare the 2 methods, values above the chosen threshold value for both methods are extracted. These values are filtered to get the storms. The process to extract the storm values and calculate the wave height of non-exceedance for a selected return period are as follows:

1. Wave heights exceeding the thresholds for a minimum of 24 hours are extracted.
2. To ensure an independent storm selection criterion, a look ahead at the next 72 hours following a wave height above the threshold which has lasted a minimum of 24 hours is done. If there is another wave height within this timespan satisfying a similar condition, the bigger value of the two is selected as they are considered as 1 storm.

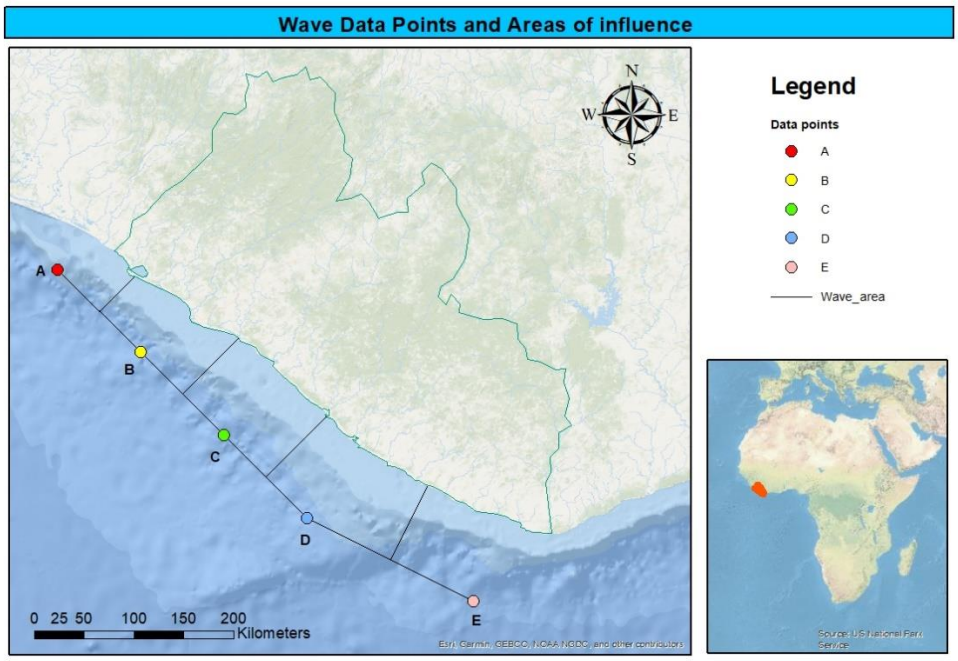

Figure 31: Assumed areas of influence of waves from the 5 offshore wave data points

3. The storm values are transformed from an s-shaped curve cumulative distribution function (CDF) to a line using the 3-parameter Weibull (1939) distribution (Weibull, 1939). The CDF is obtained by calculating the mean and standard deviation of the wave heights above the selected threshold, obtaining the frequencies of occurence of the wave heights assuming a normal distribution, and then plotting the wave heights against their respective frequencies of occurence (see *Figure 32*). The 3-parameter Weibull function is given by:

$$\mathrm{F} = 1 - exp(-(\frac{\mathrm{X}-\mathrm{A}}{\mathrm{B}})^{\gamma} \qquad (28)$$

Where $F = the\ individual\ probability\ of\ X_i\ occurring$

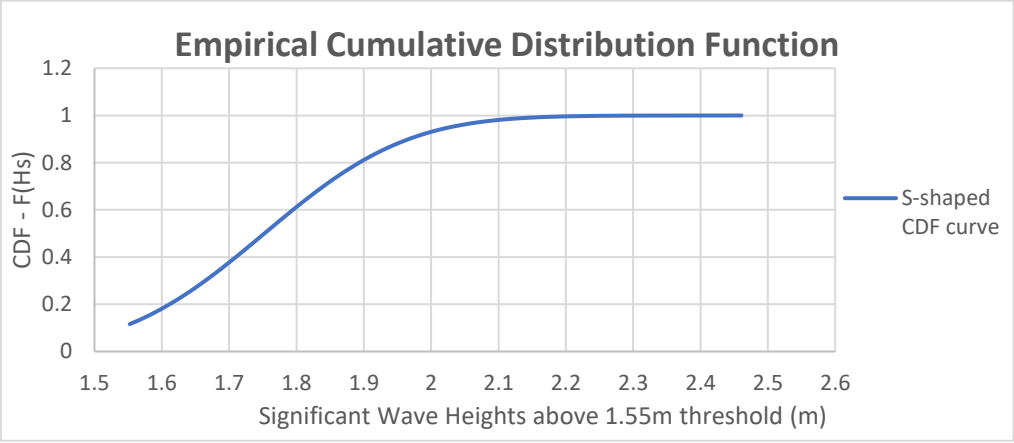

Figure 32: CDF for wave heights above 1.55m threshold. Note that the values on the x-axis start from the threshold.

The equation of the line that the s-shaped CDF curve is transformed into a line on a logarithmic scale is given by:

$$ln(-ln(1-\mathrm{F})) = \mathrm{c}\,ln(\mathrm{X}-\mathrm{A}) - \mathrm{c}\,ln(\mathrm{B}) \qquad (29)$$

Where: $y = \ln(-\ln(1-F))$

$x = \ln(X - A)$

$m = c = the\ slope\ of\ the\ line$

and: $b = -c\ln(B) = the\ intercept\ of\ the\ line$

The equation can now be read as the famous equation of line which is expressed as:

$$y = mx + b \qquad 30$$

The best fit of the line is obtained by iterating one of the parameters of which the x and y values are dependent on. The most suitable value is found when the r-squared regression value is close as possible to a value of 1, indicating the best possible fit of the values to the linear regression trendline (see *Figure 33*). Once the best fit line is obtained, the probability of non-exceedance for a wave height associated with a return period of 100 years is calculated. The wave height for that probability is then found using the equation of the line.

After the wave heights for the selected return period are found for each threshold, the standard error values are calculated and the threshold with the smallest error is selected for the next stage of the analysis as it gives the best fit of the linear regression line. As shown in Figure 34, the most stable correlation between the non-exceedance wave height and the standard error for both methods combined, occurs between threshold 1.5 m and 1.6 m. The exact value where the standard error is the lowest is 1.55 m. Compared with the threshold value of method 1, this value gives a better fit for the linear regression. However, the threshold values vary from one data point to another and will be found for each. The reason is because a lower threshold allows more waves to be extracted as storms, and if the frequency of the lower storm wave heights is high, it causes a bias in the linear regression. The data does not fit the line well and can produce wave heights higher than the highest wave height in the dataset for a return period equal to the number of years the data was collected for. The reverse happens if the threshold is too high. Also, there might be fewer storm values than the number of years the data was measured for and can produce results which are not representative of the non-exceedance wave heights for certain return periods. For example, if there are 16 storm values recorded in 23 years, then the probability of non-exceedance for a wave height within a 1 year return period is negative, which is incorrect. Therefore, the threshold which corresponds with the best-fit regression or lowest standard error value is chosen for each data point.

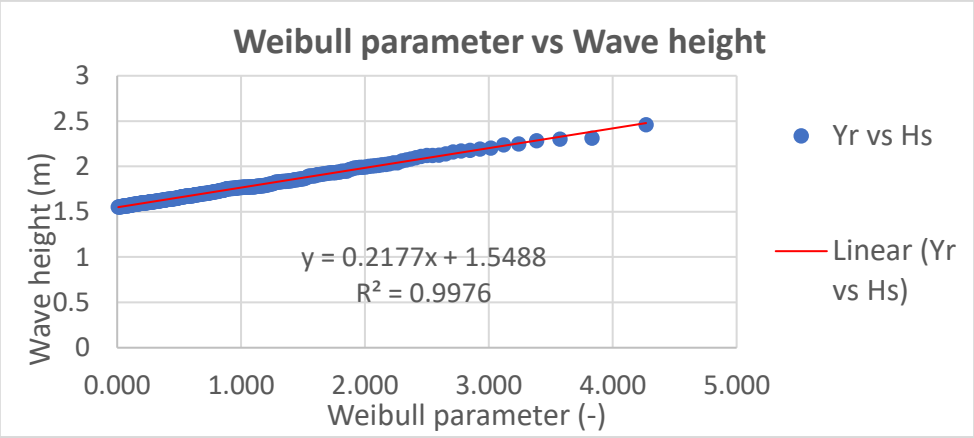

Figure 33: Weibull fit using values above 1.55m threshold for wave data point 1

Method	Threshold (m)	Wave Height for 100 year return period (m)	Standard Error (-)
2	0.5	3.015	0.0228
2	1	2.896	0.0228
2	1.4	2.714	0.0084
2	1.45	2.722	0.0092
2	1.5	2.702	0.0089
2	1.55	2.673	0.0082
2	1.6	2.672	0.0090
2	1.65	2.919	0.0090
1	1.66	2.663	0.0099
2	1.7	2.671	0.0111
2	1.8	2.611	0.0095
2	1.9	2.583	0.0099
2	2	2.196	0.1118

Table 10: Values used in Threshold selection analysis of method 2

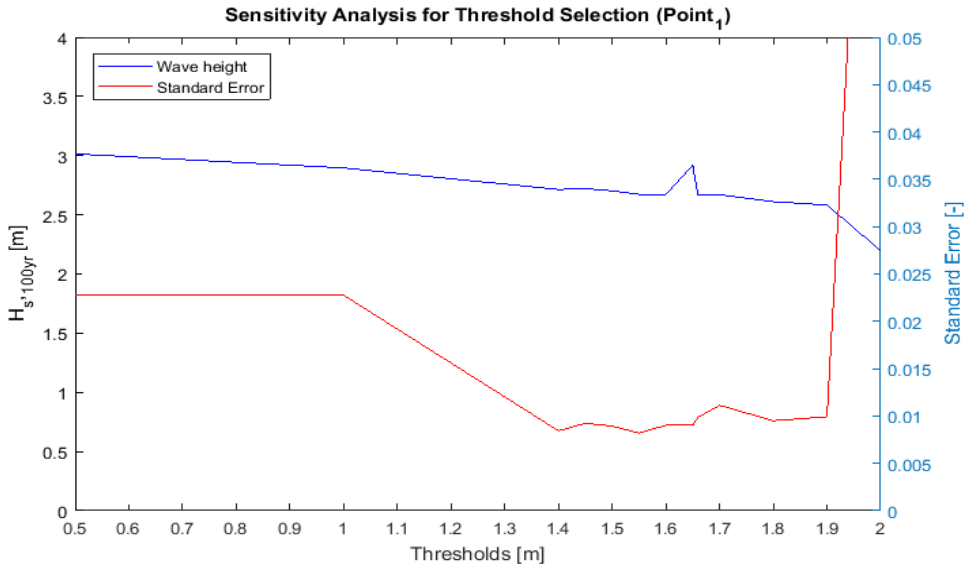

Figure 34: Threshold selection criterion for method 2

5.2.2.2 Selection of wave heights for propagation

To obtain the wave height representative of the directions they originate from including their frequency of occurrence from said directions, a directional coefficient was found. The wave height value at the 99th percentile in each direction and all the values higher than that was extracted for each direction. The mean of the extracted values was found for each direction and divided by the max of the means to get the directionality coefficient.

The wave height for the 100 year return period was then multiplied by the directionality coefficient for each direction. For the propagation, the peak period is required. To find this value, all the wave heights are plotted against their associated periods, and the power law shown in equation 31 allows the peak period to be extracted for the non-exceedance wave height found for each direction.

$$T_p = aH_s{}^b \qquad 31$$

5.2.2.3 Annual maxima method

For this method, the highest annual wave height value is selected. Since the study covers 23 years, there are 23 values in total. These values are extracted along with their associated wave periods. The same data processing procedures carried out for the P.O.T method as explained in section 5.2.2.1

Threshold selection for P.O.T method is done for the annual maxima values to obtain the wave heights and peak periods required for propagation. However, the storm filtering process is not required here as the maximum yearly values are already extracted and is therefore not included in the data processing techniques.

5.2.3 P.O.T vs Annual Maxima

For the extreme wave climate analysis, a choice between which procedure gives the most extreme scenario is required. To make a comparison, the non-exceedance wave heights for each direction found using both methods for a return period of 100 years are propagated to the breaker line. The maximum breaking wave heights for both methods are extracted and compared. The method with the higher value is used to calculate the equilibrium beach response to storms, the timescale required for equilibrium, and the volume eroded from the beach during the storm.

The LWT is used to propagate the waves obtained from the P.O.T and the annual maxima methods. Again, for this sensitivity analysis, a return period of 100 years is used, data point 1 is considered, and the threshold value for the P.O.T method is 1.55m.

Wave direction	Return Period (years)		Wave heights (m)	Peak Period (Tp)	Probability of non-exceedance		Wave heights (m)	Peak Period (Tp)	Probability of non-exceedance
		Annual Maxima				P.O.T (1.55 m threshold)			
SbE	100		2.33	11.44	99.0000%		2.42	11.46	99.9233%
S			2.20	11.27			2.29	11.22	
SbW			2.34	11.46			2.43	11.48	
SSW			2.44	11.60			2.54	11.69	
SWbS			2.57	11.76			2.67	11.92	
SW			2.13	11.17			2.22	11.08	
SWbW			1.42	10.00			1.47	9.45	
WSW			1.39	9.94			1.44	9.36	
WbS			1.12	9.38			1.16	8.61	

Table 11: Wave heights and peak periods for LWT propagation

Using LWT propagation, the wave heights at the breaker line for the P.O.T method were generally higher than the annual maximum values. This could be because the annual maxima method might have neglected some large storm values during a year. Also, in calm meteorological years, the yearly maximum values might alter the analysis by causing a bias towards low wave height values. Meanwhile, the advantage of using the P.O.T method is that it uses more values per year and can pick up storm values irrespective of the number of storms per year. The more storm values, the more emphasis is placed on higher wave heights, depending on the threshold selected. Therefore, the threshold selection method and the defining criteria for storms are important as they can heavily influence the analysis. Going forward, the P.O.T method is preferred and will be used where necessary for the remainder of this study. *Table 12* shows the values obtained at the breaker line for both methods and the direction from which the maximum wave height at breaking emanates.

P.O.T		Annual Maxima		Method Selected
Hsb (m)	Wave Direction	Hsb (m)	Wave Direction	P.O.T
3.32	SWBS	3.20	SWBS	

Table 12: Wave height values at the breaker line for the P.O.T and Annual maxima methods#

5.2.4 Storm Surge

As shown in equation $R_\infty = S\,(x_b - \frac{h_b}{m})\,B + h_b - S2$ (18,

the storm surge value is required to calculate the beach's response to storms and the subsequent volume eroded from the beach during the storm. Storm surge is an increase in water level resulting from shear stress by onshore wind over the water surface (Kamphuis, 2000). As a result, the water level sometimes increases temporarily at the same time as major wave action (Kamphuis, 2000). During a storm surge, the water level at a downwind shore will be raised until gravity (acting on the slope of the water surface) counteracts the shear stress from the wind (Kamphuis, 2000). The combination of the storm surge and wave action is said to be the cause of most of the world's disastrous flooding and coastal damage (Kamphuis, 2000). Therefore, it is important to consider the effects of a storm surge on the water level in extreme scenarios. Wind-generated shear stress is considered as the main driving force of a surge (Kamphuis, 2000). The computations carried out for the storm surge use depth-averaged 2-dimensional equations of motion and continuity.

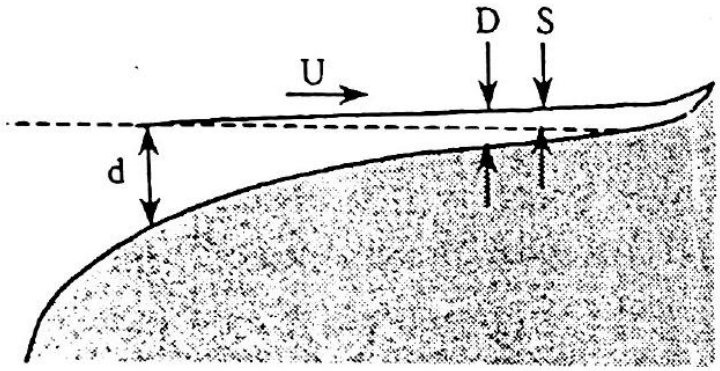

Figure 35: Kamphius definition sketch for a storm surge for an open shore (Kamphuis, 2000)

Assuming a stationary case for simple problems, the equations can be reduced to a one-dimensional computation as seen below:

$$\frac{dS}{dx} = \frac{\varsigma(U\cos\phi)^2}{gD}$$

Where: S is the storm surge (the setup of the water level by the wind);

x is the distance over which the storm surge is calculated;

ς is a constant = 3.2×10^6;

U is the wind speed;

ϕ is the angle between the wind direction and the x-axis;

D is the new depth of water (h + S);

5.2.4.1 Wind contribution to storm surge

To calculate the wind's contribution to the surge level, an extreme scenario is considered. That is, winds which blows in a direction normal to the shoreline are considered for the calculation assuming the shoreline has one general orientation from northwest to southeast. For simplicity, it is assumed that the effects of the wind start at the continental shelf break for the Liberian coast, rather than a random deep water location. Using Google Earth, the section of the coast with the narrowest shelf is

preferred. This represents the shortest cross-shore distance from any point along the shelf break to the coast.

The shelf break point geographic coordinates are referenced to the World Geodetic System (WGS 84). These coordinates are transformed to projected coordinates of the WGS Mercator Auxiliary Sphere. The transformation is kept in the same coordinate system to reduce errors. A constant slope is assumed from the breaker line to the shelf break. Another assumption is that the shelf width is constant along the coast. This assumption means, the wave conditions from point 1 used in the extreme value analysis prediction can be used. The wind speed and direction were calculated from the horizontal and vertical wind components in the ERA-Interim dataset. These values were then sorted according to directions (see windrose in Figure 38). From the 2 shoreline orientations considered, the worst case scenario involves winds blowing from the Southwest-by-south direction based on the 32-point compass. The upper and lower ranges of said directional bin are 208.125 and 219.375 degrees respectively.

Figure 36: Location of the point (green pin) on the shelf break used to calculate the wind contribution to the storm surge

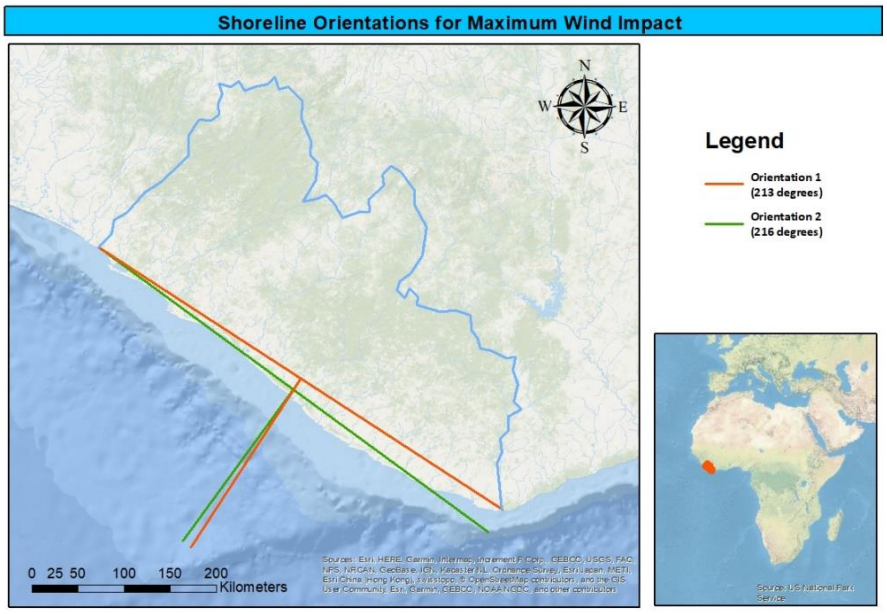

Figure 37: Map showing the 2 shoreline orientations assumed for obtaining the worst possible wind direction

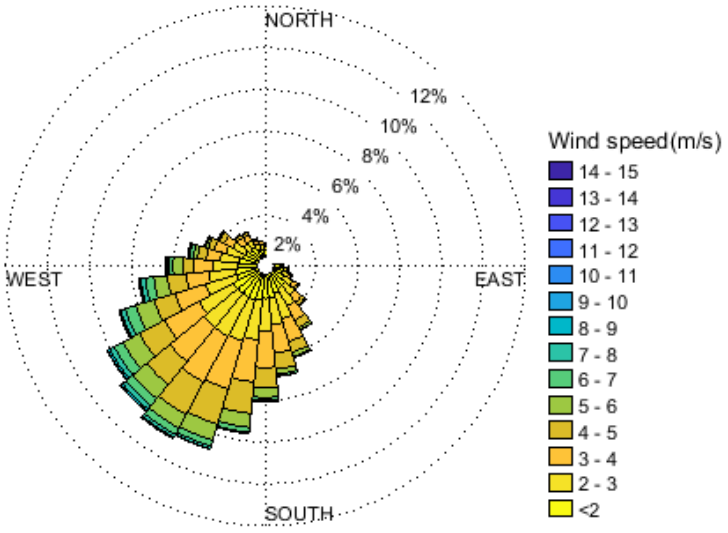

Figure 38: Wind rose for data point 1

Interestingly, for point 1, the wind with the maximum wind speed in the dataset blows from the SSW direction instead of the SWBS direction which is said to have the most impact on the coast. Considering the impact of the wind in the surge calculation, and the extreme scenario being looked at, the highest wind speed is used to calculate the wind set-up or contribution towards the surge. Assuming a constant beach profile slope, the distance between the breaker line and the shelf-break point is divided into 25 sections. Dean's equilibrium profile method is used to calculate the water depth at each position along that distance. The wind set-up is then calculated using Kamphius' (2000) procedure (Kamphuis, 2000).

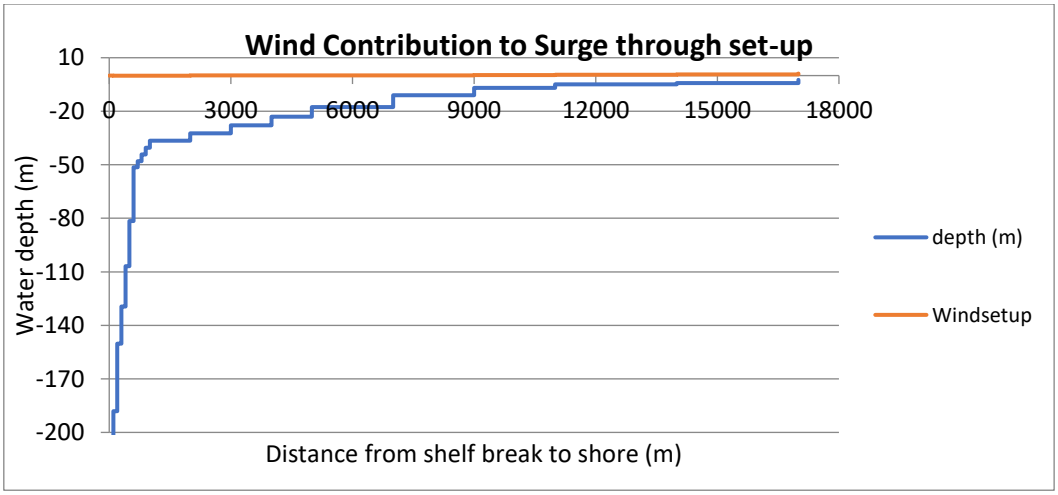

Figure 39: Cross-section of the beach profile from the shoreline to the shelf break (right to left)

5.2.4.2 Atmospheric pressure contribution to storm surge

According to Kamphius (2000), a barometric surge will accompany a storm surge since strong winds are the result of large pressure fluctuations (Kamphuis, 2000). If there is a barometric pressure difference between the sea and the shore, an additional water level rise is generated and represented by the equation below (Kamphuis, 2000):

$$\Delta \mathrm{h} = \frac{\Delta \mathrm{p}}{\rho \mathrm{g}} \qquad (32)$$

Where: $\Delta h = the\ change\ in\ the\ water\ level\ [m]$

$$\Delta p = the\ barometric\ pressure\ difference\ [kPa]$$

$$\rho = the\ density\ of\ seawater\ [kg/m^3]$$

Equation xxx results in a water level rise of 0.1 m for each kPa of pressure difference (Kamphuis, 2000). This conversion factor is used in the analysis to obtain the atmospheric mean sea level pressure contribution to the storm surge. Below is an outline of the procedures used to extract low pressure values which increases the vulnerability of the sea state to high wind velocities, and convert them to surge units using Kamphius (2000) conversion factor (Kamphuis, 2000):

- A time series of the mean sea level pressure data was made by plotting the pressure against time interval of the measurement (6 hours).
- The mean of the data was calculated and subtracted from each pressure value to demean the data, the plot the demeaned data against time.
- The data below the zero line of the demeaned time series was extracted.
- The mean and minimum of the values below the zero line were calculated and converted to surge units by using the relationship introduced by Kamphius (2000) given by:

$$1kPa = 0.1m\ water\ level\ rise$$

- The absolute values of the mean and minimum values were found and the maximum of the 2, which is the minimum of the values below the zero line in the demeaned data, is used as the atmospheric mean sea level pressure contribution to the storm surge.

5.2.5 Total value for storm surge

The total storm value is obtained by adding the wind set-up and atmospheric mean sea level pressure contributions. It is important to note that there is an uncertainty surrounding the dependency of the storm surge on swell waves emanating from the South of the Atlantic ocean. From existing literature, it is known that wind-sea waves are generated by the weak local monsoon, and rarely exceed 1.25 m in height, with a maximum period of 3-4 seconds, and are generated from the southwest (Allersma & Tilmans, 1993). The swell waves which are more frequent, have higher wave height values, and are favoured in the exteme value analysis applied here, arrive from directions between south and south-west (Allersma & Tilmans, 1993). Considering that the surge is caused by the local winds, of which the dominant direction for data point 1 is the southwest (see *Figure 38*), it is assumed to be constant along a coastal stretch under the influence of the selected data point. Also, the dominant direction of the waves for the entire coast shifts more towards the west as you move from northwest to southeast of the coast.

Once the total storm surge value is obtained, the convolution method is applied for all the return periods considered (1, 5, 10, 25, and 50). The entire procedure is then repeated for the remaining sectors of the coast exposed to waves from the data points considered in the study.

5.2.6 Seasonal Variations

There are generally 2 seasons in Liberia: the rainy and dry seasons. The rainy season is approximated to run from May to October, and the dry season runs from about November to April of the following year (Climates to Travel, n.d.). This is the time frame used to obtain the seasonal wave and wind data. However, a return period of 1 year is not considered in this section of the study as in the case of the dry season, the total values obtained above the selected threshold were smaller than 23, the number of years considered. The general threshold selected applies to the seasonal variation to remain consistent with the storm filtering and P.O.T method. It was observed that the wind hitting the coast

is roughly constant throughout the year but reduces from northwest to southeast. Therefore, it is not accounted for as a factor causing seasonal variations of the coastal morphology due to storm surges as the wind contribution to the set-up is assumed to be approximately constant. The storms defined in this study consider a 72 hours timespan between successive storms. Therefore, the convolution method was applied for the beach's response to seasonal storms as it fits within the timescale under consideration (Stive et al., 2002). Based on the results obtained for point 1, the wave climate does not vary significantly during a change of season. Significant here refers to the difference in the shoreline retreat with a magnitude less 10 centimeters. Henceforth, it is assumed in this study that the seasonal variation is negligible in terms of how the beach or shoreline responds to storm surges.

5.3 Assessing the shoreline retreat due to SLR on long-term time scales

In the previous chapter of this paper, we assumed that the beach and surf zone may display a 2-dimensional behaviour under cross-shore wave forcing, and that the amount of sediment in the active zone remains constant (Bosboom, Judith; Stive, 2015). A key factor in that assumption is the time and spatial scale considered, as distinguished by Stive et al (2002) (Stive et al., 2002). The beach is said to be a sand-sharing system on episodic scales (Morton, 2003). That is, it returns to its equilibrium state after a storm event and no sediment is lost from the system. However, on engineering or long-term scales, a number of processes exist which violate the assumptions made for the shoreline variability over short-term scales (Bosboom, Judith; Stive, 2015). For example, alongshore transport gradients due waves approaching the shoreline at an oblique angle or due to changes in shoreline orientation can lead to either shoreline advance or retreat (Bosboom, Judith; Stive, 2015). This is explained in section **5.1.7 Shoreline Orientations and waves angle of approach**of this paper. Also, loss of sand from the beach to sediment sinks (dunes and nearshore offshore canyons) due aeolian or wind-driven transport may occur over long-term scales, but is not the focus of this study (Bosboom, Judith; Stive, 2015). Interestingly, another 'virtual' sink due to relative sea level rise, in which no sediment is loss from the system at least according to Bruun (1962), causes shoreline retreat also (Bosboom, Judith; Stive, 2015). The shoreline retreat due to SLR is the focus of this chapter.

5.3.1 The Bruun Rule

Bruun argued that the "response of the upper shoreface to an increased MSL is so fast that the equilibrium upper shoreface profile will adjust to the same profile, but relative to the new MSL" (Bosboom, Judith; Stive, 2015). The 'Bruun rule' as it is popularly known assumes that the shoreface has a profile that is in equilibrium with the hydrodynamic forcing, in the absence of sediment sinks and sources (Bosboom, Judith; Stive, 2015). The shoreface is defined as shown in *Figure 40*.

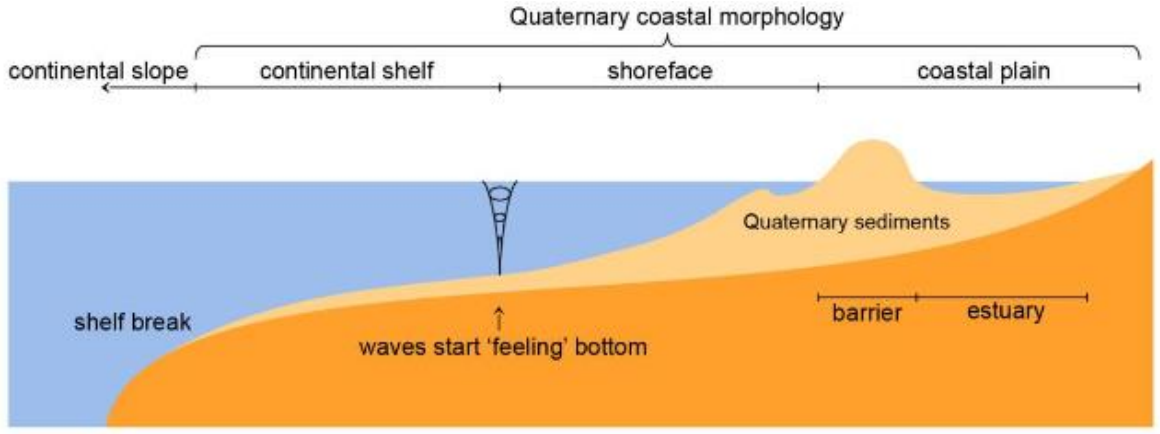

Figure 40: Spatial boundaries of the coastal zone showing the shoreface. The seaward boundary point of the shoreface is the depth of closure (Bosboom, Judith; Stive, 2015)

The shoreline retreat due to SLR is the focus of this chapter and will be calculated using the famous Bruun formula given by:

$$\text{Horizontal Retreat} = \text{RSLR (L/d)} \qquad (33)$$

Where: $RSLR = the\ relative\ Sea\ Level\ Rise\ predicted\ by\ IPCC$

$L = the\ length\ over\ which\ the\ erosion\ and\ sedimentation\ takes\ place$

$d = doc + B = the\ corresponding\ active\ height\ of\ the\ profile$

$Doc = annual\ closure\ depth$

$B = the\ height\ of\ the\ active\ berm$

The active length of the profile is calculated using the Dean (1977) profile used in earlier chapters on this paper. The berm height of the active profile is calculated using Sunamura and Okazaki's formula (Okazaki & Sunamura, 1994). However, the breaking wave height parameter used in this equation is found by propagating all the waves from deep water to the breaker line, and then taking the mean of the breaking wave height values. To calculate the length of the active profile, Dean's profile equation is used with the closure depth being the height of the profile instead of the breaker depths as used in other sections of the study.

5.3.1.1 Closure Depth

Depth of closure is widely used within coastal engineering as an empirical measure of the seaward limit of *significant* cross-shore sediment transport on sandy beaches (Nicholls, Larson, Capobianco, & Birkemeier, 1998). More fundamentally, it is an important parameter which distinguishes 2 cross-shore zones with different levels of morphodynamic activity (Nicholls et al., 1998).

Hallermeier (1981) developed the only analytical approach to estimate an annual depth of closure on sandy beaches (Nicholls et al., 1998). It is a function of extreme wave conditions and in a generalised time-dependent form is (Nicholls et al., 1998):

$$\text{doc}_{l,t} = 2.28\text{H}_{l,t} - 68.5(\text{H}_{l,t}{}^2/\text{gT}_{l,t}{}^2) \qquad (34)$$

Where: $doc_{l,t} = the\ predicted\ depth\ of\ closure\ over\ t\ years\ referenced\ to\ the\ mean\ low\ water$

$H_{l,t} = non-breaking\ significant\ wave\ height\ that\ is\ exceeded\ 12\ hours\ per\ t\ year$

$T_{l,t} = the\ associated\ wave\ period$

This method explicitly recognises that some sediment movement will occur seaward of the depth of closure (Nicholls et al., 1998). In this study, the annual depth of closure is used. That is, the offshore deep water wave height exceeded for 12 hours within a year. To obtain this wave height, the wave heights are divided into bins of 0.1 meter interval and the cumulative frequencies for each bin are calculated. Wave data point 1 is used as an illustration of the method used here. The probability of a wave being exceeded 12 hours (0.5 day) in a year is then given by:

$$\text{Prob of annual 12 hrs exceedance} = \frac{365-0.5}{365} = 99.86\% \qquad (35)$$

From *Table 13*, this wave height falls between bins 21 and 22, indicating a wave height between 2.1 and 2.2 meters respectively. A wave height of 2.14 meters corresponding to the probability of exceedance for 12 hours in a year was found using the linear interpolation formula below:

$$y = y_1 + (x - x_1)\frac{y_2 - y_1}{x_2 - x_1} \quad (36)$$

To find the associated period, a joint distribution table of wave height and periods was produced highlighting the frequency of occurrence of waves heights in each period bin. The period bin interval is 0.5 second. Weighted average period values were found by multiplying the upper limit of each period bin by the number of waves within the joint wave height-period bin and dividing that product by the total number of waves within the wave height bin. The wave height bin used here is where the calculated wave height exceeded 12 hours in a year falls. The sum of the weighted averages is then used as the associated wave period.

Bin number	Bin	Frequency	Cumulative %
1	0.1	0	0.00%
2	0.2	0	0.00%
3	0.3	0	0.00%
4	0.4	0	0.00%
5	0.5	0	0.00%
6	0.6	0	0.00%
7	0.7	73	0.22%
8	0.8	1021	3.26%
9	0.9	3330	13.17%
10	1	5180	28.58%
11	1.1	5702	45.55%
12	1.2	5006	60.45%
13	1.3	4233	73.04%
14	1.4	3262	82.75%
15	1.5	2414	89.93%
16	1.6	1537	94.51%
17	1.7	839	97.00%
18	1.8	504	98.50%
19	1.9	227	99.18%
20	2	140	99.60%
21	2.1	73	99.81%
22	2.2	42	99.94%
23	2.3	15	99.98%
24	2.4	5	100.00%
25	2.5	1	100.00%
26	2.6	0	100.00%
27	2.7	0	100.00%
28	2.8	0	100.00%
29	2.9	0	100.00%
30	3	0	100.00%

Table 13: Table showing frequency of occurrence of deep-water wave heights from wave data point 1

5.3.1.2 Relative Sea Level Rise Predictions

The SLR predictions for the region were extracted from the IPCC's global prediction values stated in chapter 13 of the Intergovernmental Panel on Climate Change (IPCC) Fifth Assessment Report (Church, J A; Clark, P U; A. Cazenave; Gregory, J M; Jevrejeva, S; Levermann, A; Merrifield, M A; Milne, G A; Nerem, R S; Nunn, P D; Payne, A J; Pfeffer, W T; Stammer, D; Unnikrishnan, 2013).

	RCP 4.5			RCP 8.5		
	Lower limit	**Mean**	**Upper limit**	**Lower limit**	**Mean**	**Upper limit**
Regional	0.32	0.51	0.72	0.48	0.68	0.87
Global	0.36	0.53	0.71	0.52	0.74	0.98

Table 14: Regional and Global SLR projections for RCP 4.5 and 8.5 with medium confidence

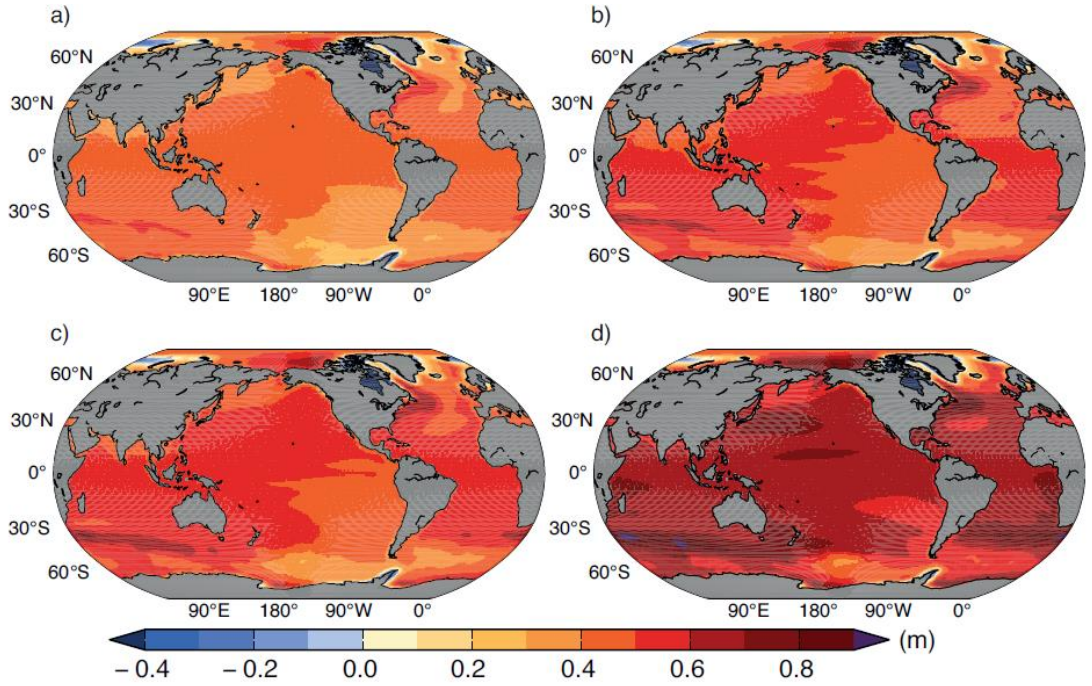

Figure 41: Ensemble mean regional relative sea level change (meters) for the RCP scenarios (a) 2.6, (b) 4.5, (c) 6.0, and (d) 8.5 between 1986-2005 and 2081-2100 (Church, J A; Clark, P U; A. Cazenave; Gregory, J M; Jevrejeva, S; Levermann, A; Merrifield, M A; Milne, G A; Nerem, R S; Nunn, P D; Payne, A J; Pfeffer, W T; Stammer, D; Unnikrishnan, 2013)

The values in Table 14 matches with the IPCC's projections for the mean SLR shown in Figure 41. For this study, only the regional projections of RCP 4.5 and 8.5 are considered. RCP used in this document refers to 'Representative Concentration Pathways' which are four greenhouse gas concentration describing four possible future climate scenarios depending on the amount of greenhouse gases (GHG) emissions in the years to come. The numbers attached to the RCP label are named after a possible range of radiative forcing values in the year 2100 relative to pre-industrial values (+2.6, +4.5, +6.0, and +8.5 W/m2, respectively) (Pachauri, 2014).

In this study, the regional values are used as they are more representative of the study area than the global projections. This is better explained in the 2013 Sea Level Change report from the IPCC Fifth Assessment Report shown below:

> *"Regional sea level changes may differ substantially from a global average, showing complex spatial patterns which result from ocean dynamical processes, movements of the sea floor, and changes in gravity due to water mass redistribution (land ice and other terrestrial water storage) in the climate system. The regional distribution is associated with natural or anthropogenic climate modes rather than factors causing changes in the global average value*

> *and include such processes as a dynamical redistribution of water masses and a change of water mass properties caused by changes in winds and air pressure, air–sea heat and freshwater fluxes and ocean currents. Because the characteristic time scales of all involved processes are different, their relative contribution to net regional sea level variability or change will depend fundamentally on the time scale considered"* (Church, J A; Clark, P U; A. Cazenave; Gregory, J M; Jevrejeva, S; Levermann, A; Merrifield, M A; Milne, G A; Nerem, R S; Nunn, P D; Payne, A J; Pfeffer, W T; Stammer, D; Unnikrishnan, 2013).

The shoreline retreat due to SLR will be calculated for each data point (1 to 5), and the results will be presented in the next chapter of this paper

CHAPTER 6: RESULTS AND DISCUSSION

This chapter presents the results of the calculations and analysis done in this study. However, prior to displaying the results, specific results are presented and discussed. For the mean wave climate, the bulk longshore sediment transport rates using the CERC and Kamphius equations are compared and the Kamphius' expression is selected as being more representative of the actual sediment transport conditions albeit with justifications. This is followed by a display of the influence of the shoreline orientations and change in wave conditions on the sediment transport rates. Next, the transport rates obtained by Kamphius' equation are tested against the values calculated using the SDS change rate data (volume calculation explained in section 5.1.10 **Satellite Derived Shoreline**). For the extreme climate, the relationship between the beach's response and the return period is presented. The difference in retreat rates using the RCP 4.5 and 8.5 is shown for the long-term conditions.

The results are presented in a chart format for one orientation. This chart comprises of a general description, and the morphological, and hydrodynamic characteristics of a coastal stretch on medium term scale, the shoreline retreat values due to storm surge, the volume of sediment eroded above the MSL and the peak storm surge level, the timescale required for the beach to return to equilibrium, and a rate parameter on short-term scale, and finally the shoreline due to SLR on long-term scales. For the short and long-term scales, the parameters calculated using an extreme value analysis are presented for 6 selected return periods. The results for the remaining orientations can be found in the Appendices (section xxx).

6.1 CERC vs Kamphius

In this section, the bulk longshore sediment transport rates using the CERC and Kamphius formulas are compared to test their predictive capabilities. Based on the results obtained, the CERC equation predicts sediment transport volumes over a magnitude more than Kamphius'. When plotted on the same magnitude scale as seen in Figure 42, the CERC formula gives values in an order of magnitude of millions of cubic meters while the Kamphius equation gives sediment transport rates in an order of hundred of thousands.

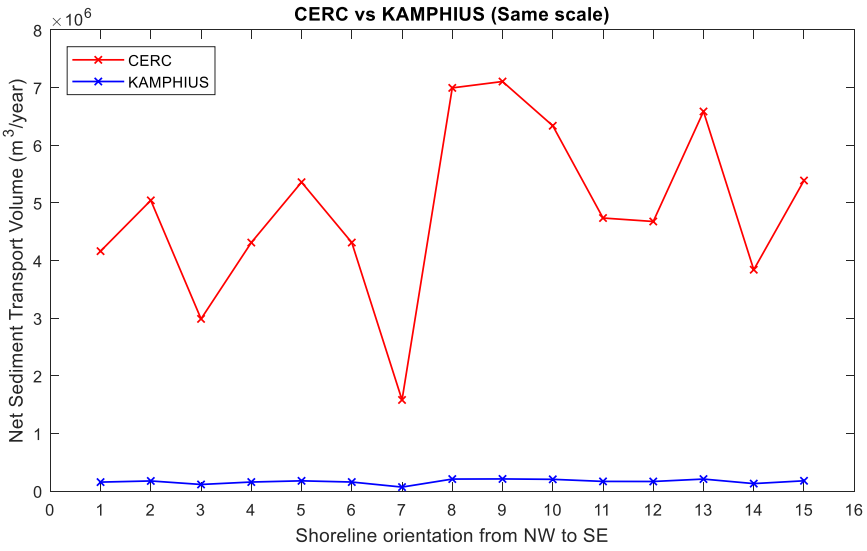

Figure 42: Net sediment transport prediction using CERC and Kamphius' equations.

In terms of the variation with regards to the transport rates for different shoreline orientations, both formulas follow a similar pattern as shown in Figure 43.

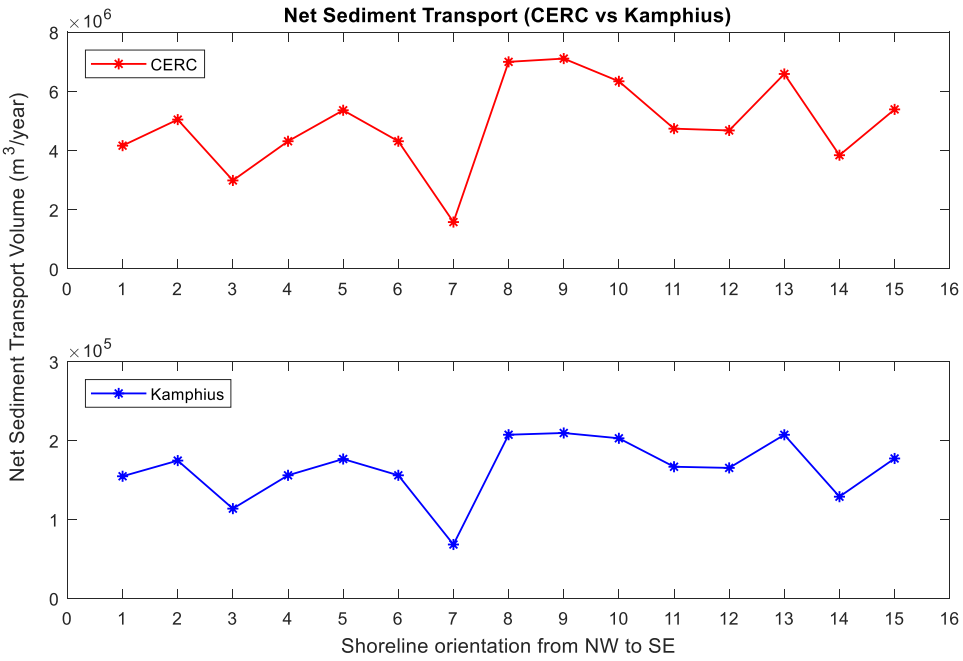

Figure 43: Transport rates across shoreline orientations

From the graphs shown in this section, the CERC formula seems to overpredict sediment transport rates. This is expected due to the overreliance on certain parameters in the CERC formula, and/or the lack of consideration for other requirements which affect sediment transport. Kamphius (1991) conducted 3-dimensional hydraulic model experiments with regular and irregular waves to study alongshore sediment transport rate (Kamphuis, 1991). In his experiments, he applied the CERC formula to see how well it fits the model data. Interestingly, an expression which did not represent the data well based on a best fit regression line fitted the data even better than the CERC equation and with less error too (Kamphuis, 1991). To represent all the data used, an expression which compares well with published field data was developed, linking sediment transport rate to wave steepness, beach slope, relative grain size, and breaking angle (Kamphuis, 1991). This expression given by equation $Q = 6.4x10^{4} * H_{sb}{}^{2} * T_{p}{}^{1.5} * m_{b}{}^{0.75} * D_{50}{}^{-0.25} * \sin^{0.6}(2\varphi_{b})$ (14 considers the influence of important transport-related parameters such as the wave period, grain size, and beach slope (Bosboom, Judith; Stive, 2015).

Compared to the CERC equation, the dependency of the transport rate on the wave-breaking angle is smaller. The dependence of transport rates on grain size is however weak, and the scale effects is negligible due to the effects of incorrect beach slope and grain size cancelling out each other (Kamphuis, 1991). There is also an interdependence between parameters in Kamphius' expression. For instance, higher waves will provide flatter beach slopes for the same grain size, and coarser materials tend to form steeper slopes under constant hydraulic conditions (Bosboom, Judith; Stive, 2015). Based on the reasoning used by Kamphius in his formulation to consider important parameters left out by the CERC equation and the fact that it compares better with published field data, it is considered more representative of the actual sediment transport rates along a uniform coast. Henceforth, the bulk longshore sediment transport rates obtained using his expression will be compared with the transport rates obtained using the SDS data.

6.2 Shoreline Orientation influence on sediment transport

Alongshore sediment transport occurs when waves approach the coast at an angle other than 90˚. Waves approaching the shore hold a certain amount of energy. As they break, there is an exchange of momentum which causes a radiation stress (Bosboom, Judith; Stive, 2015). This stress can move fluid and sediments. However, based on the formulations of the so-called radiation stress, it is greatest when the waves approach the shoreline at an angle of 45˚. This implies that the angle of approach is crucial in sediment transport estimation. Kamphius in his formula assumed a severe wave breaking approach angle thus giving the parameter more influence than it already had when predicting sediment transport rates. This influence of this approach angle at breaking depends on the orientation of the shoreline. Figure 44 shows that for a 7 degree increase in the shoreline orientation with respect to the true north, the sediment transport volume increase by about 37% under the same wave conditions.

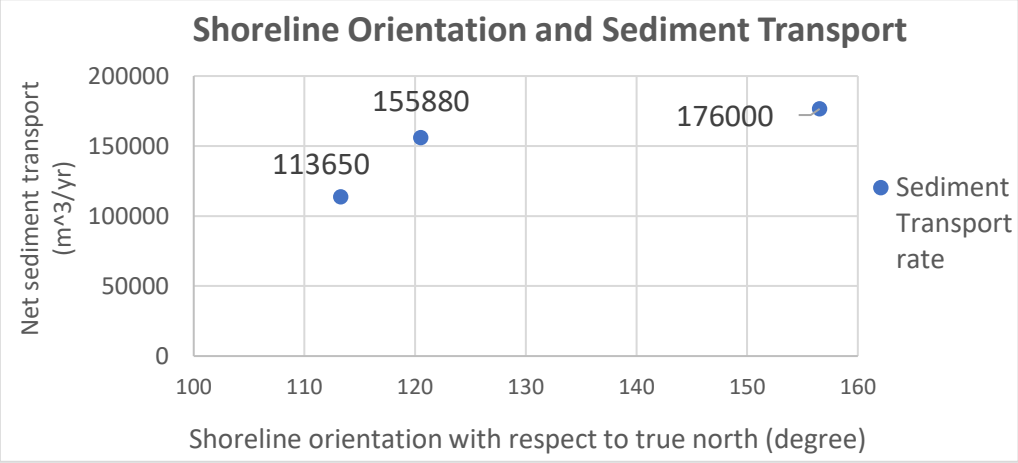

Figure 44: Influence of shoreline orientation on sediment transport

6.3 Wave conditions and sediment transport

The wave height is the most important parameter which determines how much sediment is moved provided the waves approach the shoreline obliquely. The waves travel with the energy which they dissipate at breaking. In the CERC and Kamphius equations, the wave height is squared, thus giving it a higher weight in predicting sediment volumes or rates. A 1 meter increase in wave height doubles the amount of sediment transport holding all factors constant.

6.4 Kamphius' vs SDS data bulk transport predictions

Compared with Kamphius' equation which predicted a north-western net transport direction, the SDS values showed that for 4 orientations (7, 12, 13, and 14 – green arrows read from left to right), the net transport moves towards the south-east. Figure 45 shows the net transport directions predicted by Kamphius and the SDS change rate data. A reason for the shift in transport direction could be due to the method used to calculate the transport rates using the change rates. The alongshore distance between 2 transects was multiplied by the area of the profile (see 5.1.10 **Satellite Derived Shoreline**). It was assumed that no sediments move southeast of the most north-western transect, thus allowing for a southeast alongshore distance to be used. Therefore, for a coastal stretch wherein the shoreline accretion rates (positive values) are more prevalent than the erosion rates (negative values), the net transport direction is positive and points towards the southeast.

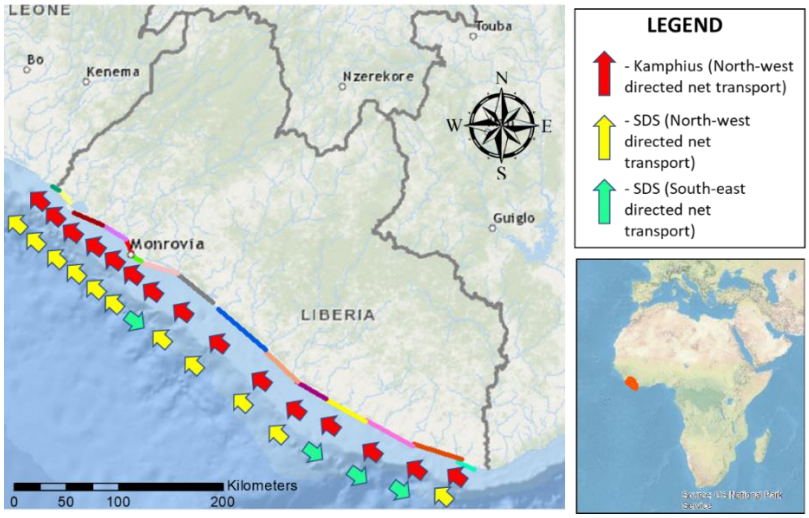

Figure 45: Net sediment transport directions using the Kamphius and SDS methods

Figure 46 displays the net transport rates using the SDS data. Values below zero indicate a southeast drift direction. From the graph, few points can be drawn. They are as follows:

- The shift in direction between orientation 6, 7, and 8 from northwest-southeast-northwest could be because of Cape Mesurado. The protrusion of the shoreline in this area serves as a littoral drift divide explained by the coastal cell concept (Motyka & Brampton, 1993). At a drift divide, sediment flow in opposite directions.
- The high transport rate at shoreline orientation 9 explains the narrow beach width west of the harbour as shown in Figure 5. Sediments are blocked by the eastern harbour breakwater and accumulate over time. The downdrift coast west of the harbour is starved of sediments, thus causing an imbalance in the sand-sharing system.
- For shoreline orientations 12, 13, and 14, the waves approaching the coast are predominantly from the southwest (see Figure 47), hitting the coast at about 43% of the time, 10% more than waves from the nearest most frequent direction. These waves also are of higher magnitude. As they approach the coast, their crests get parallel to the depth contours closed to the coast. Due to the shoreline orientation in this area, coupled with higher and more frequent waves coming from the southwest direction, a significantly higher amount of sediments is moved in the southeast direction.

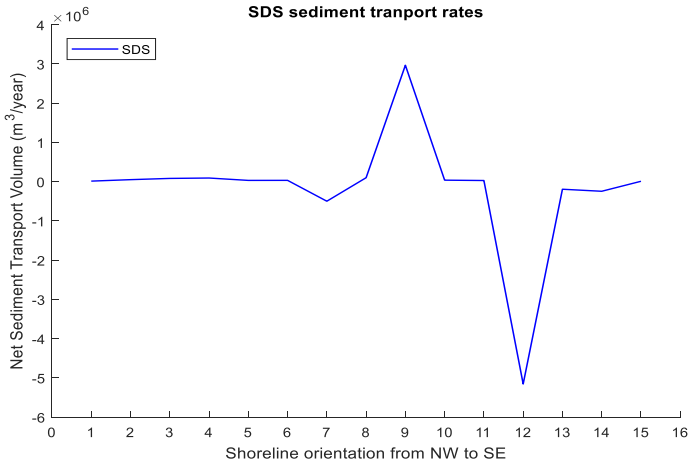

Figure 46: Net longshore sediment transport predictions using SDS data. Values below zero indicate a southeast transport direction.

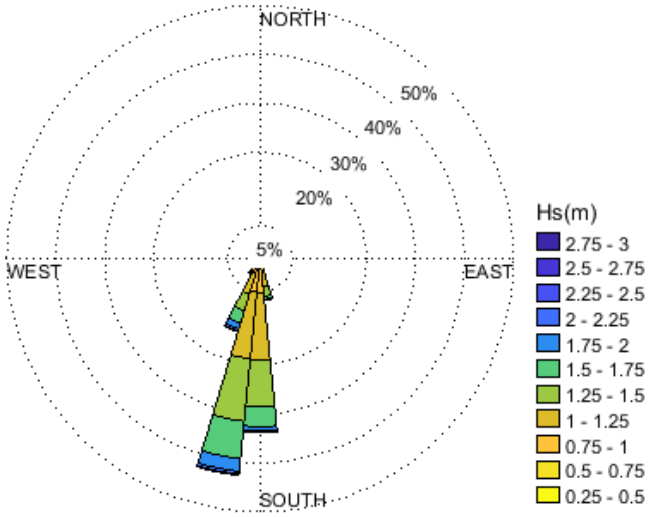

Figure 47: Wave rose for wave data point 4.

6.5 Beach response to storm conditions for different return periods

There is a linear relationship between the equilibrium beach response due to storms and the return period. A wave height exceeded once in a larger return period year will cause more damage to the beach as shown in Figure 48. This is because the beach will have adapted to a certain hydrodynamic forcing condition and hence its morphology is suited to such. A sudden rare increase in the forcing larger than the maximum value experienced will cause a major shift in equilibrium (assuming the beach returns to its equilibrium state – something which never truly happens as the morphodynamic cycle never stops). The beach will need time to adjust to this new forcing and might lose a large amount of sediments before then.

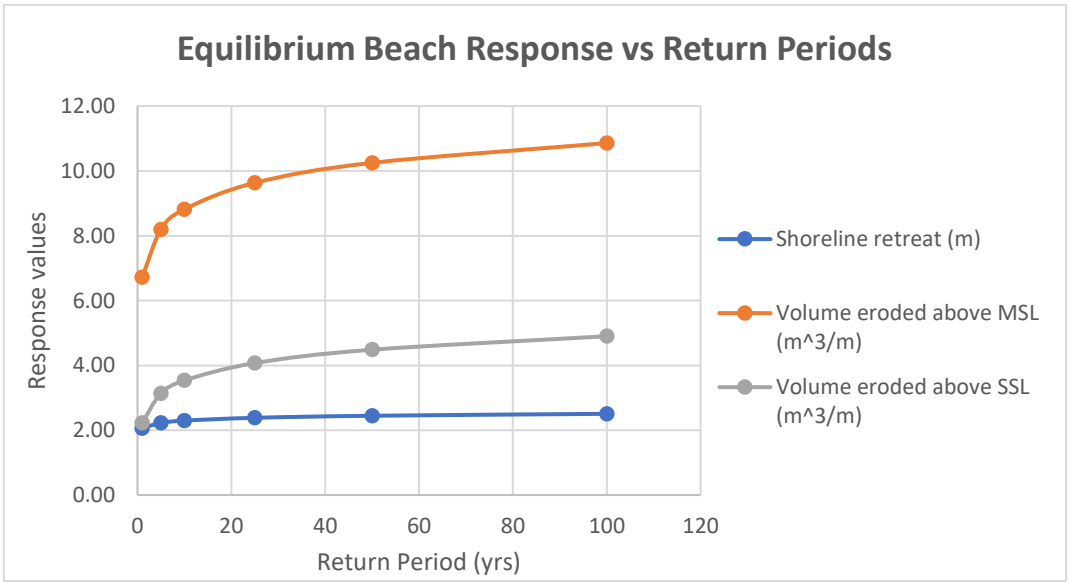

Figure 48: Beach response in return period number of years

6.6 Shoreline retreat rates for different RCP Scenarios

The long-term shoreline retreat rates are higher for a more pessimistic relative SLR projection. As is shown in Figure 49, the rate of retreat for RCP 8.5 compared to RCP 4.5 increases by about 20% for a 15 cm increase in relative SLR. At this rate, a relative SLR of 75 cm will cause a 100% increase in retreat

rates, and a meter increase in SLR would potentially trigger an increase in shoreline recession by about 135%.

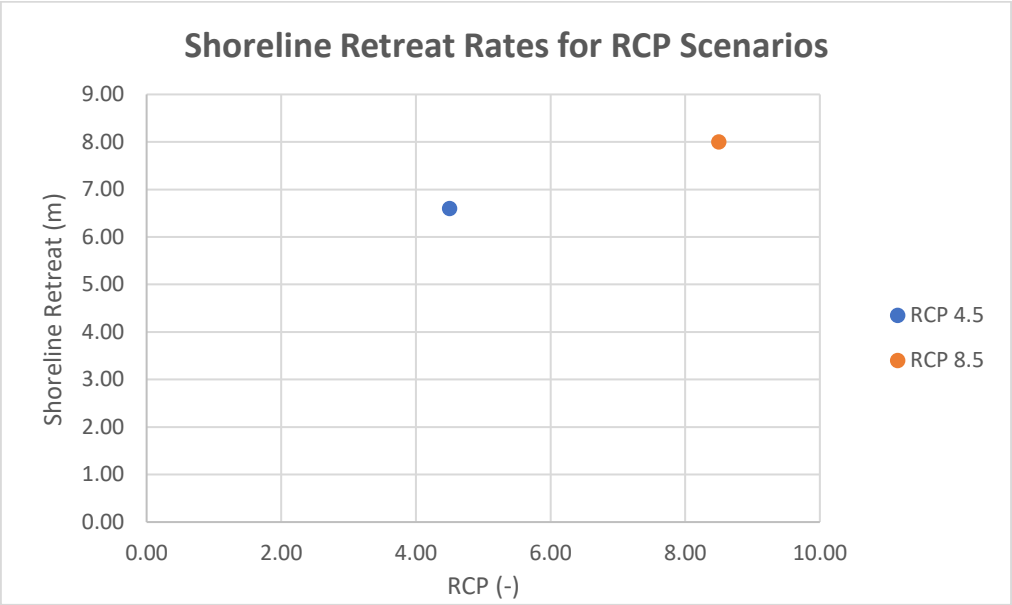

Figure 49: Shoreline retreat due to SLR for different RCP scenarios

Coastal Stretch: LIB_1	Abbreviations : OC - Open Coast; BB - Barrier Beach; L - Lagoon; HR - Harbour; TDI - Tidal Inlet & Deltas; LK - Lake; R - River; J - Jetty											
County: Grand Cape Mount	Mano River - Yonkale		Location (Lat and Lon boundaries)		Northwest	11.48987 ˚W	6.920687 ˚N					
					Southeast	11.453077 ˚W	6.884538 ˚N					
General Description		Morphodynamics		Hydrodynamics								
Length (m):	5984	Type of coast:	OC	Mean Wave Climate								
Berm height - mean wave climate (m):		Evolutive state:		Quadrant:	III							
Mean:	2.1	Evolutive behaviour:	Erosive	Mean Hs(m):	1.85							
Max:	3.8	Mean evolution (m/yr):	-1.20	Mean Tp (sec):	10.40							
Min:	1.1	Mean erosion (m/yr):	-1.20	Most frequent dir (deg)	191.25		SbW	46.2%				
Foreshore Slope:		Length of erosive zone (m):	5984	2% Run-up (m)	0.61		Stdev	0.18				
Mean:	0.02	Mean accretion (m/yr):	-	Extreme wave climate								
Max:	0.03	Length of accretive zone (m):	-	Extreme surge direction	Return period (yrs)							
Min:	0.02	Length of equilibrium zone (m):	-	SWbS	1	5	10	25	50	100		
Sediment:		Presence of obstacles (YES/NO):	NO	Non-exceeded Hs (m)	2.03	2.27	2.36	2.49	2.58	2.67		
D50 (mm):	0.25	Type:	-	Equilibrium response to storm surge (m):	2.06	2.23	2.30	2.38	2.45	2.51		
Standard deviation:	0.59	Number:	-	Volume eroded from MSL (m^3/m):	6.72	8.19	8.82	9.63	10.25	10.86		
Color:	Brownish	Morphodynamic state:	4 - 5	Volume eroded from peak storm surge level (m^3/m):	2.23	3.14	3.54	4.07	4.48	4.90		
Mean beach orientation: (˚with respect to true North)	125	Wright & Short label	Intermediate	Timescale of equilibrium response (hrs):	0.24	0.28	0.29	0.31	0.33	0.34		
		Closure Depth	4.62	Long-term wave climate								
		Bulk longshore sediment transport rate capacity		Mean breaking wave height (m):	1.53							
		SE directed transport (m^3/yr)	260	Standard deviation:	0.40							
		NW directed transport (m^3/yr)	154900	IPCC SLR Regional prediction:	Upper limit (Pessimistic Scenario)							
		Net (m^3/yr)	154600	SLR regional predictions	RCP 4.5			RCP 8.5				
		Gross (m^3/yr)	155160		0.72			0.87				
		Cap (m^3/yr)	560	Shoreline Retreat Rates (m):	6.6			8.0				

Figure 50: Coastal conditions for shoreline orientation

CHAPTER 7: LIMITATIONS OF THE STUDY

In this chapter, a brief description of the uncertainties involved in the study is given.

7.1 ERA-Interim wave data

The wave data used by ERA-Interim is an average over 6 hours found by an interpolation method. As it is measured in real time over a smaller interval, a lot of values may be lost in the data. Taking the mean value over 6 hours do not allow for a rigorous analysis. A validation method is therefore required. For example, wave data from a wave buoy should be compared with the wave heights obtained by ERA-Interim. Shanas and Kumar (2013) compared wave data from ERA-Interim with wave data from buoys at a deep water and shallow water location in the eastern Arabian Sea. They concluded that the wave height values from both sources had a correlation value of 0.85 with a root mean square error of 0.87 and 0.53 for deep and shallow waters respectively (Shanas & Sanil Kumar, 2014). They asserted that ERA-Interim underpredicts the significant wave height value by 15% in deep water, and overpredicts it by 9% (Shanas & Sanil Kumar, 2014). Shanas and Kumar (2013) also pointed out a significant scattering when the wave periods and directions were compared. It is however unclear what the performance of ERA-Interim dataset is in other regions as the study area and that should be of concern for further research along the Liberian coast.

7.2 Assumptions used in LWT Propagation

The propagation method used in the study considers the wave motion only. In reality, the waves have a mass moving at a certain speed, thus momentum is being carried along by waves as they approach the coast. This implies that LWT does not consider the transfer of momentum as the waves propagate from deep to shallow water. It also does not count for the residual horizontal orbital particle velocity in the direction of propagation referred to as Stoke's drift (Bosboom, Judith; Stive, 2015). Although LWT considers wave transformation processes such shoaling and refraction as waves propagate from deep to shallow water, bottom friction is not accounted for. This phenomenon has the tendency of reduce the wave energy before it reaches the breaker line. This may overestimate breaking wave heights at the breaker line which subsequently overpredicts sediment transport in the surf zone to a power of 2 for each 1 m wave height overestimation. Bottom friction often works in combination with shoaling when the waves encounter the seabed. LWT also does not account for wave-to-wave and wave – current interaction. Depending on the direction of water currents, the wave heights could be enhanced or reduced to a significant amount (Bosboom, Judith; Stive, 2015). However, with the data obtained for the study, it is an acceptable method of propagation to obtain rough wave breaking characteristics as there is not sufficient information for a more rigorous numerical modelling propagation tool such as SWAN (Simulating waves nearshore).

7.3 Uncertainty in SDS change rate data

The satellite imagery used to obtain the SDS change rate data underwent a lot of filtering and pre-processing. Human errors and errors encountered by the satellite can increase the amount of uncertainty in the data. Low precision change rate predictions (higher root mean square error) for the transects could alter the results obtained. The average uncertainty in change rate prediction is about 0.6 and the average root mean square error is about 20. This is expected as the standard deviation of the dataset is 1.01.

7.4 Assumptions made for storm surge calculations

Based on the local wind direction and the lack of information on the influence of storm winds from the south of the Atlantic Ocean, one surge value was used for a whole sector. A worst case scenario was also used wherein the wind speed from a direction normal to the shoreline was ignored in favour of a higher wind speed. This might overpredict the storm surge value and produce higher retreat and erosion rates than the actual conditions.

7.5 The Bruun Rule

The Bruun rule assumes that all sand transport occurs normal to the shoreline in the cross-shore direction (Ranasinghe & Stive, 2009). This restricts the Bruun rule to performing as a two-dimensional model as it does not account for any 3-dimensional variability that is common along natural coastlines (Ranasinghe & Stive, 2009). Thus, it does not make realistic predictions in areas adjacent to headlands, or engineering structures, lagoon and estuary inlets, deltas and

other areas with significant gradients in alongshore sediment transport (Ranasinghe & Stive, 2009). Determining how far away from one of these areas can the Bruun rule be applied successfully is a challenging task and is not considered in this study. The uncertainty surrounding what depth of closure value to used also alters the predictions of the Bruun rule. However, most of Liberia's coastline are free of interventions and the Bruun rule can be used as a first estimate tool in predicting long-term retreat rates due to SLR.

7.6 Hallermeier's closure depth equation

The predictive closure depth equation of Hallermeier only serves as a conservative morphological boundary during erosional events, rather than a sediment transport boundary (Nicholls et al., 1997). As the time scale of observation increases, the location of the depth of closure along the beach profile changes (Nicholls et al., 1997). Nicholls et al (1998) concluded that on a scale from events up to years (short and medium time scales), the closure depth is primarily a function of direct external forcing (cross-shore redistribution of sediment by waves), indirect external forcing (sediment loss/gain by littoral transport and the resulting profile translation) and internal system dynamics (bar dynamics) (Nicholls et al., 1998). They therefore claimed that Hallermeier's closure depth equation cannot be expected to predict the actual closure, but rather it predicts distributional properties such as the limit (Nicholls et al., 1998). This adds more uncertainty to the study.

7.7 Kriebel and Dean's convolution theory

The convolution theory used to calculate the beach's response to storm-surge contains an unrealistic feature in its approach. It assumes that the upper contours of the beach profile would erode throughout the storm event whereas in nature, they would be activated only during the extreme high water levels (Kriebel et al., 1993). However, the authors believe that the convolution method is a useful analytical tool in situations where preliminary beach-profile response calculations are required (Kriebel et al., 1993). This was proven in their paper by comparing the beach response calculated with the convolution method and measured values of 2 storm events (Kriebel et al., 1993).

Other general formulations and theories, such as the Cowan's breaker index, the Kamphius' conversion of sea level pressure to surge values etc., add more uncertainty to the results obtained. Each of them comes with some limitations and therefore, the results obtained using them require calibration before being used for any coastal management related purpose. Most importantly, the lack of information and/or willingness from local governmental authorities in Liberia responsible for the coastal zone to provide a more robust information made this study more challenging and difficult.

CHAPTER 8: CONCLUSION AND RECOMMENDATIONS

This study aims to provide first estimate values as a hint explaining the general coastal processes and response shaping the coast over different time and spatial scales. In the absence of robust data, it is difficult to carry out robust analysis of the coastal zone. With such an information gap needing to be filled, the study uses simple analytical methods and formulas to arrive at generic results. It is hereby highly recommended that the results obtained in this study should never be used for coastal management purposes unless real time data is collected and used to validate them.

A first attempt to validate these results would be an improved coastal monitoring strategy or policy. The importance of coastal monitoring procedures can not be furthered underestimated as it gives the necessary information to act upon when managing the coast. The installation of wave buoys along the coast, implementation of regular beach profile surveys, the usage of aerial photographs taken at regular time intervals, an attempt to perform a sediment budget analysis of the coastal system are measures which can improve the coastal management procedures in Liberia. There is a need to understand the sediment transport processes occurring at harbours, tidal inlets and barrier beaches, river outlets etc…

A sediment budget analysis wherein the sediment sources, sinks, and pathways are identified can help a lot in preparing coastal management adaptation strategies (coastal protection using hard and/or soft approaches) to control and/or reduce current erosion rates along the Liberian coast. Without understanding our coastal system, attempts to implement adaptation strategies to combat coastal erosion will be misguided and might cause more harm than good, especially with the current SLR projections made by the IPCC.

CHAPTER 9: REFERENCES

Alamy Ltd. (n.d.). Aerial view of West Point, the poorest suburb of the city of Monrovia, Liberia, taken from the top of the ruins of Hotel Ducor. Retrieved June 7, 2018, from https://www.alamy.com/stock-photo-aerial-view-of-west-point-the-poorest-suburb-of-the-city-of-monrovia-73553511.html

Allersma, E., & Tilmans, W. M. K. (1993). Coastal conditions in West Africa-A review. *Ocean and Coastal Management*, *19*(3), 199–240. https://doi.org/10.1016/0964-5691(93)90043-X

Allsop, W. (2015). Influence of steep seabed slopes on breaking waves for structure design, (December).

Barbara Tasch. (2017). RANKED: The 30 poorest countries in the world. Retrieved June 7, 2018, from http://uk.businessinsider.com/the-25-poorest-countries-in-the-world-2017-3/#5-niger-gdp-per-capita-1113-907-26

Barber, D. (2008). Traditional mariners' compass points. Retrieved May 27, 2018, from http://tamivox.org/dave/compass/index.html

Berrisford, P., Dee, D., Fielding, K., Fuentes, M., Kallberg, P., Kobayashi, S., & Uppala, S. (2009). The ERA-Interim Archive. *ERA Report Series*, *1*(1), 1–16. Retrieved from http://www.ecmwf.int/publications/library/do/references/list/782009

Bosboom, Judith; Stive, M. J. . (2015). *Coastal Dynamics I, lecture notes CIE4305* (Version 0.). Delft: Delft Academic Press.

British Geological Survey; Liberian Geological Survey. (n.d.). Geology. Retrieved June 9, 2018, from https://www.bgs.ac.uk/LGS/geology.html

Brosen_windrose.svg. (n.d.). A 32-point compass rose. Retrieved June 3, 2018, from https://commons.wikimedia.org/w/index.php?curid=11999587

Camenen, B., & Larson, M. (2007). Predictive Formulas for Breaker Depth Index and Breaker Type. *Journal of Coastal Research*, *234*(234), 1028–1041. https://doi.org/10.2112/05-0566.1

Chester K. Wentworth. (2018). A Scale of Grade and Class Terms for Clastic Sediments. *The University of Chicago Press Stable*, *30*(5), 377–392. Retrieved from http://www.jstor.org/stable/30063207

Church, J A; Clark, P U; A. Cazenave; Gregory, J M; Jevrejeva, S; Levermann, A; Merrifield, M A; Milne, G A; Nerem, R S; Nunn, P D; Payne, A J; Pfeffer, W T; Stammer, D; Unnikrishnan, A. S. (2013). *Sea Level Change*. *Climate Change 2013: The Physical Science Basis. Contribution of Working Group I to the Fifth Assessment Report of the Intergovernmental Panel on Climate Change [Stocker, T.F., D. Qin, G.-K. Plattner, M. Tignor, S.K. Allen, J. Boschung, A. Nauels, Y. Xia,* (Vol. 13). Cambridge, United Kingdom and New York, NY, USA.: Cambridge University Press.

Climates to Travel. (n.d.). Temperature, rainfall, prevailing weather conditions, when to go, what to pack. Retrieved June 5, 2018, from https://www.climatestotravel.com/climate/liberia

Davis, R. A., & Hayes, M. O. (1984). What is a wave-dominated coast?, *60*, 313–329.

Dean, R. G., & Dalrymple, R. A. (1991). Water Wave Mechanics for Engineers and Scientists. In Philip L.F Liu (Ed.), *Advances Series on Ocean Engineering* (Vol. 2). Farrer Road Singapore: World Scientific Publishing Co. Pte. Ltd.

Deltares.nl. (n.d.). Deltares. Retrieved May 25, 2018, from https://www.deltares.nl/en/

DEPARTMENT OF THE ARMY, Waterways Experiment Station, Corps of Engineers, C. E. R. C. (1984). *Shore protection manual: Volume I and II*. *U.S. Army Engineer Waterways Experiment Station* (Vol. 1 & 2). https://doi.org/10.5962/bhl.title.47830

ECMWF. (2012). Part VII : ECMWF Wave Model IFS DOCUMENTATION – ECMWF WAVE MODEL Table of contents Numerical scheme, (June), 1–79.

Finkl, C. W. (2004). Coastal Classification : Systematic Approaches to Consider in the Development of a

Comprehensive Scheme.

Hadden, B. R. L. (2006). The Geology of Liberia : a Selected Bibliography of Liberian Geology , Geography and Earth Science, (May), 5–6.

Hagenaars, G., de Vries, S., Luijendijk, A. P., de Boer, W. P., & Reniers, A. J. H. M. (2018). On the accuracy of automated shoreline detection derived from satellite imagery: A case study of the sand motor mega-scale nourishment. *Coastal Engineering*, *133*(December 2017), 113–125. https://doi.org/10.1016/j.coastaleng.2017.12.011

Healy, Terry; Wang, Ying; Healy, J.-A. (2002). Muddy Coasts of the World: Processes, Deposits and Functions. In *Proceedings in Marine Science*. Elsevier.

Hennermann, K. (2017). ECMWF: What is ERA-Interim. Retrieved May 25, 2018, from https://software.ecmwf.int/wiki/display/CKB/What+is+ERA-Interim

Hinkel, J., Brown, S., Exner, L., Nicholls, R. J., Vafeidis, A. T., & Kebede, A. S. (2012). Sea-level rise impacts on Africa and the effects of mitigation and adaptation: An application of DIVA. *Regional Environmental Change*, *12*(1), 207–224. https://doi.org/10.1007/s10113-011-0249-2

Johnson-sirleaf, E. (2008). GOVERNMENT OF THE REPUBLIC OF LIBERIA 2008 NATIONAL POPULATION AND HOUSING CENSUS : PRELIMINARY RESULTS, (June).

Kamphuis, J. W. (1991). Alongshore Sediment Transport Rate. *Journal of Waterway, Port, Coastal, and Ocean Engineering*, *117*(6), 624–640. https://doi.org/10.1061/(ASCE)0733-950X(1991)117:6(624)

Kamphuis, J. W. (2000). *Introduction to Coastal Engineering and Management*. *Advanced Series on Ocean Engineering* (Vol. 16). https://doi.org/10.1007/s13398-014-0173-7.2

Kriebel, D. L. ., Dean, R. G. ., & Members, A. (1993). Convolution for time-dependent beach-profile response. *Journal of Waterway, Port, Coastal, and Ocean Engineering*, *119*(2), 204–226.

Liberian Hydrological Services. (n.d.). Rivers. Retrieved June 10, 2018, from http://lhsliberia.com/hydrology-for-the-curious/rivers/

Liberian Hydrological Services. (2016). Rainfall data. Retrieved June 6, 2018, from http://lhsliberia.com/rainfall-data/

Lorenc, A. C. (1981). A Global Three-Dimensional Multivariate Statistical Interpolation Scheme. *Monthly Weather Review*. https://doi.org/10.1175/1520-0493(1981)109<0701:AGTDMS>2.0.CO;2

Luijendijk, A., Hagenaars, G., Ranasinghe, R., Baart, F., Donchyts, G., & Aarninkhof, S. (2018). The State of the World ' s Beaches. *Scientific Reports*, 1–11. https://doi.org/10.1038/s41598-018-24630-6

Maps of World. (2013). Liberia River Map. Retrieved June 9, 2018, from https://www.mapsofworld.com/liberia/river-map.html

Maps of World. (2015). Political Map of Liberia. Retrieved June 9, 2018, from https://www.mapsofworld.com/liberia/liberia-political-map.html

Morton, R. A. (2003). *An Overview of Coastal Land Loss: With Emphasis on the Southeastern United States*. Retrieved from https://pubs.usgs.gov/of/2003/of03-337/waves.html

Motyka, J. M., & Brampton, A. H. (1993). Coastal management - mapping of littoral cells, (1622174).

Nicholls, R. J., Birkemeier, W. a, & Hallermeier, R. J. (1997). Application of the depth of closure concept. *Proceedings of the Coastal Engineering Conference*, *4*, 3874–3887. https://doi.org/10.9753/icce.v25

Nicholls, R. J., Larson, M., Capobianco, M., & Birkemeier, W. A. (1998). DEPTH OF CLOSURE: IMPROVING UNDERSTANDING AND PREDICTION Robert J. Nicholls , Magnus Larson , Michele Capobianco and William A. Birkemeier. In *Coastal Engineering Proceedings* (pp. 2888–2901). International Conference on Coastal Engineering (ICCE). Retrieved from https://icce-ojs-tamu.tdl.org/icce/index.php/icce/article/viewFile/5810/5478

Okazaki, S., & Sunamura, T. (1994). Quantitative Predictions for the Position and Height of Berms. *Geographical Review of Japan*, *67*(2), 101–116.

Pachauri, R. K. (2014). *Climate Change 2014 Synthesis Report*.

Ranasinghe, R., & Stive, M. J. F. (2009). Rising seas and retreating coastlines. *Climatic Change*, *97*(3), 465–468. https://doi.org/10.1007/s10584-009-9593-3

Robb, James M.; Schlee, John; Behrendt, J. C. . (1973). Bathymetry of the Continental Margin off Liberia, West Africa. *Research U.S. Geological Survey*, *1*(5), 563–567. Retrieved from https://pubs.usgs.gov/journal/1973/vol1issue5/report.pdf

Saket, A., Peirson, W. L., Banner, M. L., & Allis, M. J. (1994). Wave breaking onset of two-dimensional wave groups in uniform intermediate depth water, (1994), 1–15.

Scott, B. R., & Colby C. H. (1965). Effects of Water Temperature on the Discharge of Bed Material. *Geological Survey Professional Paper*, (462–G).

Shanas, P. R., & Sanil Kumar, V. (2014). Comparison of ERA-Interim waves with buoy data in the eastern Arabian Sea during high waves. *Indian Journal of Marine Sciences*, *43*(7), 1343–1346.

Sistermans, P. G. J. (2002). Graded Sediment Transport by Non-breaking Waves and a Current, (January).

Sorensen, R. M. (2006). *BASIC COASTAL ENGINEERING*. (Springer, Ed.) (Third Edit). New York: Springer.

Stive, M. J. F., Aarninkhof, S. G. J., Hamm, L., Hanson, H., Larson, M., Wijnberg, K. M., … Capobianco, M. (2002). Variability of shore and shoreline evolution, *47*, 211–235.

Stockdon, H. F., Holman, R. A., Howd, P. A., & Sallenger, A. H. (2006). Empirical parameterization of setup , swash , and runup, *53*, 573–588. https://doi.org/10.1016/j.coastaleng.2005.12.005

The Bruce Murray Space Image Library. (n.d.). Wentworth (1922) grain size classification. Retrieved May 31, 2018, from http://www.planetary.org/multimedia/space-images/charts/wentworth-1922-grain-size.html

Titus, J. G. (1990). WESTERN AFRICA, THE AMERICAS, THE MEDITERRANEAN BASIN, AND THE REST OF EUROPE. In *Miami Conference on Adaptive Responses to Sea Level Rise and other impacts of Global Climate Change: Changing Climate and the Coast* (Vol. 2).

United Nations Development Programme. (2016). Strengthening Liberia's capability to provide climate information and services to enhance climate resilient development and adaptation to climate change.

United Nations Development Programme. (2018). Enhancing Resilience of Vulnerable Coastal Areas. Retrieved March 23, 2018, from http://www.lr.undp.org/content/liberia/en/home/operations/projects/environment_and_energy/enhancing-resilience-of-vulnerable-coastal-areas-.html

USAID; U.S. Geological Survey. (n.d.). Ecoregions and Topography of Liberia. Retrieved June 10, 2018, from https://eros.usgs.gov/westafrica/ecoregions-and-topography/ecoregions-and-topography-liberia

Weibull, W. (1939). A Statistical Theory of the Strength of Materials. *Ingeniorsvetenskapsakademiens*.

Wikimedia Foundation Inc. (2018). Sandstone. Retrieved May 31, 2018, from https://en.wikipedia.org/wiki/Sandstone

Wiles, D. L. (2005). Coastal Zone Vulnerability and Adaptation to Climate Change in Liberia. *Training Workshop on Adaptation and Vulneration to Climate Change. Mozambique*.

Wilson, G. (2012). Wilson, Garmonyou. Retrieved June 7, 2018, from http://allafrica.com/stories/201210181174.html

Woodroffe, C. D. (2007). The Natural Resilience of Coastal Systems: Primary Concepts. *Managing Coastal Vulnerability*, 45–60.

World Sea Temperature. (2018). Monrovia Sea Temperature. Retrieved May 31, 2018, from https://www.seatemperature.org/africa/liberia/monrovia.htm